ENZYME BEHAVIOR IN SYNTHETIC MATERIALS AND STRUCTURAL IMPLICATIONS FOR RATIONAL DESIGN

A Dissertation
Submitted to the Graduate Faculty
of the
North Dakota State University
of Agriculture and Applied Science

By

Jasmin Kaye Farmakes

In Partial Fulfillment of the Requirements
for the Degree of
DOCTOR OF PHILOSOPHY

Major Program:
Chemistry

November 2020

Fargo, North Dakota

North Dakota State University
Graduate School

Title

Enzyme Behavior in Synthetic Materials and Structural Implications for Rational Design

By

Jasmin Kaye Farmakes

The Supervisory Committee certifies that this ***disquisition*** complies with North Dakota State University's regulations and meets the accepted standards for the degree of

DOCTOR OF PHILOSOPHY

SUPERVISORY COMMITTEE:

Dr. Zhongyu Yang
Chair

Dr. Kenton Rodgers

Dr. John Hershberger

Dr. Bingcan Chen

Approved:

11/15/2020	Gregory Cook
Date	Department Chair

ABSTRACT

Combining enzymes with synthetic materials is the new frontier of biocatalysis, materials science, and protein engineering. Enzymes are biological macromolecule catalysts with incredible efficiency and specificity that are desirable for use in a variety of different fields. However, commercial applications have been limited by the stability and reusability of un-altered enzymes. An avenue for overcoming the challenges to harnessing enzyme power is to combine enzymes with materials to create an enzymatically-active material that has enhanced stability and activity. Unfortunately, the catalytic activity of the hybrid material is often lower than that of the enzyme alone. The activity of an enzyme is directly dependent on its structure and dynamics. Therefore, a deeper understanding of enzyme structure and dynamics upon incorporation into materials will provide the data necessary to rationally design enzymatically-active materials with the desired features.

This dissertation explores the behavior of a model enzyme, T4 Lysozyme, with two different artificial material systems, metal-organic frameworks and polyethylene glycol. The underlying structural rationale for the behavior is probed using a variety of techniques, notably, Electron Spin Paramagnetic Resonance. Herein, the implications of structural alterations on activity and opportunities for exploitation are discussed. T4 Lysozyme is a perfect model for this study because it has a well characterized structure-activity relationship, thus providing a vast literature understanding which can be pulled from to verify and assist with interpretation of data.

The structural basis of enzyme activity alteration in artificial materials can be used to rationally design systems with desired characteristics. After successfully demonstrating the tunability of proteins in artificial materials using T4L as a model, human Cu/Zn superoxide dismutase 1 was chosen for continuing studies due to its importance in diseased states. However, the superoxide dismutase mutant chosen is aggregation prone, which makes it difficult to express recombinantly in large amounts. Therefore, an efficient protocol for producing the superoxide dismutase protein was developed to set the stage for future studies.

ACKNOWLEDGEMENTS

I would like to express gratitude to the people who supported me in my journey through graduate school. First, I would like to thank the members of my advisory committee, Dr. Zhongyu Yang, Dr. Kenton Rodgers, Dr. John Hershberger, and Dr. Bingcan Chen, for the guidance and support they provided. I would like to emphasize an extra-special thanks to Dr. Yang who not only imparted wisdom but also fostered growth by including me in the development, writing, and editing of manuscripts and grants.

To the members of the Yang group, thank you for always being willing to help and for sharing your knowledge. Thank you Sunanda for convincing me to join the group and for supporting me on days when I was ready to give up. Thank you Dr. Pan for your hard work and infectious enthusiasm. Thank you Qiaobin for being a gracious officemate and friend.

Additionally, I am grateful to those who collaborated with us for their insight. Some I would like to thank by name are: Dr. Scott Payne, Dr. Angel Ugrinov, Dr. Yongki Choi, and Dr. Coray Colina. Special thanks to Dr. Aravinda Munasinghe, your advice has been invaluable.

In the great sea of academia, it is easy to feel adrift without friends to commiserate with. I am grateful that I had Levi, Quinlyn, Krystal, and Wendy sharing this journey with me. Thank you, Levi, for helping me learn quantum mechanics and brightening up my bonfires. Thank you, Quinlyn, for helping me hold my head high and reminding me that I am a strong independent woman on days that I forgot. Thank you, Krystal, for your supportive advice and proof-reading services. Thanks to Wendy for babysitting and always answering my weird medical questions. A very big thank you to Coach Chelsea Crosby, I would not have survived 2020 without you and the ladies of the group.

Last, but not least, I would like to thank the people and programs who provided monetary support and supplies that made this journey possible. A very big thank you to Jim and Sue Swenson who supported my academic journey by providing me with a full-tuition scholarship that paid for my undergraduate degree. Without this scholarship I would not have graduated with a degree in chemistry. Thank you to the Central Alumni Scholarship and to the Edwin Fremont Ladd Endowed Scholarship which paid for much-needed supplies that helped me keep up with classes. Additionally, the support of the Upward Bound program, McNair Scholars program, Lutheran Social Services, and Disability Support Services, were vital to my success. Thank you to everyone who donates to and works for these programs.

DEDICATION

To the homeless youth. Don’t let your current circumstances keep you from dreaming.

TABLE OF CONTENTS

LIST OF TABLES

LIST OF FIGURES

LIST OF SCHEMES

LIST OF ABBREVIATIONS

AFM	Atomic Force Microscopy
ALS	Amyotrophic Lateral Sclerosis
Asp	Aspartate
BDC	Terephthalic acid
°C	Degrees Celsius
Ca	Calcium
CaBDC	MOF made of Calcium and terephthalic acid
$CaCl_2$	Calcium Chloride
CD	Circular Dichroism Spectroscopy
Cu	Copper
CNT	Carbon Nanotubes
CW	Continuous Wave
DCM	Dichloromethane
DCU	Dicyclohexylurea
DD	Deionized-distilled
DDH_2O	Deionized-distilled water
DNA	Deoxyribonucleic acid
DMF	N,N-Dimethylformamide
DTT	Dithiothreitol
E. Coli	Escherichia coli bacteria
EDTA	Ethylenediaminetetraacetic acid
EDX	Energy-Dispersive X-ray
EPR	Electron Paramagnetic Resonance Spectroscopy
FALS	Familial Amyotrophic Sclerosis

FDA	Food and Drug Administration
Fe	Iron
FTIR	Fourier Transform Infrared Spectroscopy
GHz	GigaHertz
Glu	Glutamic Acid
GO	Graphite Oxide
HEPES	4-(2-hydroxyethyl)-1-piperazineethanesulfonic acid
HEWL	Hen Egg White Lysozyme
His	Histidine Amino Acid
His-tag	Tag of 6 Histidine Amino Acids
IDP	Intrinsically Disordered Protein
IPTG	Isopropyl β- d-1-thiogalactopyranoside
IR	Infrared Spectroscopy
kDa	kilodaltons
$KMnO_4$	Potassium Permanganate
LB	Luria Broth
Lys	Lysozyme
M	Molarity
mM	Millimolar
MES	2-(N-morpholino)ethanesulfonic acid
MeOH	Methanol
Mg	Milligram
Mn	Manganese
Min	Minutes
MOF	Metal-Organic Framework

MOPs	3-(N-morpholino) propanesulfonic acid
mRNA	Messenger RNA
MTSL R1	S-(1-oxyl-2,2,5,5-tetramethyl-2,5-dihydro-1H-pyrrol-3-yl)methyl methanesulfonothioate
M.W.	Molecular Weight
MWCO	Molecular Weight Cut Off
NaCl	Sodium Chloride
NDSU	North Dakota State University
Nm	nanometer
NMR	Nuclear Magnetic Resonance Spectroscopy
NO_3	Nitrate
OD	Optical Density
PBS	Phosphate-buffered saline
PEG	Polyethylene Glycol
PXRD	Powder X-Ray Diffraction
Rcf	Relative Centrifugal Force
ROS	Reactive Oxygen Species
SDSL	Site-Directed Spin Labeling
SDS-PAGE	Sodium dodecyl sulfate polyacrylamide gel electrophoresis
SEM	Scanning Electron Microscopy
SOD1	Superoxide Dismutase 1
T4L	T4 Phage Lysozyme
TCEP	tris(2-carboxyethyl)phosphine
TEM	Transmission Electron Microscopy
THF	tetrahydrofuran

UV	Ultraviolet
XRC	X-Ray Crystallography
ZIF	Zeolitic Imidazolate Framework
Zn	Zinc

LIST OF SYMBOLS

Å	Angstrom
β	Beta
G	Gauss
μm	Micrometer
Ω	Omega
H	Magnetic Field Strength
μM	Micromolar
ΔE	Change in Energy
h	Plank’s Constant
s	Second
π	Pi
r	Effective Radius
k	Boltzmann’s Constant
T	Absolute Temperature
L	Liter
mA	Milliamp
ml	Milliliter
C	Celsius
U	Units
μL	Microliter
kV	Kilovolt
η	Solution Viscosity
τ_c	Rotational Correlation Time
γ_e	Gyromagnetic Ratio

ν	Frequency
μ	Magnetic Moment
m_s	Spin Quantum Number
g_e	g-factor of a Free Electron
B_0	External Applied Magnetic Field
m_I	Nuclear Spin Angular Momentum
T_1	Spin-Lattice Relaxation
T_2	Spin-Spin Relaxation

LIST OF APPENDIX FIGURES

1. INTRODUCTION TO ENZYMATICALLY-ACTIVE MATERIALS

1.1. Overview

Combining enzymes with synthetic materials is the new frontier of biocatalysis, materials science, and protein engineering. The introduction of a synthetic partner provides the enzyme properties/characteristics of the synthetic material, which can improve the stability or reusability of the target enzyme and result in a hybrid material that possesses catalytic activity. The activity of the hybrid material depends on the structure, dynamics, and orientation of the incorporated enzyme. Both the preparation and characterization of enzymatically-active materials have been explored in the literature with exciting findings and varied challenges. This chapter will start with a general introduction of enzymes, with special emphasis on two model enzymes chosen to represent monomeric and dimeric enzymes. Next, an introduction to three popular synthetic materials that are often combined with enzymes, polymers, Metal-Organic Frameworks (MOFs), and graphite oxides (GOs) is presented. Lastly, the purpose of this dissertation is introduced.

1.2. Versatility of Enzymes

Metabolism is a network of chemical reactions that utilize and produce energy in organisms. However, many of these vital reactions would progress too slowly to sustain life without a catalyst. Organisms rely on enzymes, which are macromolecule catalysts, to catalyze reactions and carry out specific tasks. When compared to the uncatalyzed reaction, enzymes can increase the rate of a reaction by 100 million to 10 billion times[1–3]. The carefully molded structure of an enzyme provides high specificity and efficiency that is currently unrivaled by any synthetic catalyst[4–7]. Because the power of an enzyme cannot be easily replicated, and enzymes are environmentally friendly, it is desirable to use enzymes to catalyze reactions whenever possible[1]. Many different enzymes have evolved to serve specific purposes and to catalyze the vast and varied reactions necessary for maintenance and growth of living organisms. This provides a large pool of enzymes that are desirable for use as bio-catalysts in food science, material science, pharmaceuticals, and healthcare.

Throughout recorded history, humans have used enzymes in food preservation and production, but it wasn't until 1877 that the term enzyme was used to describe these biocatalysts[1]. The Nobel Prize in Chemistry 1946 was divided between James Sumner for his discovery that enzymes can be crystallized, and to John Northrop and Wendell Stanley for their preparation of enzymes and virus proteins in pure forms[1]. These pioneering works in enzyme purification set the stage for the future of enzyme utilization. Still, large scale microbial production of enzymes didn't begin until the 1960's[2,6,7]. Enzymes are now used in many large-scale industrial processes including, but not limited to, pharmaceuticals, textiles, cleaning, food production and preservation. Two examples of commonly used large-scale industrial enzymes, amylase and lipase, demonstrate the versatility of enzymes in commercial applications.

Amylase is an enzyme that catalyzes the breakdown of starch into sugar molecules during the digestion process. In metabolism, the sugar molecules that are produced by the amylase hydrolysis reaction are converted by other enzymes into glucose that can be used as energy. The action of amylase has applications in several commercial industries, but is especially helpful for food production and detergents[1,8]. In the food industry, amylase facilitates the baking of breads and brewing of alcohol by breaking the large, cheap, and widely available starch molecules down into sugars that are readily fermented by yeast. In the case of detergents, amylase is of great use because it can remove food stains by breaking down starches that are clinging to the fabric. Amylase is additionally beneficial in detergents because it can remove stains in an ecofriendly manner, and thus, has replaced more harsh methods of cleaning.

Similarly, lipases are enzymes that aid in the digestion of fats. In metabolism, lipases break down dietary fats so they can be used for energy and are also involved in cell signaling processes[1]. In the food industry, lipase can be used to modify food flavor by breaking fats into short-chain fatty acids and alcohols. For example, lipase can effectively remove fat when processing raw meats into packageable products[1,9,10]. In the detergent industry, lipase can prevent the formation of greasy fat residues and remove stains in fabric that are caused by fats. Just like amylase, lipase has replaced some harsh chemical detergents to create more eco-friendly products. In addition to their usefulness in the food and detergent industries, amylase and lipase have both been administered to patients to treat pancreatic insufficiency by replacing missing enzymes[11].

Unfortunately, the full potential uses of enzymes have been limited by stability and reusability. The applications mentioned above for amylase and lipase are all one-time use in mild conditions with no possibility of recapture for reuse or recycling. Combining materials with enzymes allows for a hybrid that is more stable, catalytically active, and reusable[3,7,12]. The first report of an enzymatically active material was published in 1916 when it was noticed that invertase could be immobilized via adsorption to charcoal and subsequently separated from the solution via centrifugation[13,14]. Since then, a host of different materials have been combined with enzymes in many different ways to create enzymatically-active hybrids. However, upon incorporation into materials, enzyme activity is typically altered. Enzyme activity is dependent on factors including protein structure and dynamics, orientation, and access to the active site. Understanding the interplay of factors, especially changes in structure and dynamics, is vital for tuning enzyme activity in materials.

1.3. Lysozyme in Enzymatically-Active Materials Study

One enzyme that has been at the forefront of protein activity and structure studies is Lysozyme. According to some reports, egg whites were used by early Romans to treat eye infections, and similarly, breast milk has been used as a topical antibiotic; both egg whites and breast milk contain considerable amounts of lysozyme[15]. Between 1880 and 1920, the antibacterial properties of various lysozyme-containing substances including milk and egg whites were published. However, it was not until 1922 that Alexander Fleming coined the term lysozyme after observing the bacteriolytic action of nasal mucous from a person suffering from a head cold[16–18]. Although lysozyme from hen egg white (HEWL) was crystallized by Edward Abraham in 1937, it took until 1965 for the structure to be described after David Chilton Phillips obtained a 2 angstrom resolution model using X-ray crystallography[15]. The full amino acid sequence of HEWL was published in 1962, making it the first protein fully sequenced that contains all twenty common amino acids, as well as the first protein to have its three dimensional structure solved using X-ray diffraction techniques[19,20].

Using the structural information, a mechanism for lysozyme catalytic action was proposed by David Chilton Phillips in 1967 and is referred to as the 'Phillips' mechanism, which is shown in Figure 1.1[21]. We now understand that lysozyme can kill bacteria by cleaving peptidoglycan cell walls. The peptidoglycan walls are made from polymers of alternating N-acetylmuramic acids bonded via a β(1-4) glyosidic linkage to N-acetylglucosamines; these strands are cross-linked with short peptide bridges at the lactyl groups of the muramic acid residues[17]. In HEWL, the glutamic acid 35 residue (Glu 35) donates a proton to the glyosidic bond, thus protonating the glyosidic oxygen and cleaving the C-O bond. The aspartate 52 residue (Asp 52) stabilizes the intermediate by acting as a nucleophile to generate glycosyl-enzyme[20].

Then, the intermediate reacts with a water molecule, which results in the final hydrolysis product and regenerated enzyme.

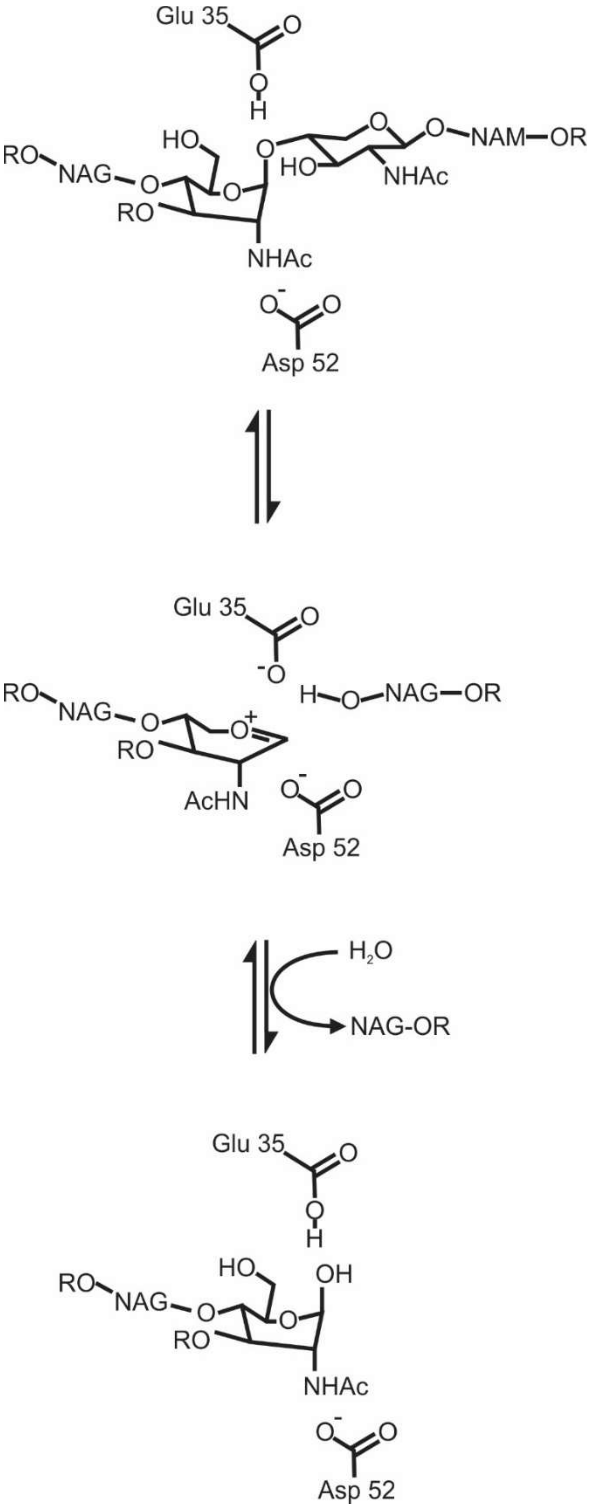

Figure 1.1. Phillips Mechanism of HEWL activity.

HEWL is cheap to produce in large quantities, commercially available, and thus, popular for use in food products and pharmaceuticals including products such as, chewing gum, cosmetics, and baby formula[22]. However, HEWL causes an immunological response in humans and an allergic reaction for some people, which has driven research into the production of other types of lysozyme[17]. Furthermore, many bacteria have evolved mechanisms to evade lysozyme action; lysozyme is not effective at killing all types of bacteria, especially gram-negative bacteria, which have extra membranes around their cells walls[17]. Recent research has indicated that in addition to wall cleavage, lysozyme also helps fight infection by modulating host immune response and can reduce inflammation which has become increasingly more important as antibiotic resistant infections rise[16]. Therefore, lysozyme is a desirable target for biomedical applications such as treating infections, inflammation, and cancer[22]. Due to the enormous potential opportunities, microbial production of novel recombinant lysozymes (especially human variants) is an active area of research.

Still, the recapture and reuse of free lysozyme is hampered by the same challenges mentioned for amylase and lipase, namely, poor stability in harsh conditions and the inability of recapture for reuse. To overcome these limitations, lysozymes have been investigated in combination with a variety of different materials via adsorption, covalent linkages, and co-precipitation. Notably, T4 Bacteriophage lysozyme (T4L) is a popular choice for studying protein stability and structure because it is easily produced in laboratory conditions, tolerant of changes in amino acid sequence, and readily crystalizes[23]. Beginning in the 1990's, T4L was used to study protein folding as well as to develop NMR techniques, and thus, has a well-established and characterized structure-function relationship[24]. T4L has also been used as an expression partner to stabilize and crystalize more difficult proteins due to its stability and easy expression. Although the amino acid sequence of T4L is non-homologous to HEWL, the catalytic function is the same[25].

Therefore, T4L is a good model enzyme for studying enzyme structural changes upon incorporation into enzymatically active materials because it has a desirable function, is stable, easy to produce, and has a widely-investigated structure-function relationship. The vast literature understanding of T4L can aid in the assessment and interpretation of data, which is especially helpful in systems that are challenging to probe. Furthermore, the resistance to appreciable change due to amino acid alterations makes it a prime candidate to be mutated for site-specific covalent attachments. Understanding the structural changes of proteins upon interaction with materials provides opportunities to selectively tune and enhance enzyme activity. In this dissertation, T4L will be used as a model protein to probe structural alterations of proteins upon addition to materials. The materials used herein are polyethylene glycol (PEG), graphite oxide (GO), and two different Metal Organic Frameworks: ZIF and CaBDC (made from calcium and terephthalic acid).

1.4. Potentials of Superoxide Dismutase in Antioxidant Materials

While T4L has antibacterial applications and is a great model enzyme for structure studies, superoxide dismutase is desirable for applications in antioxidant materials and disease states. Oxidative stress is involved in many disease states including cancer, diabetes, and neurodegenerative conditions[26]. Reactive oxygen species (ROS) are generated in the process of normal metabolism as well as from outside sources, but oxidative stress occurs when more ROS are present than the natural antioxidant defenses can handle[26–28]. Antioxidant molecules and enzymes are an integral part of preventing the ROS from oxidizing essential macromolecules like DNA, protein, and lipids.

Superoxide dismutase (SOD) is a powerful antioxidant enzyme responsible for the dismutation of two superoxide anions to hydrogen peroxide and molecular oxygen. The mechanism of human superoxide dismutase 1, which is used in this dissertation, is shown in Figure 1.2. It is an especially important enzyme because dismutation is the first step in the detoxification process of superoxide anions in cells[26]. As a metalloenzyme, it requires a metal cofactor to catalyze the reaction. Various isoforms of SOD exist in both prokaryotes and eukaryotes with different metal cofactors. The typical cofactors are iron(Fe), zinc(Zn), copper(Cu), and manganese(Mn). Cu/Zn-SODs are predominant in eukaryotes and can be found in almost all human tissues[27,29,30].

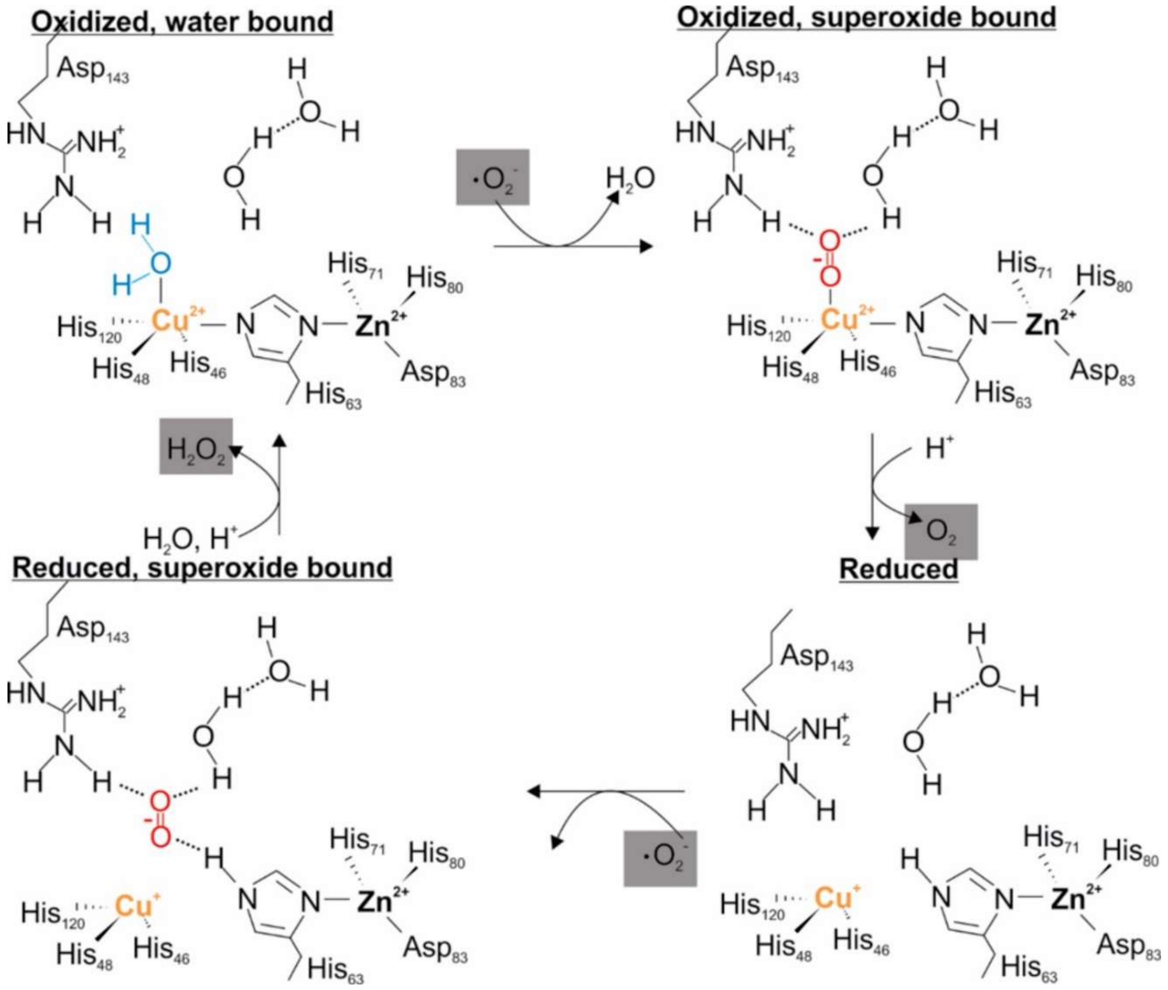

Figure 1.2. Mechanism of Human Superoxide Dismutase 1.

The widespread distribution of the SOD enzymes and the importance of keeping ROS at optimal levels underlies why a lack of SOD is observed in many pathologies occurring in both humans and animals[26,29]. In addition, the natural levels of SOD decrease with age, and free radical formation increases, which contributes to the aging process[27]. SOD has also been shown to exhibit protective effects against irradiation, carcinogenesis, and apoptosis[29,31]. Therefore, a large body of research dating back to the 1980's focuses on administering SOD as a supportive therapy, precautionary measure, or anti-aging supplement[27,29]. However, this research was greatly slowed in 1991 when bovine SOD was removed from the market. Thanks to advances in recombinant protein production technologies, recombinant SOD can be expressed and purified from bacterial cells.

Human Cu/Zn SOD1 is a homodimer, localized mainly in intracellular cytoplasmic spaces, that has been linked to Familial Amyotrophic Lateral Sclerosis (FALS)[32]. ALS is a disease caused by progressive motor neuron degeneration that is characterized by stiff muscles, weakness, twitching, and eventual death. FALS cases are caused by different point mutations in the SOD1 gene which produces aggregation-prone SOD proteins[32]. Studies have shown that the progression of ALS is not due to a loss of SOD action, but a gain of toxic function[28]. Therefore, any strides made in delivering SOD enzymes is not beneficial for treatment of FALS. Instead, understanding the underlying aggregation mechanisms of the mutant SODs is vital for developing therapeutics to prevent or treat this devastating disease. However, the production of the familial ALS mutants is complicated by their aggregation-prone nature.

In this dissertation, a mutant of human superoxide dismutase 1 is expressed in E. Coli and purified from the soluble fraction of the cell lysate in Chapter 5. Protein isolation from inclusion bodies is sometimes necessary for aggregation-prone enzymes that cannot be purified from the soluble fraction of the cell lysate. However, purification from the soluble fraction is preferable to isolation from inclusion bodies because it involves less disruption of protein structure. The steps taken to optimize the procedure can be generalized to other mutants of SOD, which all aggregate differently, but also for other aggregation prone proteins as well. The production of SOD can be used for future structure studies or for incorporation into materials.

1.5. Enzymatically Active Polymer-Based Materials

Polymers are molecules that are made from many repeated units. Natural biopolymers such as collagen, hemoglobin, peptides, and DNA play essential roles in organisms. Plastics such as styrene and silicone are examples of commonly used synthetic polymers. Synthetic polymers are attractive materials because they can be made with many tunable properties to fit different needs[33]. Using synthetic polymers for biomedical therapeutics has been a topic of interest since the 1940's, but it wasn't until 1970 that the first report of polymers stabilizing proteins was published[34–36]. In the early years, polymers were studied as plasma expanders, wound dressing materials, and antiseptics; in the 1960's synthetic polymer-based drugs began to emerge[37].

Polyethylene glycol (PEG) is a common polymer choice for biomedical applications because it has low immunogenicity, toxicity, and cost. First isolated in 1859, PEGs are synthetic uncharged hydrophilic polymers made of repeating ethylene glycol units joined by an ether linkage[38]. Polymer chains of PEG can be synthesized as either linear or branched and can be prepared in a variety of sizes with different functional end groups. The FDA has approved PEG for use in pharmaceuticals and is used in a variety of products including laxatives, lubricants, skin creams, and toothpastes. PEG is an especially unique polymer because it is soluble in both hydrophobic and hydrophilic solvents and can be used to increase the solubility of a drug.

Attaching PEGs covalently to a protein, aptamer, or drug is termed "PEGylation" and has been shown to increase the circulation time and stability of drugs[34,37,39]. The first PEGylated therapeutic on the market, Adagen, was approved in 1990 to treat severe combined immunodeficiency disease. Adagen is a bioengineered form of an enzyme called adenosine deaminase which has PEG covalently attached on the protein using native lysine residues. By PEGylating the adenosine deaminase, the enzyme can be injected into a patient to replace the missing native enzymes. Since the release of Adagen, many other PEGylated pharmaceuticals have been approved for market use.

Over the years, advances in polymer synthesis methods and recombinant protein production techniques have allowed for the development of many diverse enzymatically active protein-polymer hybrids[37]. Polymer synthesis has grown to include the development of co-block polymers and 'smart' polymers that are responsive to changes in the solution. These 'smart' polymers change shape depending on temperature or pH and thus, can tune hybrid functions in response to stimuli. Meanwhile, advances in recombinant protein production has allowed for site-specific point mutations which make controlled site-specific conjugation possible.

Prior to the technological advances necessary for producing an enzyme with engineered attachment sites, attachment methods were limited to native amino acids. Lysine and cysteine residues are typical targets for conjugation sites because their side chains include reactive groups[40]. Non-specific attachment can be done by adding an active group to the end of the polymer to react with the lysine or cysteine residues that are native to the protein. This method of attachment is effective, but difficult to control and typically results in a heterogeneous product, which is not ideal for bio-medical applications. Drugs such as Adagen which were made using non-mutated enzymes and non-specific attachment are being replaced by drugs using new technologies.

Still, the biopharmaceutical properties of a designed enzymatically-active material cannot be easily anticipated[39]. The accurate prediction of the final properties of a material is dependent on many factors including weight, shape, charge modification, conjugation chemistry, and protein structural changes. To continue the development of enzymatically-active materials, more data is needed to improve the modelling that provides a basis for rational design. Thus, a more fundamental understanding of the factors underlying the material properties and enzyme behavior within is required.

Although PEGylation is known to increase the stability and circulation time of the attached protein or molecule, it typically decreases the activity of an attached enzyme[34,41,42]. This decrease in activity can be a result of factors such as disruptions in structure, surface charge, and steric hinderance[40]. To continue development of protein-polymer conjugates and be able to tune enzyme activity, the underlying cause of activity loss must be investigated. T4L is a common choice for studying the effects of polymer conjugation and has been conjugated to PEG as well as other polymers in a variety of different ways.

Although T4L has been widely used for polymer conjugation, there is limited information on the comparison of changes in structure and dynamics that happen with site-specific conjugation to PEG based on location. The well-characterized structure-function relationship of T4L is useful in connecting the activity changes to the structure changes of the enzyme upon covalent polymer attachment. The activity changes of T4L conjugated site-specifically with 1.9K and 5K PEG are observed in Chapter 4 of this dissertation and the underlying reasonings discussed. By understanding the changes in enzyme structure, protein polymer hybrids can be rationally designed to maximize stability while still entirely retaining or enhancing enzyme activity. This knowledge will aid in the creation of hybrids to fit criteria needed for applications as drugs, as well as in other areas such as biomaterials or biocatalysis.

1.6. Enzymatically Active Carbonaceous Materials

As mentioned earlier, to achieve the full potential of enzymes in manufacturing and industry, the proteins need to be stabilized in harsh conditions, as well as recaptured for reuse and recycling. Immobilizing enzymes on solid supports adds stability, but is also a way to reuse the enzyme[7,43,44]. However, the immobilization can cause a decrease in protein activity for reasons including restricted access to the active site, steric crowding, restricted enzyme dynamics, and changes in structure[9,45]. In some cases, carefully designed immobilization may enhance the activity properties of the enzyme, specifically if an enzyme on a support can be locked into a more active conformation[7,9,13].

The earliest report of immobilizing enzymes on a solid support was in 1916 when it was noticed that invertase could adsorb onto charcoal (a carbonaceous material), and in 1960, enzyme immobilization was commercialized[14,46]. Since then, many different immobilization platforms have been developed including metallic nanoparticles, porous materials, and silicon-based materials[4]. However, carbonaceous solid supports including graphene, graphene oxide, graphite, and carbon nanotubes remain attractive for applications in sensor chips, micro assays, and microreactors due to their conductivity, strength, biocompatibility, and solubility[4,44,46]. Carbon-based sensors have been utilized in glucose monitors because they provide a higher sensitivity and lower detection limit as compared to previous sensors[47,48].

The early days of enzyme immobilization relied on adsorption using surface charges to make reversible non-covalent interactions such as hydrogen bonding, hydrophobic interactions, and electrostatic interactions[7,49,50]. Non-covalent interactions have the advantage of not requiring protein alterations, but are less stable and controllable than covalent interactions. The solid support can provide some stability in harsh environments; however, the harsher the environment, the more likely that the non-covalent interactions will be disrupted, and the protein will leach off. There is also little control over the amount and orientation of enzyme on the support, which makes it difficult to tune the protein function on the material[8]. Oftentimes, there is low activity due to low loading capacity or steric hinderance.

Nowadays, covalent attachment is often employed to immobilize enzymes on solid supports because it can provide a sturdier product as well as a higher level of control[51]. Controlling enzyme orientation and structure on the support is vital for tuning enzyme activity as well as producing more robust materials for use in drug delivery and catalysis. Advances in protein engineering have allowed for selective covalent attachment to solid supports through the same strategies employed for the polymer conjugation discussed above. However, another approach to prevent enzyme leaching from the solid supports is to combine multiple materials.

Carbonaceous supports have been successfully combined with a variety of different materials including mesoporous silica, metal nanoparticles, polymers and several different Metal Organic Frameworks (MOFs), typically Zeolitic Imidazolate Framework(ZIF)[47,52,53]. Many of these combinations do not involve enzymes and are useful for the manufacture of nanowires, catalysts, sensors, and materials with improved capacitance[54–57]. Layering other materials on graphene is especially popular because graphene is highly conjugated which allows for delocalized electrons that can participate in or stabilize other reactions and bonds[58]. These de-localized electrons contribute to the superior conductivity of graphene which allows it to act as a wire with rapid electron transfer between an electrode and the redox center of a protein; these properties are why graphene-based biosensors have high sensitivities and low detection limits[47,48,59]. Graphene and carbon nanotubes can be easily altered to include surface functional groups that can further facilitate covalent and non-covalent bonding.

Carbonaceous materials are especially interesting for combination with lysozyme because graphene-based nanomaterials have been shown to be biocompatible and have antibacterial properties[60]. Studies of lysozyme on carbonaceous materials have observed dramatically different bio-effects of the hybrid materials which might be explained by enzyme conformational changes[61,62]. Tuning the bio-effects of hybrid materials and preventing enzyme leaching is vital for the further expansion of these materials into applications for drug delivery and biocatalysts. Adsorbing enzymes to a graphene-based surface and then growing MOFs on top is a promising solution that can create an enzymatically active material that is biocompatible and robust[63–65]. An understanding of the orientation and structure of enzymes within a carbonaceous-enzyme-MOF combined material can give clues for combinations that can tune and enhance the activity of the enzyme.

In this dissertation, the combination of graphite oxide with two different Metal-Organic Frameworks (MOFs) and T4L is explored in Chapter 3. Graphite oxide (GO) was chosen for its low toxicity under physiological systems, large surface area (two sides), and water solubility. T4L can readily adsorb to the GO surface by electrostatic interactions between the protein and the functional groups on the GO surface without any modification to the protein. However, for the purpose of this study, T4L is modified to have a label that allows for investigation of the orientation within the material. The addition of MOF is done through co-precipitation and does not specifically require interaction with the protein. The information gathered from this study can be generalized for use in designing other immobilization platforms.

1.7. Enzymatically Active Metal-Organic Framework Materials

Metal-Organic-Frameworks (MOFs) are cage-like porous materials made from metal ions and organic linker molecules. The metal ion forms a node and the coordination number of the metal determines the possible molecular geometry[14,66]. The organic linkers act as spacers and connect the metal ions to form an open multidimensional lattice. By changing the metal or linker the final properties and architecture of the MOF can be tuned for a variety of functions. The term MOF was coined in 1995, and the crystalline structure of MOF-5 was published in 1999[14]. Since then, MOFs have been made for use in biosensors, catalysts, and importantly, as enzyme immobilization platforms[57,66–68].

Incorporating proteins into MOFs can be done via surface adsorption, covalent attachment or through encapsulation by co-precipitation and diffusion[67,69]. Encapsulation is especially attractive because it is more robust than simple adsorption, but also can be done in mild solution without any modification to the enzyme. It has been shown that enzymes encapsulated in the MOF pores retain activity and are shielded from unfolding[70]. Some enzymes can be encapsulated by diffusion into the open pores of pre-made MOFs, but co-precipitation allows for encapsulation in MOFs with small pore sizes without the enzyme unfolding[14]. Co-precipitation involves adding the metal ions, linkers, and enzymes in solution and allowing the crystals to form with the enzymes caught in the MOF defects. This technique is popular because it can be done in one-pot and mild conditions which allows for simplicity[66].

Many enzymes have been successfully incorporated into MOFs including lysozyme, cytochrome c, and trypsin[14]. It has been hypothesized that the properties and orientation of the enzyme within complexes can be tuned by adjusting the metal and ligand used. The high tunability and diverse synthesis methods have made MOFs prime candidates for use in catalytic multi-enzyme complexes[2,43]. Desirable characteristics for a protein immobilization platform are mild synthetic conditions, biocompatibility, stability, and tunability, which are characteristics of some MOFs. However, the properties of the MOF depend greatly on the metal and linker used. For example, magnetic metals can be used to enhance capacitance and provide for easy separation[71,72]. Two popular metals for use in MOFs are zinc and calcium because of their availability and biocompatibility[63,73].

Zeolitic Imidazolate Frameworks (ZIF) are a popular class of MOF that are made from zinc and imidazolate derivatives. ZIFs are attractive because they are highly stable in water, can be made through co-precipitation, have high porosity, and high thermal stability[74]. Since zinc is a common biological metal, it is generally considered safe and biocompatible, which opens possibilities for drug delivery. Furthermore, the imidazolate linker may interact with any surface accessible histidine residues to cause a preferential orientation within the material. It has been shown that enzymes can be encapsulated within the ZIF scaffolds as well as in defects on the crystal surface while retaining activity and being shielded from unfolding[63,70]. However, ZIF disassembles quickly at low pH, which makes it a candidate for pH sensitive release, but not for stabilization in acidic media.

Calcium-based MOFS are good candidates for drug delivery studies because they are stable in water and non-toxic[75]. Combining calcium and terephthalic acid (Ca-BDC) is especially promising because BDC is non-toxic at low levels[73]. However, the variability and lack of structural control of Ca-BDC MOFs is a barrier for tuning the material[73,76]. Ca-BDC confinement and release has been demonstrated with curcumin, a small molecule with anti-oxidant properties[73]. Unlike ZIF, Ca-BDC is stable in acidic media, but disassembles in phosphate buffer, which allows for selective release in different conditions. To further design calcium-based MOFs for enzyme encapsulation, the structure of the Ca-BDC MOFs and enzyme behavior upon encapsulation must be understood[75].

In this dissertation, the difference in conditional stability and orientation of our model enzyme, T4L, in two different graphite oxide-MOF composites is probed. ZIF and CaBDC were chosen because of their biocompatibility and differing pH stabilities. It was anticipated that the enzyme would orient itself differently in each material. While the high porosity of MOFs allow small substrates to diffuse in and contact the enzyme, large substrates cannot contact the active site of an enzyme buried deep within the MOF lattice. In attempt to confine more of the enzyme to the surface with the active site exposed, graphite oxide was used as a support and the MOF grown on top. The enzyme was altered to allow for the attachment of a label that provides site-specific molecular level information and encapsulated via a one-pot co-precipitation. Understanding the difference in enzyme orientation upon encapsulation with different MOFs provides information necessary for designing MOFs that can selectively tune enzyme orientation and activity.

1.8. Purpose of this Study

Combining enzymes with materials provides advancements in drug delivery, therapeutics, and catalysis that would be otherwise inaccessible due to the limited stability and reusability of enzymes alone. However, the catalytic activity of enzymatically-active materials is often poor when compared with the activity of free enzymes. A fundamental understanding of the structural changes underlying enzyme activity alteration upon incorporation in materials will provide the basis for rational design and future development of enzymatically-active hybrid materials. The aim of this work is to increase understanding of enzyme behavior within different materials so that enzyme structure and function can be tuned in future endeavors. To that end, a unique approach which can be used regardless of the background matrices of the system to reveal the underlying structural rationale for enzyme behavior is introduced in Chapter 2, namely, Electron Spin Paramagnetic Resonance Spectroscopy (EPR). Then, the behavior of a model enzyme, T4 Lysozyme, upon non-covalent incorporation into a GO-MOF composite (Chapter 3) and covalent site-specific PEGylation (Chapter 4) is explored. In addition, the systematic production of an aggregation-prone model dimeric enzyme, human Cu/Zn SOD1, is presented for future incorporation into materials (Chapter 5), which has set the basis of our further investigation of dimeric enzymes upon combination with synthetic materials. The findings herein can provide general insights into other systems and aid in the rational design and tuning of hybrid materials and protein production.

2. ELECTRON PARAMAGNETIC RESONANCE SPECTROSCOPY FOR THE STUDY OF ENZYME STRUCTURAL INTERACTION WITH MATERIALS

2.1. Overview

Enzyme function is directly related to structure and conformational dynamics. Therefore, an understanding of enzyme structure and dynamics is required for designing enzymatically-active materials with desired activity. Continuous Wave Electron Paramagnetic Resonance Spectroscopy (CW EPR) in combination with site-directed spin labelling (SDSL) can be applied to studying protein structure and dynamics in complex environments regardless of the background matrices, which makes SDSL-EPR a desirable approach for understanding complex/hybrid systems[40,77–83] . This chapter will outline the importance of enzyme structure and dynamics, as well as, the theory behind CW EPR spectroscopy and how it can probe enzyme structure and dynamics upon interaction with materials.

2.2. Enzyme Structure-Function Relationship

Enzymes are proteins that catalyze reactions with efficiency and specificity that cannot be easily replicated artificially at this time. Because the catalytic power of an enzyme is unrivaled by any synthetic catalyst and enzymes are environmentally friendly, it is desirable to utilize enzymes whenever possible[4–7]. However, the utilization of enzymes has been limited by the protein's stability and reusability (and correspondingly, cost). The impressive speed and selectivity of an enzyme is directly dependent on its structure and conformational dynamics. Therefore, stability, efficiency, and selectivity can be adjusted by altering the protein structure/dynamics.

Enzymes have 4 layers of structure that build upon each other to form the catalytic machinery. The primary structure of an enzyme is the sequence of amino acids that comprise its polypeptide chain(s). The polypeptide chain(s) then fold to produce a variety of secondary structure features including helices, barrels, turns, and loops. The tertiary structure refers to the overall three-dimensional structure and arrangement of the secondary features. In proteins that are comprised of more than one polypeptide chain, the quaternary structure defines the arrangement of chains in relation to each other. For the two proteins discussed herein, T4L has one chain and no quaternary structure whereas SOD1 is a homodimer.

The final resultant structure of a protein contains many structural features including helices, barrels, domains, binding sites, and the active site. Although the active site is where catalysis occurs, the structural features work dynamically together to give the enzyme function[84]. Amino acid residues and charges on the outside of the enzyme can guide enzyme locality as well as attract substrates. The structural packing of the internal amino acid residues adds stability and support to align domains in their proper locations while the flexibility of loops connecting domains allows for domain movement. The shape and charge of the substrate binding site/pocket restricts what substrate can enter the active site and bestows selectivity upon the enzyme.

Enzyme structure is held together by a range of different inter- and intra-molecular interactions such as peptide bonds, hydrogen bonds, electrostatic interactions, hydrophobic interactions, and disulfide bonds[4,49,85]. These forces come together to form a specifically molded scaffolding that supports the active site while retaining the dynamic flexibility necessary for catalysis to proceed[14,49]. Harsh conditions, such as those often used industrially, can denature enzymes and destroy function by disrupting the molecular forces that hold the structure together. Preserving the intricate network of interactions and bonds and thus, protein structure and dynamics, is vital for increasing enzyme stability and retaining activity in denaturing conditions[49,85].Two popular approaches to preserve enzyme structure in harsh conditions is to use protein engineering and/or synthetic materials.

Protein engineering refers to the selective modification of proteins to have desired characteristics. Advances in recombinant DNA technology and microbial protein production have provided the necessary tools to produce novel enzymes with new or improved properties[1,7,13]. The engineering is often done using site-directed mutagenesis on the DNA to add, subtract, or swap out amino acids in the primary structure. The recombinant enzyme can then be expressed microbially and purified. The structure of an enzyme can be strengthened by adding amino acids in strategic positions to create new disulfide bonds and hydrogen bonds[7]. Residues can also be added, subtracted, or swapped out to increase or decrease hydrophobic packing and other structural features[3,7,13,86]. Enzyme structure can also be adjusted by incorporating materials either non-covalently or covalently through engineering[3,7,43,87,88].

Another approach to stabilize enzymes for use in harsh conditions is to combine them with synthetic materials. Studies have shown that hybrid materials can accomplish increased structural stability as well as imparting protection from enzymatic degradation in biological systems, enhanced capture for reuse, and in certain cases, increased activity[14,46,85,88]. Unfortunately, upon incorporation into a material, an enzyme typically displays reduced activity. Activity is dependent on many factors, including protein surface charge, active site accessibility, and notably, the protein's structure and dynamics[13,14,49,89,90]. Therefore, activity alteration is not surprising because resisting structural changes in order to prevent denaturation imparts stability, but activity is largely dependent on active site access and structural fluctuations that help substrate/cofactor recognition and binding. However, interactions between enzyme and material can be used to tune protein function within materials by locking enzymes in a more active conformation or selectively gating the access site[49].

Retaining or enhancing enzyme activity within materials has potential to advance many different fields such as drug delivery, materials science, biosensors, therapeutics, and biocatalysis[13,43,44]. Despite the vast research efforts into enzymatically-active materials, exploiting the enzyme workforce for commercial use remains a challenging issue. Because of the delicate interplay of factors underlying protein structure and dynamics, even a carefully designed material can have unforeseen consequences in enzyme activity and properties[49]. To successfully tune enzyme function in hybrid materials, a strong understanding of molecular level interactions is necessary. However, the structural basis of enzyme interactions with materials can be difficult to probe due to the enzyme signals being overlapped and/or interfered by material signals. Still, there are techniques that can be used to gather information necessary to tune enzyme function in materials. A key technique used herein is Electron Paramagnetic Resonance spectroscopy.

2.3. Introduction to Electron Paramagnetic Resonance Spectroscopy

Electron Paramagnetic Resonance (EPR) Spectroscopy is a technique for studying samples with unpaired electrons. This method can be used to gather information on a variety of intrinsically paramagnetic samples such as metal complexes as well as monitoring radical generating reactions. Generally, biological samples are EPR silent because they do not naturally contain unpaired electrons. Using site-directed mutagenesis, paramagnetic spin labels can be attached site-specifically to proteins[77]. The EPR signal of the labeled proteins depends solely on the motion of the label, which makes it especially useful in complex heterogeneous samples, such as enzymatically active materials, where a high background noise would be expected using other techniques. This section will focus on the application of continuous wave (CW) EPR to the study of protein structure and dynamics utilizing site-directed mutagenesis to incorporate a paramagnetic label into the normally EPR silent proteins and the applications for studying enzymatically active materials.

2.3.1. Continuous Wave Electron Paramagnetic Signal Origins

In spectroscopy, the absorption, emission, or scattering of electromagnetic radiation upon interaction with matter is measured to glean information from and about the atomic or molecular states of the sample. Continuous Wave (CW) EPR is an absorption spectroscopy technique that utilizes microwave radiation (~GHz frequencies) to induce a transition between quantum mechanical energy levels of an unpaired electron in an applied external magnetic field. The energy transition of the electron is affected by the electron's surroundings, and therefore, can provide molecular level local information. Unlike other popular techniques, in CW EPR, the frequency of radiation is held constant, and the absorption of the transition is monitored as a function of an external magnetic field.

The origin of the EPR adsorption spectra relates back to the magnetic properties of electrons and Zeeman splitting. Electrons intrinsically have a negative charge and an angular momentum called 'spin' which gives rise to a magnetic moment (μ). Due to these properties, electrons have magnetic dipoles and can be thought of as tiny bar magnets. The spin of an electron can be parameterized by its spin quantum number (m_s) of ±1/2. Naturally, the spins of the electrons are randomly oriented in all directions. However, when placed in a magnetic field, the magnetic moment of the electron will orient either parallel (-1/2), or antiparallel (+1/2) to the magnetic field, just as a bar magnet would. As shown in Figure 2.1, the alignment of spin in relation to the field produces 2 energy levels, which is the Zeeman splitting.

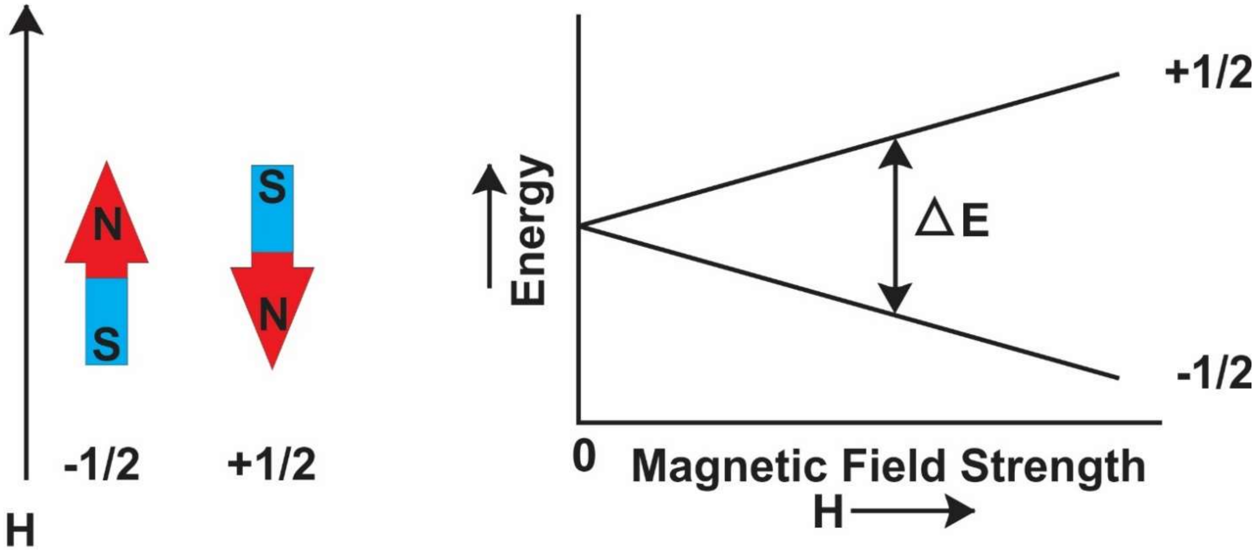

Figure 2.1. Zeeman Splitting. Allowed energy states of the electron's magnetic moment with respect to the applied external magnetic field(H).

The magnetic moment (μ) of an electron can be described mathematically as:

$$\mu = m_s g_e \beta B_0 \tag{2.1}$$

Wherein, m_s is the electron quantum spin number, g_e is the g-factor of a free electron, β is the Bohr magneton conversion constant, and B_0 represents the applied magnetic field. Therefore, the difference between the two energy states (ΔE) of a free electron in a constant applied external field B_0 is:

$$\Delta E = g_e \beta B_0 \tag{2.2}$$

To relate the change in energy states of the electron described in equation 2.2, we can make use of Plank's law, which states:

$$\Delta E = h\nu \tag{2.3}$$

With h being plank's constant and ν being the frequency of radiation. Combing equations 2.2 and 2.3 gives us an equation 2.4 which describes the central resonance condition of EPR.

$$h\nu = g_e \beta B_0 \tag{2.4}$$

As mentioned earlier, in CW EPR, the frequency of the radiation is held constant, and the magnetic field is swept. When the magnetic field strength satisfies the parameters of the resonance condition equation (2.4), absorption is observed. This equation also shows that the energy levels are dependent on the applied field such that when there is no field, $B_0 = 0$, there will be no energy transition.

In theory, the absorption spectra could be attained by applying a fixed external magnetic field and varying the frequency. However, due to the relatively small energy gap that is being probed, a resonance cavity is used to create standing waves of radiation that can induce the energy transition. A resonator is a fixed piece of equipment and must be tuned to a specific frequency, so it is more practical to fix the frequency and modulate the magnetic field. Furthermore, the difference in spin states of the electrons is small, and therefore, the net absorption is small. To enhance the signal, the external field is modulated with a secondary field. Therefore, the first derivative of the absorption spectrum is detected and recorded. A sample spectrum of a free unpaired electron and its first derivative is presented in Figure 2.2.

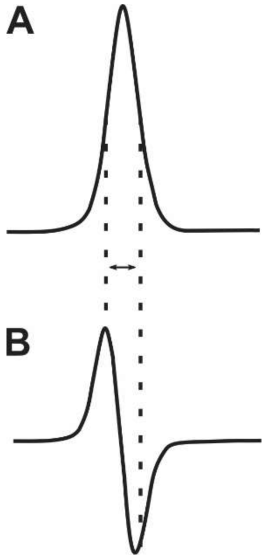

Figure 2.2. Absorption lineshape (A) and the first derivative (B).

2.3.2. Electron Paramagnetic Resonance Spin Labeling

For a single unpaired free electron, a sharp transition between Zeeman levels as shown in Figure 2.2, would be expected. However, in real paramagnetic samples where the unpaired electron is delocalized in certain molecular orbitals, the net absorbance spectrum is further split by spin-orbit coupling and hyperfine interactions. In the case of proteins, which are generally EPR silent due to a lack of unpaired electrons, a paramagnetic sensor must be introduced into the system. This sensor should be attached site-specifically and be sensitive to changes in the environment. A spin label is a molecule that contains a stable free radical and can be attached to a protein to serve as a paramagnetic sensor.

Nitroxide derivatives are popular choices for spin labels wherein the unpaired electron resides in the 2p orbital of the nitrogen[81,91]. To protect the radical from disproportionation reactions and limit the flexibility, the nitroxide group is often incorporated into a 5 or 6 membered ring with a quaternary carbon. The resulting spin label radicals are stable at temperatures up to 80 °C and in a pH range from 3-10, which makes them well-suited for protein studies. To attach the spin label to a protein, the label generally contains a "positioning group" which can guide and attach the label to the desired site. Methane thiosulfonate or hydroxysuccinimide groups can react with thiols, which make them desirable groups for attaching at cysteine residues. Some labels use functional groups that can attach to solvent-accessible lysine residues. Figure 2.3 shows example EPR spin labels with attachment groups highlighted. The spin label used herein (and also the most popular spin label for proteins), R1, is denoted with a black box[77–79,81,84,91].

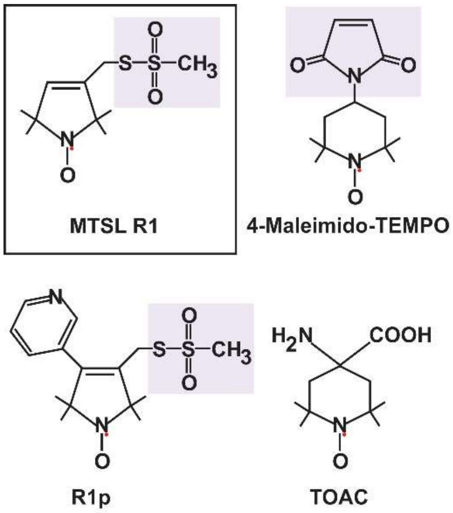

Figure 2.3. Common spin labels. Positioning groups are highlighted. R1 is outlined using a black box.

Previously, the main limitation of spin labelling proteins was the natural abundance of cysteine and lysine residues, and thus, a lack of selection in labelling site[77]. However, the advances in DNA technology, genetic engineering, and microbial production has allowed for the birth of site-selective labelling via site-directed mutagenesis. Site-Directed Spin Labeling (SDSL) is a technique pioneered by Dr. Wayne Hubbell wherein a native residue is mutated to a cysteine residue and reacted with a spin label[77,79,80,92]. While both cysteine and lysine residues are popular choices for attaching moieties to proteins, cysteine is especially useful because of its low natural abundance. Oftentimes, native cysteines are involved in disulfide bridges or are not solvent accessible, so they are ineligible for label attachment. However, any native cysteine residues that can compete for labelling must be mutated to a nonreactive group (ca. a serine or alanine) to ensure that the label is attached to only one residue.

The resulting CW EPR spectra of the spin labeled protein will depend on the identity, location, and motion of the label. Herein, the paramagnetic properties of the nitroxide spin label R1, highlighted in a black box in Figure 2.3 above, are utilized to gather structural information on spin-labeled T4 Lysozyme. The signal of the R1 label is anisotropic, and thus, can impart motion dependent information on protein structure and dynamics. The theoretical basis of the CW EPR signal lineshape of free R1 in solution is introduced below.

2.3.3. Spin-Orbital Coupling and Hyperfine Splitting of R1

The spectrum of an electron in a spin label differs from that of a free electron due to its interaction with the atomic/molecular orbitals as well as the nuclear spins, or, in other words, the spin-orbital coupling and hyperfine splitting which cause a spectral shift in g-value and magnetic field, respectively. The ability of R1 to confer structural information stems from the spin-orbital coupling which causes a g-shift that is orientation dependent. As mentioned earlier, an electron can be thought of as a tiny bar magnet because its charge and angular momentum produce a magnetic moment. This magnetic moment can be described mathematically using equation 2.1.

The g-factor is a dimensionless proportionality constant that can relate the magnetic moment of a particle to its angular momentum quantum number. For a free electron, the value of g_e is known to be 2.0023, but when the electron is placed in an orbital, the spin of the electron becomes coupled to the orbital angular momentum, thus changing the total angular momentum. The magnitude of the g-shift from spin-orbital coupling will depend on the degree of restriction that the electron experiences. Since g_e describes a completely unrestricted electron, as the degree of restriction increases, so too does the deviation from g_e.

The electron in R1 is in the axially symmetric 2p orbital of the nitrogen, and as such, is not uniformly restricted like it would be in a spherically symmetric s-orbital. Therefore, the molecule has different g values for each orientation with respect to the applied magnetic field. For nitroxide radicals, the g-values have been found to be gxx=2.0089, gyy=2.0061, and gzz=2.0027, with the axis system as shown in Figure 2.4[81,91]. The g-factor anisotropy is not visible in the spectrum of R1 that is tumbling freely in solution due to motional averaging, but it will allow the label to confer structural information when attached to a protein, which will be discussed in section 2.2.4.

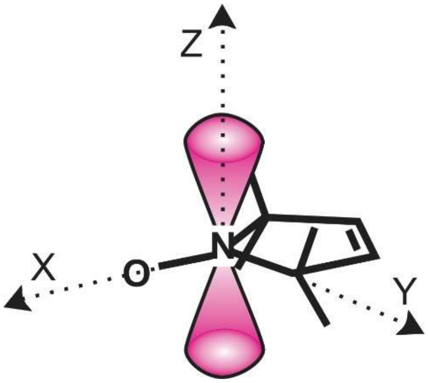

Figure 2.4. Principal axis system for R1.

In addition to the g-shift that occurs from the spin-orbital coupling, the magnetic field felt by the electron is affected by the local magnetic fields. An electron in an orbital is basically a circulating current, which gives the orbital its own magnetic moment. The magnetic moments from the electron spin and orbital angular momentum interact as two tiny bar magnets would to change the net magnetic field experienced by the electron. The local orbital magnetic moment can either oppose the applied field to give a lesser effective field or it can align with the field to give a stronger effective field. This effect is analogous to 'shielding' in NMR. However, in the case of R1, broadening from the orbital magnetic field is small when compared to the hyperfine splitting interactions discussed below[81,91].

Hyperfine splitting is a result of interactions between the electron magnetic moment and nearby nuclear magnetic moments. Just as an electron and orbital can be thought of as tiny bar magnets due to angular momentum and charge, so too can a nucleus be imagined as a tiny bar magnet. Similar to normal-sized bar magnets, the magnetic moment of the electron can be influenced by the magnetic moments of nearby nuclei and the degree of interaction will depend on the proximity. In the R1 label, the electron generally resides near the N-O bond, and therefore, the nitrogen and oxygen atoms would be expected to contribute the most to the hyperfine splitting pattern[81,91].

The local magnetic fields given off by the nucleus and the orbital can align with or against the applied magnetic field to change the magnetic field that the electron experiences. This is mathematically described in equation 2.5, with H representing magnetic field strength.

$$H_{effective} = H_{applied} + H_{orbital} + H_{hyperfine} \tag{2.5}$$

As we know from the core EPR resonance equation, 2.4, when the magnetic field (B_0) satisfies the equation, absorption is observed. However, the applied magnetic field necessary to induce the transition will depend on the net effective field. Therefore, some electrons will require a smaller (or larger) applied field to induce the transition. However, the effect of the local magnetic fields is directly dependent on the magnitude and orientation of each with respect to the applied magnetic field. While electrons and nuclei typically align themselves based on spin quantum number with the field, orbitals do not. This will cause fluctuations in the $H_{effective}$ as R1 moves through solution.

^{14}N, which is naturally abundant and assumed to be the predominant isotope in R1, has a nuclear spin value of 1 and corresponding spin states of (m_I) -1,0, and +1. The 3 nuclear spin states describe the orientation of the nuclear magnetic moment in respect to the applied magnetic field. Therefore, the 3 nuclear bar magnets can strengthen, weaken, or not change the applied magnetic field. Each of these 3 options interact with the 2 different Zeeman levels of the electron to give 6 total energy states. Out of these 6 states, only 3 of the energy transitions are observed due to EPR selection rules. Therefore, the characteristic spectra of free R1 in solution has 3 peaks as shown in Figure 2.5. The magnitude of the splitting is around 15 G, which is clearly distinguishable on spectra.

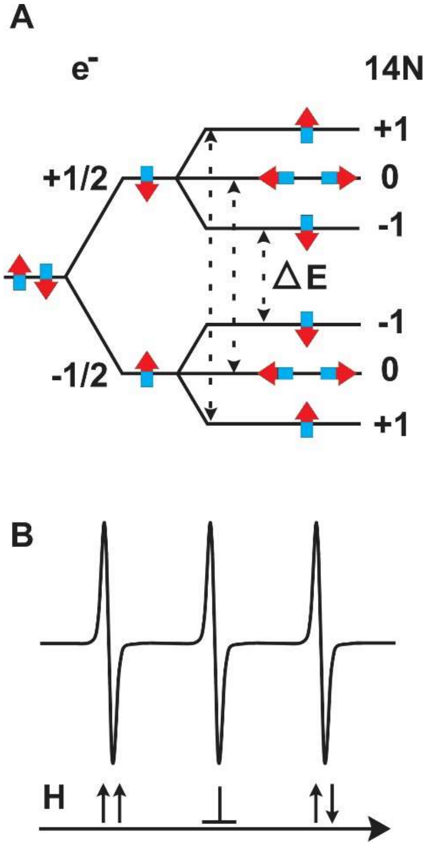

Figure 2.5. Hyperfine interactions of R1. A) Energy level splitting pattern. The allowed energy transitions are marked with dotted lines. The orientation of the electron spin and nuclear spins are represented on the energy levels as bar magnet arrows. B) CW EPR spectrum of free R1 in solution. The orientation of the spins from the electron and nucleus with respect to each other are shown under each peak.

Because the electron is somewhat delocalized, it may have additional hyperfine splitting with adjacent non-zero nuclear spins. The magnitude of splitting depends on the abundance of the interaction and the distance of the interaction, just as the distance affects field interactions of bar magnets. Because the electron is generally nearest the nitrogen nucleus, the splitting from the nitrogen dominates the spectra. There is no splitting contributed by the naturally abundant ^{16}O because its nuclear spin value is 0. The low natural abundance ^{13}C and high abundance ^{1}H both have nuclear spin values of ±½. These additional splittings are roughly 1 G in magnitude and as such, simply appear as a slight broadening of the EPR lines.

Spin-orbital coupling and hyperfine interactions give rise to the characteristic 3-line spectra of free R1 in solution. However, it is signal anisotropy that is useful for probing protein structure and dynamics. When R1 is attached to a protein, the signal will broaden based on the net motion of the R1 at that particular attachment site. The 3 main motions that appear in the spectra are the protein tumbling, backbone dynamics, and R1 intrinsic motion. Combined with site-directed spin labelling, information from the R1 site-specific motion can impart valuable insight on protein structure and dynamics. The origin and uses of R1 spectral broadening due to protein structure and dynamics is discussed below.

2.3.4. Spectrum Changes of R1 in Solution upon Attachment to Proteins

When probing proteins, it is the orientation-dependent site-specific broadening that makes a CW EPR signal useful for reporting information on a molecular level. Upon attachment to a protein, the signal of the R1 spin label will predictably broaden. The spectra broadening relates back to anisotropy averaging and spin relaxation which will be discussed below. The 3 main motions that are visible in the R1-protein spectra are the rotational tumbling, intrinsic R1 motion, and protein backbone dynamics.

As discussed earlier, an unpaired electron has two energy states when placed in a magnetic field due (Zeeman splitting). The EPR signal records the absorption of microwave energy that excites an unpaired electron from the lower energy state to the higher energy state. The energy of the two states relate back to the electron spin magnetic moment orienting either with or against the magnetic field. Prior to absorption, there is a greater number of electrons in the lower energy state aligned parallel to the applied magnetic field. For equilibrium at X-band frequency (around 9.8 GHz) and room temperature, the population difference is only around 0.1 % of the total spins[91].

Even though the difference is small, there is still a bulk magnetization parallel to the direction of the magnetic field. When the microwave radiation is applied, the energy levels become equalized and the net magnetization parallel to the field becomes 0 and the net magnetization on the transverse plane becomes 1. The process of the system returning to equilibrium is called relaxation. Relaxation occurs in two ways, spin-lattice relaxation and spin-spin relaxation. *Spin-lattice* relaxation time constant is denoted as T_1 and is the time it takes for the net magnetization to return to approximately 63 % of the original value. *Spin-spin* relaxation time constant is denoted as T_2 and describes the exponential decay of the net magnetization back to equilibrium along the transverse plane.

The net magnetization process can be described using a series of equations (Bloch equations) that take spin relaxation into account. The Bloch equations relate the intensity of absorption as a function of applied magnetic field strength. One of the equations is presented herein as equation 2.6.

$$i(H_{applied}) = \frac{2T_2}{1+{\gamma_e}^2{T_2}^2(H_{applied}-H_{effective})^2} \qquad (2.6)$$

In equation 2.6, γ_e represents the gyromagnetic ratio that relates the angular momentum to the magnetic moment of the electron. H represents the magnitude of the respective magnetic fields as described in equation 2.5. The spin-spin relaxation is presented in the equation as T_2. The equation shows that the spin-spin relaxation rate, fluctuations in $H_{effective}$, and the g-value all determine lineshape.

Many factors can affect the relaxation rate of the system, but the tumbling motion is a primary mechanism for a paramagnetic molecule in solution[81,91]. The tumbling motion of the molecule refers to the 4-dimensional procession through orientations that the molecule spontaneously undergoes in solution. As discussed previously, the spin-orbit coupling and hyperfine interactions alter the magnitude of the applied field necessary to induce the transition due to local field interactions. The local fields provided by the orbital and nearby nucleuses are dependent on their orientation with respect to the applied magnetic field. Therefore, as the molecule tumbles through solution, the local magnetic field will fluctuate, thus altering the relaxation process, and consequently, signal lineshape.

The tumbling process is described by a factor called the correlation time, denoted by τ_c. When the correlation time is smaller than the maximal difference in g-values, motional averaging hides the anisotropy from the spectrum. When the motion is slowed, the individual contributions from each g-value become more prominent in the spectra. In Figure 2.6, the simulated X-band spectra of R1 in solution with different correlation times is presented. As the time increases, the spectrum becomes increasingly broadened until it begins to resemble a powder spectrum.

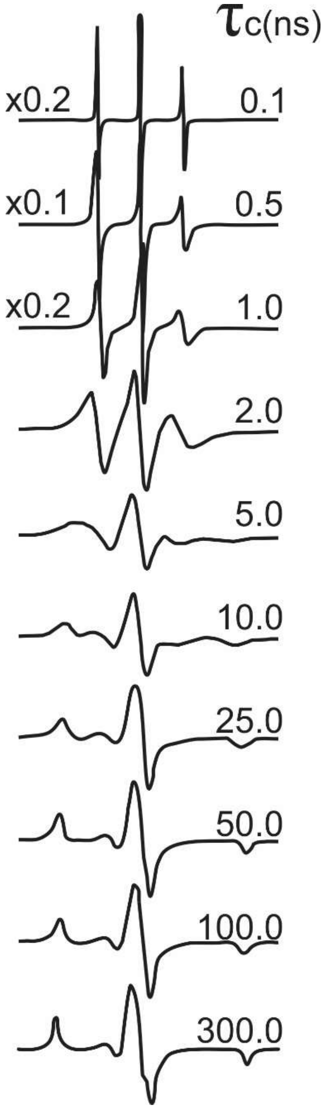

Figure 2.6. Effect of tumbling rate on EPR spectra. Simulated X-band EPR spectra of R1.

The correlation time can be described mathematically using equation 2.7 wherein η represents the solution viscosity, r is the effective radius of the molecule, k is Boltzmann's constant, and T is absolute temperature.

$$\tau_c = \frac{4\pi\eta\ \ ^{3}}{3kT} \qquad (2.7)$$

Equation 2.7 shows reliance on 2 important features: 1) effective radius of the molecule, 2) the viscosity of the solution. A reliance on temperature is also shown, however, for protein studies the temperature variance is not large enough to significantly alter the correlation time[81,91].

The radius of R1, and thus its circumference, is very small, which allows it to process through the possible orientations quickly. It is this fast motion that results in an averaged g-value and sharp spectrum peaks. However, proteins are large molecules and will have a much larger radius than R1. Therefore, it is expected that simply attaching R1 to a macromolecule will result in a longer correlation time, which is observed. The change in tumbling rate will depend on the size of the molecule that the R1 is attached to; larger molecules will have slower tumbling rates.

The tumbling of R1 can be slowed by attachment to a macromolecule but also by changing the viscosity of the solution. In the case of protein study via CW EPR, the solution generally has low viscosity. However, the viscosity of the solution can be changed to purposefully effect the correlation rate. This may be done to simulate crowding or in attempt to separate out the correlation factor from the other features displayed in a spectrum (intrinsic R1 motion and backbone dynamics) which will be explained below.

The intrinsic motion of the R1 label refers to the movement of the label about the attachment bond. The R1 spin label is attached to a protein with a cysteine mutation via the reaction scheme shown in Figure 2.7. The R1 spin label is designed to be a rigid structure to protect and confine the free radical electron. The nitrogen of the nitroxide group is incorporated into a planar 5-member ring, and thus, rotation along the covalent bonds to carbon is restricted. However, there is no restriction along the disulfide bond that is used to attach the label to a protein or other molecule.

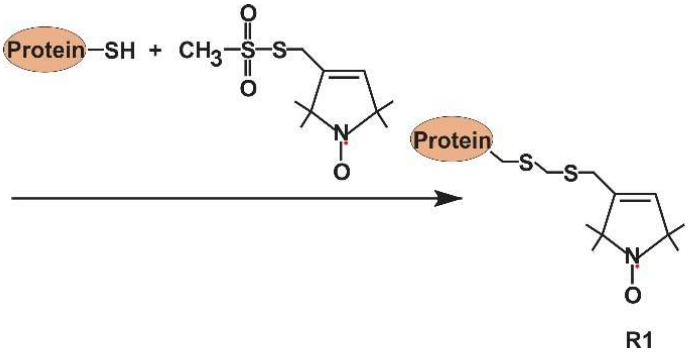

Figure 2.7. Reaction scheme for R1 attachment. Protein not shown to scale.

Therefore, the nitroxide may wobble along a rotational axis about the disulfide bond. Figure 2.8 shows a simplified representation of the intrinsic motion. In this representation, the rotational motion along the ZY plane is largely unrestricted and therefore allows for the averaging of g_{yy} and g_{zz}. The averaging in the g_{xx} direction will largely depend on the rotational tumbling and local backbone dynamics at that site. This intrinsic motion of the nitroxide label will always be present in spectra whether the label is attached to a protein or other solid support molecule.

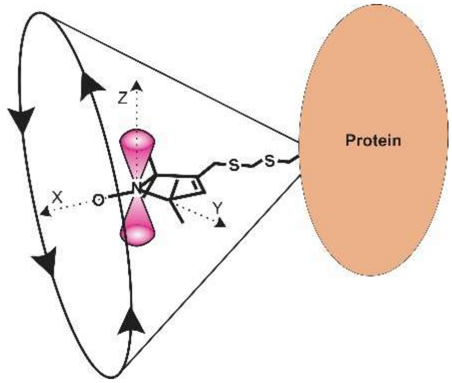

Figure 2.8. Intrinsic spin label motion. Protein is not scaled to size. Rotation is visualized by the cone.

In addition to the protein tumbling and intrinsic R1 motion, the CW EPR spectra are sensitive to changes in local backbone dynamics. The backbone dynamics of a protein at a labeled site will affect the g-value averaging as well as the relaxation process. As discussed above, the label will have restricted g_{xx} averaging when attached to the protein. The rotational tumbling can produce motion in the X direction, but the local backbone dynamics can as well. If the label location is fluctuating in the X direction it can provide averaging that would not be present in a static molecule. If all other factors are held constant, a label at a more mobile location on the same protein would have a sharper peak due to averaging.

In practice, both the anisotropies of the g-tensor and hyperfine tensor (A) will contribute to the resultant spectra. The hyperfine interaction contains both a constant, the Fermi contact, usually ~15 G for a Nitroxide, and an orientation dependent term (due to the magnetic dipolar interaction), so the motion of the spin label on the host protein contributes to the final spectra. In one extreme case, where fast rotational tumbling averages all orientation dependent terms (ca. in the case of a free label, Figure 2.9, left top), only the Fermi contact contributes to the final spectral splitting, which results in three sharp lines. In another extreme case, when all orientations contribute to the final spectra due to high restriction in motion (ca. when a label is in contact with some species or frozen, Figure 2.9, left bottom), the hyperfine tensor (A_{xx}=~5 G, A_{yy}=~5 G, A_{zz}=~35 G) will contribute to the final spectra, resulting in a highly split, wide spectrum (Figure 2.9, right bottom panel). The real experimental data fall in between these two extreme cases and can be analyzed via spectral simulation. Note that, due to the complex motions of the label on the host protein, as well as the protein motions, it is extremely difficult to assign peaks to specific hyperfine or g-splittings at X-band. High frequency EPR may help such peak splitting, which is beyond the scope of this dissertation.

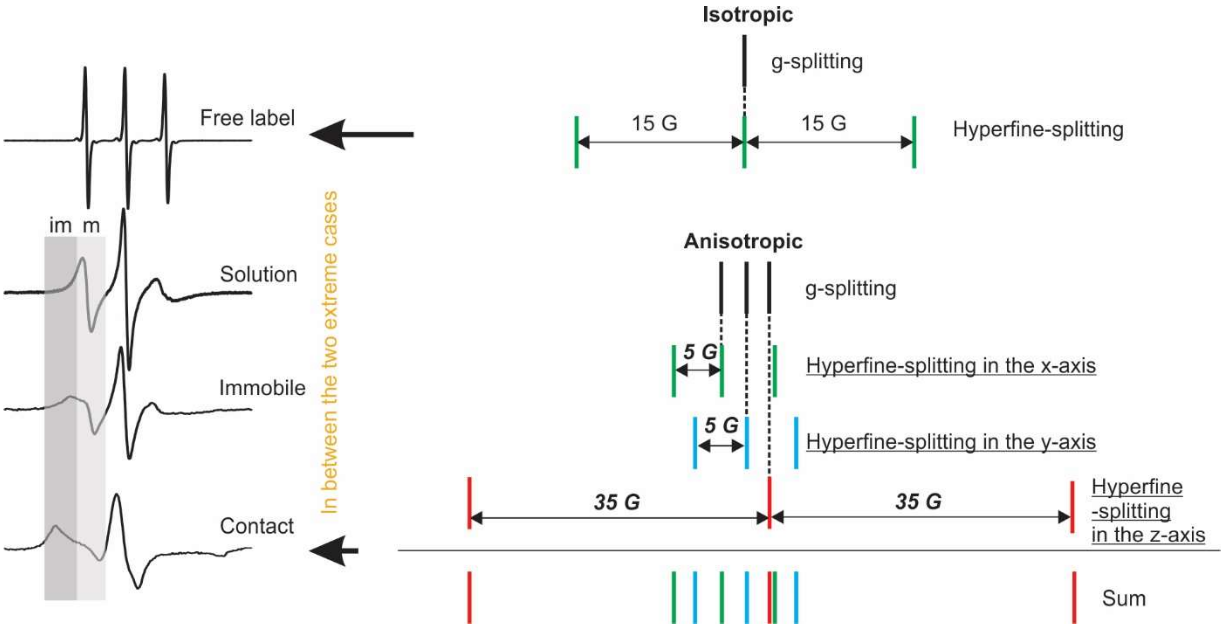

Figure 2.9. Spectral splitting from g-tensor and hyperfine interactions under two extreme conditions (right) and the commonly seen experimental EPR spectra (left). The spectral splitting from each tensor is difficult to resolve at X-band EPR due to overlap.

In conclusion, the main features in the CW EPR spectrum of a protein labeled with R1 are the protein rotational tumbling, intrinsic spin label motion, and the backbone dynamics. Each of these features contribute to the net spectrum obtained. Therefore, CW EPR is not a definite measurement, but rather, a comparative tool. We can gain information by comparing the signals of different label locations along a protein backbone. The application of CW EPR in studying protein structure and dynamics in synthetic materials will be discussed in section 2.3.5 below.

2.3.5. Application of CW EPR to Protein-Materials Interface

The naturally/physiologically folded protein structure and dynamics are integral to enzyme function. However, many diseases are caused by misfolded proteins and understanding the structural changes that cause disfunction is necessary for prevention and treatment. In addition to the health implications of protein study, a thorough understanding of protein structure can provide the information necessary to produce tunable enzymatically-active materials and harness the enzyme catalytic power artificially. Therefore, many research efforts have focused on elucidating the structure and dynamics of proteins. Many diverse methods have been developed to access structural information of proteins. Two well-established and common methods are X-Ray Crystallography (XRC) and Nuclear Magnetic Resonance Spectroscopy (NMR). However, intrinsically disordered proteins, membrane-bound proteins, and enzymes in materials pose challenges to being studied with these techniques. EPR is a good complementary technique that can acquire information that would be otherwise inaccessible.

X-ray crystallography is a technique of probing the molecular structure of a crystal via the diffraction pattern of applied X-ray radiation. Applying this technique to proteins requires that the protein be organized into a set pattern within a protein crystal. Some proteins, such as lysozyme, readily crystalize into well-ordered units. However, making protein crystals is not a trivial task. To make crystals, the protein sample must be very pure, highly concentrated, and align itself in a set conformation which can be difficult to achieve and impossible for some samples. Still, XRC remains a popular and powerful technique for determining protein structures due to its high resolution, typically 2-5 Å.

Nuclear magnetic resonance spectroscopy is similar to EPR spectroscopy in that it probes resonance of quantum spin values within an applied magnetic field; except that the resonance being probed is of the nuclear spin and the magnetic field is held constant with the radio wave frequency varied. Unlike EPR, the resonance observed is from all nuclei with a non-zero spin value rather than only the signal from the label. Therefore, protein NMR is limited to smaller proteins and often incorporates isotropic labels to aid in spectra deconvolution. Protein NMR, unlike XRC, does not require the protein to be crystalized, but rather can obtain structure information of proteins in the solution state or other native states like EPR. Like XRC, protein NMR requires a highly purified sample, which can be difficult to achieve.

Dr. Wayne Hubbell pioneered work on SDSL in the 1990's to develop EPR methods that could be used in systems that were challenging for other techniques such as disordered proteins, membrane bound proteins, and complex systems[77–81,84,91,92]. Intrinsically disordered proteins (IDP) are proteins that lack a fixed structure and can rapidly undergo structure and dynamics changes depending on their environment. Therefore, IDP's are difficult to crystalize and often require interactions with other proteins or lipids that would complicate the signal. Similarly, membrane-bound proteins suffer from lipid background signals, difficult crystallization, and are often too large for NMR. EPR can be done using SDSL on complex systems of arbitrary sizes in solution, which makes it a prime candidate for studying IDP's and membrane-bound proteins.

As mentioned in section 1.2, Lysozyme was the first protein to have its three-dimensional structure solved using X-ray diffraction techniques in the 1960's and it was used as a model enzyme to develop NMR techniques in the 1990's. The wealth of information on lysozyme structure from various techniques provides a library of literature to aid in the assessment and interpretation of data. Therefore, it is a natural progression that lysozyme would be chosen to develop SDSL. Using a variety of different experiments on the well-characterized lysozyme, researchers were able to show that the CW EPR signal was sensitive to the structure and dynamics at the labeled site[77,79,81,84,91,92]. It was also discovered that the EPR signal could show large-scale conformational changes. The EPR data agreed with the XRC and NMR data available, which validated EPR as a good complementary technique. The computation and data gathered from the lysozyme studies laid the foundation for computer programs that can be used to deconvolute spectra from other more complex systems.

The study of enzymes in combination with materials is plagued by many of the limitations that IDP's and membrane-bound proteins pose, namely, difficulty in crystallization and complex background signals. Because EPR has proven effective in probing the structure and dynamics of these complex systems, it is a prime choice for studying the protein-material interface. EPR has been successfully applied to a variety of different enzyme-materials combinations including gold nanoparticles, protein-polymer hybrids, carbon nanotubes, graphite oxide, and metal-organic frameworks to name a few[40,82,83,93]. In this dissertation, EPR is applied to Graphite Oxide-Metal Organic Framework composites to probe lysozyme orientation within the compound, which will be expounded on in chapter 3.

2.3.6. EPR Conclusion

Understanding protein structure and dynamics is important for a variety of applications. However, the detailed molecular mechanisms of proteins can be difficult to probe, especially for proteins in enzymatically-active materials. EPR is a unique technique that was developed to study IDPs and membrane-bound proteins in solution which was challenging for XRC and NMR. EPR can be performed on systems regardless of size, complexity and purity, which makes it an ideal technique for studying enzymatically-active materials. The data obtained from EPR can also be used to improve molecular modeling techniques, which are important for rational design.

2.4. Concluding Remarks

By combining multiple techniques, we can build a model that provides the molecular-level information necessary to understand proteins, create therapeutics, and synthesize tunable enzymatically-active materials. In this dissertation, CW EPR is utilized to probe the orientation of T4 lysozyme within graphite oxide-metal organic framework composites. This technique can be applied to a variety of enzyme-materials systems to gather more structure and dynamics information. A deeper understanding of enzyme-materials interactions will aid in the rational design and development of tunable enzymatically-active materials.

3. ENZYME IMMOBILIZATION ON GRAPHITE OXIDE (GO) SURFACE VIA ONE-POT SYNTHESIS OF GO/METAL−ORGANIC FRAMEWORK COMPOSITES FOR LARGE SUBSTRATE BIOCATALYSIS[1]

3.1. Abstract

Although enzyme immobilization has improved many areas, biocatalysis involving large-size substrates is still challenging for immobilization platform design because of protein damage in the often “harsh” experimental conditions required for these reactions. Our recent efforts indicate the potential of using Metal−Organic Frameworks (MOFs) to partially confine enzymes on the surface of MOF-based composites while offering sufficient substrate contact. Still, improvements are required to expand the feasible pH range and efficiency of substrate contact. In this contribution, it was discovered that Zeolitic Imidazolate Framework (ZIF) and a new calcium-carboxylate based MOF (CaBDC) can both be coprecipitated with a model large-substrate enzyme, lysozyme (lys), to anchor the enzyme on the surface of graphite oxide (GO). Lys activity was observed against its native substrate, bacterial cell walls, indicating lys was confined on composite surfaces. Remarkably, lys@GO/CaBDC displayed a stronger catalytic efficiency at pH 6.2 as compared to pH 7.4, indicating CaBDC is a good candidate for biocatalysis under acidic conditions as compared to ZIFs which disassemble under pH < 7. Furthermore, to understand the regions of lys being exposed to the reaction medium, site-

---

[1] The work discussed in this chapter was co-authored by Jasmin Farmakes, Isabelle Schuster, Amanda Overby, Lina Alhalhooly, Mary Lenertz, Qiaobin Li, Angel Ugrinov, Yongki Choi, Yanxiong Pan, and Zhongyu Yang. The work was previously published in ACS Applied Materials and Interfaces[83]. Jasmin Farmakes, Yanxiong Pan, and Zhongyu Yang were responsible for the data interpretation and conclusions put forth in this chapter. Jasmin Farmakes performed the majority of the experimental work and data collection including the EPR spectra, activity data, FTIR spectra, and TEM images. Yanxiong Pan prepared the graphite oxide and assisted in data collection, experimental troubleshooting, and manuscript revision. Yongki Choi and Lina Alhalhooly collected the AFM data. Angel Ugrinov collected the powder x-ray diffraction data and assisted in interpretation. Isabelle Schuster, Amanda Overby, and Mary Lenertz prepared reagents, buffers, and participated in some experimentation alongside Jasmin Farmakes. Qiaobin Li aided in the experimental design and sample preparation. Jasmin Farmakes wrote the manuscript and participated in the revision process.

directed spin labeling (SDSL) electron paramagnetic resonance (EPR) spectroscopy was utilized. The data showed a preferential orientation of lys in GO/ZIF composite, whereas a random orientation in GO/CaBDC. This is the first report on immobilizing solution-state large-substrate enzymes on GO surface using two different MOFs via one-pot synthesis. These platforms can be generalized to other large-substrate enzymes to carry out catalysis under the optimal buffer/pH conditions. The orientation of enzyme at the molecular level on composite surfaces is critical for guiding the rational design of new composites. This work has been published in *ACS Appl. Mater. Interfaces* 2020, 12, 23119-23126.

3.2. Introduction

Immobilizing enzymes on solid surfaces offers enhanced enzyme stability, reusability, and catalytic efficiency, thus improving cost-efficiency in biocatalysis[8,9,12]. However, the reactions are often limited to relatively mild conditions to avoid enzyme damage[94,95]. This places limitations on reactions that are more efficient in, or require, harsher conditions that may denature the protein such as elevated temperature, organic solvents, and/or extreme pHs[96,97]. Encapsulating enzymes in porous materials, such as mesoporous nanoparticles[98–101] or (reversible) micelles, offers enhanced enzyme stability under those harsh conditions[102–105]. However, it is challenging for the encapsulated enzymes to contact large-size substrates[66,67,69,106]. On the other hand, many desirable biocatalysis reactions involve large substrates such as polysaccharides, fibers, or cells, and require or prefer harsh conditions[102,107–109]. This raises an intrinsic conflict of requirements: to protect the enzyme from harsh environments while still exposing the enzyme (especially the active site).

Recent works suggest a potential compromise: co-crystallization of enzymes with Zn^{2+} and imidazolate to create enzyme@ MOF biocomposites that allow portions of the enzymes to be entrapped below the surface of the MOF crystals with other portions (likely the active site) above[110]. It has been shown that the partially exposed enzymes are active for large-substrate biocatalysis and have enhanced stability in ZIF-8[82]. However, ZIF-8 is unstable under acidic pHs, and thus, the composite disassembles to release the trapped enzymes[111]. Also, some enzymes are completely buried under the crystal surface and unable to participate in large-substrate biocatalysis, which reduces the cost-efficiency[110]. A potential solution to both drawbacks which has been explored is to build ZIF-8 scaffolds on carbon nanotubes (CNTs) so that more enzymes are encapsulated on the surface[63]. The π–π stacking interactions between the CNTs and ZIF added stability to the ZIF scaffolds so that only a small portion of ZIF was disassembled in acidic pHs (less than 5.5). Still, the pH stability and loading capacity could be further improved. Other efforts on improving enzyme@MOF acid stability include a polymer hybridized ZIF; but this method requests complex synthetic expertise[112]. A more recent solid-state mechanochemical encapsulation approach can encapsulate enzyme powders in an acid-stable MOF, UiO-66[113]. However, many enzymes are unavailable or not functional in the solid state.

In this work, the co-precipitation of enzyme, metal and ligands on the surface of graphite oxide (GO) was explored for its promising advantages in enzyme immobilization. It was found that the enzyme loading capacity can be enhanced on the zero curvature GO surfaces as compared to CNTs. Also, in addition to Zn^{2+} and imidazolate, the Ca^{2+} and disodium terephthalate (BDC-Na_2) can coprecipitate on GO surface together with the enzyme in the aqueous phase, generating an acid-stable, enzyme@GO/CaBDC composite. Given the stability of GO/ZIF and GO/CaBDC in different pHs and even different buffers (ZIF is stable in the more biological relevant PBS buffer but CaBDC is not), platforms were established that can immobilize enzymes for large substrate biocatalysis under different conditions (acidic conditions: GO/CaBDC; basic conditions: GO/ZIF; PBS buffer: GO/ZIF). These platforms were tested using a model large substrate enzyme, T4 lysozyme (T4L), which catalyzes the hydrolysis of β-1,4 glycosidic bonds of bacterial cell walls[20]. For both GO/ZIF and GO/CaBDC composites, lysozyme activity was observed, indicating partial exposure of lysozyme on both surfaces. Then the exposed regions of lysozyme on the surfaces was probed using site-directed spin labeling electron paramagnetic resonance spectroscopy (SDSL-EPR) as detailed in our recent works, which adds to the understanding of structural basis governing the activity[63,77,82].

This is the first report on immobilizing large-substrate enzymes on GO surface using two different MOFs via aqueous-phase one-pot synthesis. In comparison to enzyme adsorbed on GOs, GO/ZIF or CaBDC composites offer enhanced immobilization because MOF scaffolds can effectively prevent leaching[10,114]. In addition, no chemical modifications of the enzyme are required, which minimizes enzyme perturbation that is a concern for covalent linking based immobilization. In comparison to existing GO/MOF (often GO/ZIF) works, this work includes large-substrate enzymes for biocatalytic reactions[64,65]. The advantage of GO/ MOF composites compared to enzyme@ZIF composites is the reduced the number of enzymes completely buried under the composite surface and unable to participate in catalysis[74,82,115]. Thus, the composites discussed herein can potentially enhance the cost-efficiency for large-substrate biocatalysis. Artificial enzymes based on GOs and/or MOFs offer enhanced stability and cost-efficiency as compared to native enzymes; however, immobilizing native enzymes on GOs/MOFs offer enhanced selectivity against specific substrates[116–119]. More importantly, our work is the first demonstrating the feasibility of using CaBDC MOF to host enzymes for acidic biocatalysis. Solid-state mechanochemical encapsulation of powder-state enzymes into the acidic stable UiO-

66[113] is also promising, but our method is applicable to the encapsulation of solution-state enzymes which is preferential for proteins. The developed GO/ZIF and GO/CaBDC platforms can be generalized to other large-substrate enzymes to carry out catalysis under optimal buffer/pH conditions. The orientation of enzyme at the molecular level on composite surfaces reported herein provides further understanding of protein activity in composites and is invaluable for the rational design of new composites.

3.3. Materials and Methods

Graphene nanoplatelets aggregates were obtained from Alfa Aesar (submicronparticles, S.A. 500 m^2 /g) and all other chemicals are purchased from Sigma-Aldrich. All lysozyme mutants were created, expressed, purified, and spin labeled according to prior works[120]. Graphene oxide was obtained by oxidizing the graphite using $KMnO_4$ under 36 °C for 3 h, followed by washing and dialyzing to pH 7. The enzyme@GO/ZIF composites were created by first protecting the protein with poly vinylpyrrolidone (PVP) so that the reaction could be carried out in methanol (MeOH). The PVP-protected enzyme was added to the GO solution and allowed to incubate for 10 min. Then, $Zn(NO_3)$ and imidazolate were added sequentially to the mixture, followed by wash and resuspension. The enzyme@GO/CaBDC composites were prepared by adding $CaCl_2$ to GO aqueous solution, followed by addition of enzyme and BDC. The lysozyme activity was measured using a commercial lysozyme activity kit (Micrococcus lysodeikticus, ATCC No. 4698, Sigma-Aldrich). All EPR spectra were acquired using a Varian E-109 spectrometer with a cavity resonator. The stability tests were conducted by subjecting each composite to 1 M NaCl, 4.5 pH, and 5.7 pH, followed by monitoring EPR spectra at 0, 0.5, 1, 2, 5, 24, and 48 h. AFM imaging was preformed using a commercial atomic force microscope (NT-MDT NTEGRA AFM). The samples were imaged in semicontact mode with a resonant frequency of 190 kHz AFM probes (Budget sensors) under ambient conditions. TEM images were acquired by loading each composite to copper TEM grids. The images were captured using a JEOL JEM-2100 LaB6 transmission electron microscope running at 200 kV. Infrared (IR)spectra were recorded on a Nicolet Impact 410 FTIR spectrometer. Powder X-ray diffraction (PXRD) data were collected on a Bruker AXSD8 Advance A25 Powder X-ray diffractometer (40 kV, 40 mA) using Cu Ka (l = 1.5406 Å) radiation.

3.4. Results and Discussion

3.4.1. Composite Design

Lysozyme (lys) is a good model enzyme because of its widely investigated structure−function relationship using various techniques including SDSL-EPR as well as the large physiological substrate, bacterial cell walls[121–123]. Lys also has a large physiological substrate, bacterial cell walls, and therefore, potential applications for natural antibiotic products, which are greatly needed[124–126]. GO was selected as the immobilization platform in this work because it is easily dispersed in aqueous solution, can be conveniently separated from a reaction mixture, has large surface to volume ratio, and high thermal stability[114,127–129]. GO has been utilized for enzyme immobilization, although physical adsorption often suffers from leaching and chemical bonding can cause enzyme perturbation[130–133]. The MOFs, ZIF, and CaBDC, were chosen because of their capability to coprecipitate on GO surfaces with enzymes in mild solutions. Also, the different selection of metals and ligands can potentially lead to different properties and applications of the resultant composites.

3.4.2. Sample Preparation

Commercial graphene nanoplatelets aggregates were purchased from Alfa Aesar (submicron particles, S.A. 500 m2 /g) and oxidized by the Hummers method as described in the literature[134]. Eight lys mutants (44C, 65C, 72C, 89C, 109C, 118C, 131C, and 151C) were created using site-directed mutagenesis, expressed, purified, and spin labeled using procedures as described in prior works[63,82,135]. The lys@ GO/ZIF composites were created by mixing each mutant with GO in water, followed by the addition of $Zn(NO_3)$ then imidazole. The sample was then placed on the nutator overnight to be washed and resuspended with water the following day. Similarly, lys@GO/CaBDC were prepared by adding $CaCl_2$ to GO aqueous solution, followed by the addition of protein and BDC. The solution was allowed to sit overnight on a nutator then washed and resuspended as the ZIF composites were. All samples were washed three times and resuspended using water prior to data collection.

3.4.3. Characterization of lys@GO/MOF Composites

Fourier transformation infrared (FTIR) and powder X-ray diffraction (PXRD) were carried out to confirm the formation of the composites. Upon lys encapsulation, the FTIR spectra (Figure 3.1 A,B) display an additional peak at ∼3500 cm−1 as compared to both GO/MOFs without lys, indicating the presence of protein in the composites. The PXRD data on lys@GO/ZIF and lys@GO/CaBDC indicate that the presence of GO and protein did not change the diffraction patterns significantly as judged by comparison to those of pure ZIF and CaBDC. Note that the 20−25° broad peak in Figure 3.1 C,D are attributed to GO and partially reduced GO, respectively. Taken together, these data confirm that lys is captured within both GO/MOFs, and that the crystals containing lys have crystal scaffolds similar to the composites without protein.

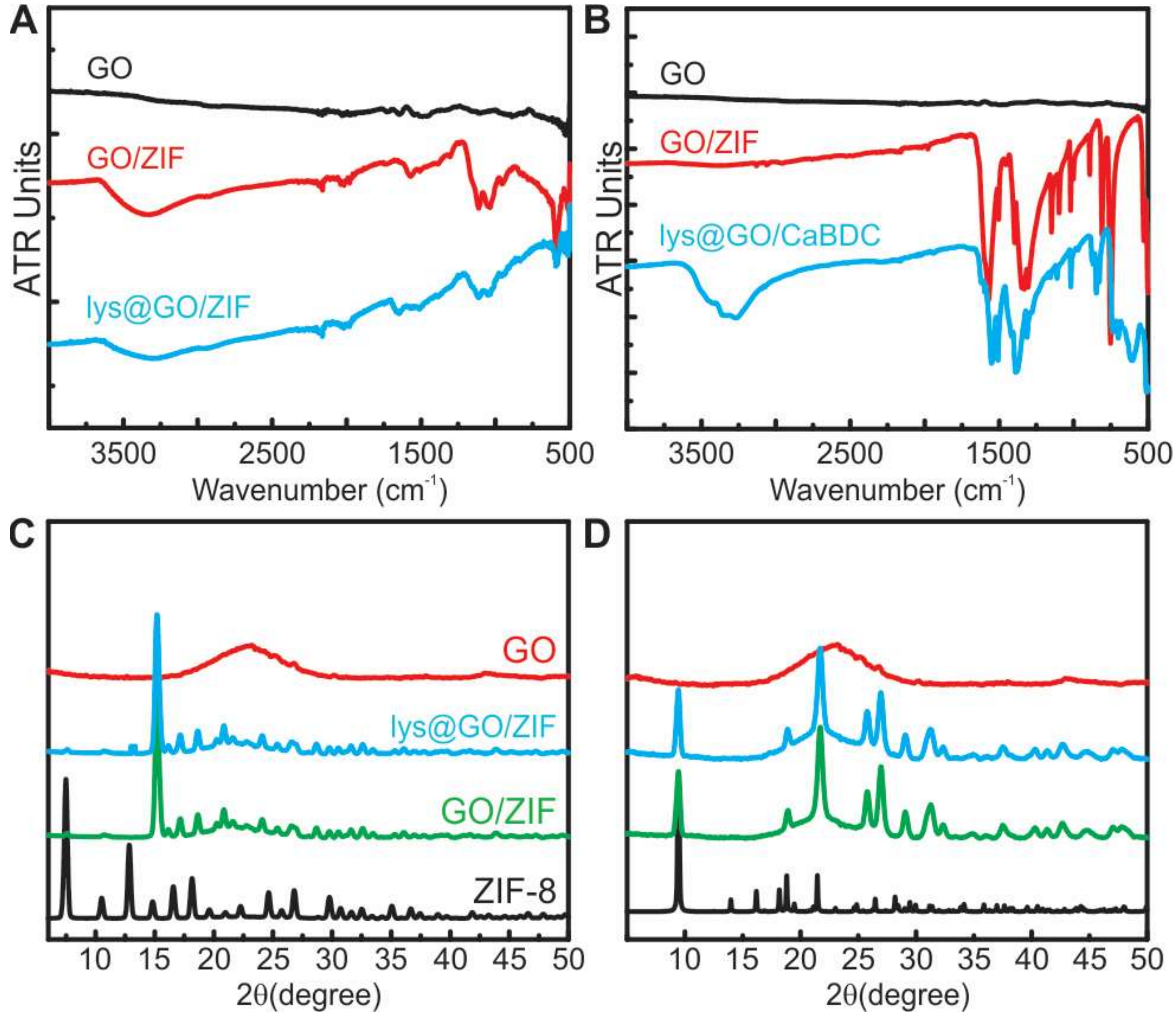

Figure 3.1. Attenuated total reflection (ATR) FTIR (A,B) and PXRD (C,D) characterization of the formation of the lys@GO/ZIF or lys@GO/CaBDC.

To visualize the formation of MOF crystal on the GO surface, the scanning electron microscope (SEM) was employed. GO exhibits a relatively smooth surface (Figure 3.2A). Upon formation of ZIF on GO, considerably small papillae were coated on the GO surface (Figure 3.2B). Encapsulation of lys in GO/ZIF results in larger papillae (Figure 3.2C), likely because lys serves as nuclei during the formation of ZIF. Upon coating with CaBDC, sharp, needlelike particles are formed on GO surfaces (Figure 3.2D). Lys, again, induced the formation of large particles on GO surfaces (Figure 3.2E). To confirm the presence of relevant elements on each GO surface in the involved composites, energy-dispersive X-ray (EDX) spectroscopy was employed (data not shown). Overall, Zn or Ca were detected in the GO/ MOF composites while the percentage of nitrogen increases in lys@GO/ZIF or lys@GO/CaBDC as compared to composites without lys encapsulation, both of which confirm the formation of the desired composites.

Transmission electron microscopy (TEM) and atomic force microscopy (AFM) were also acquired to visualize the morphologies of the formed composites. TEM images (Figure 3.2 G,I) show crystals on top of/incorporating the GO sheets into their structures. Upon lys encapsulation, defects in the crystal surface are visible, likely due to enzyme incorporation. The AFM data of lys encapsulated GO/MOFs (Figure 3.3) also indicate formation of rough surfaces, consistent with TEM.

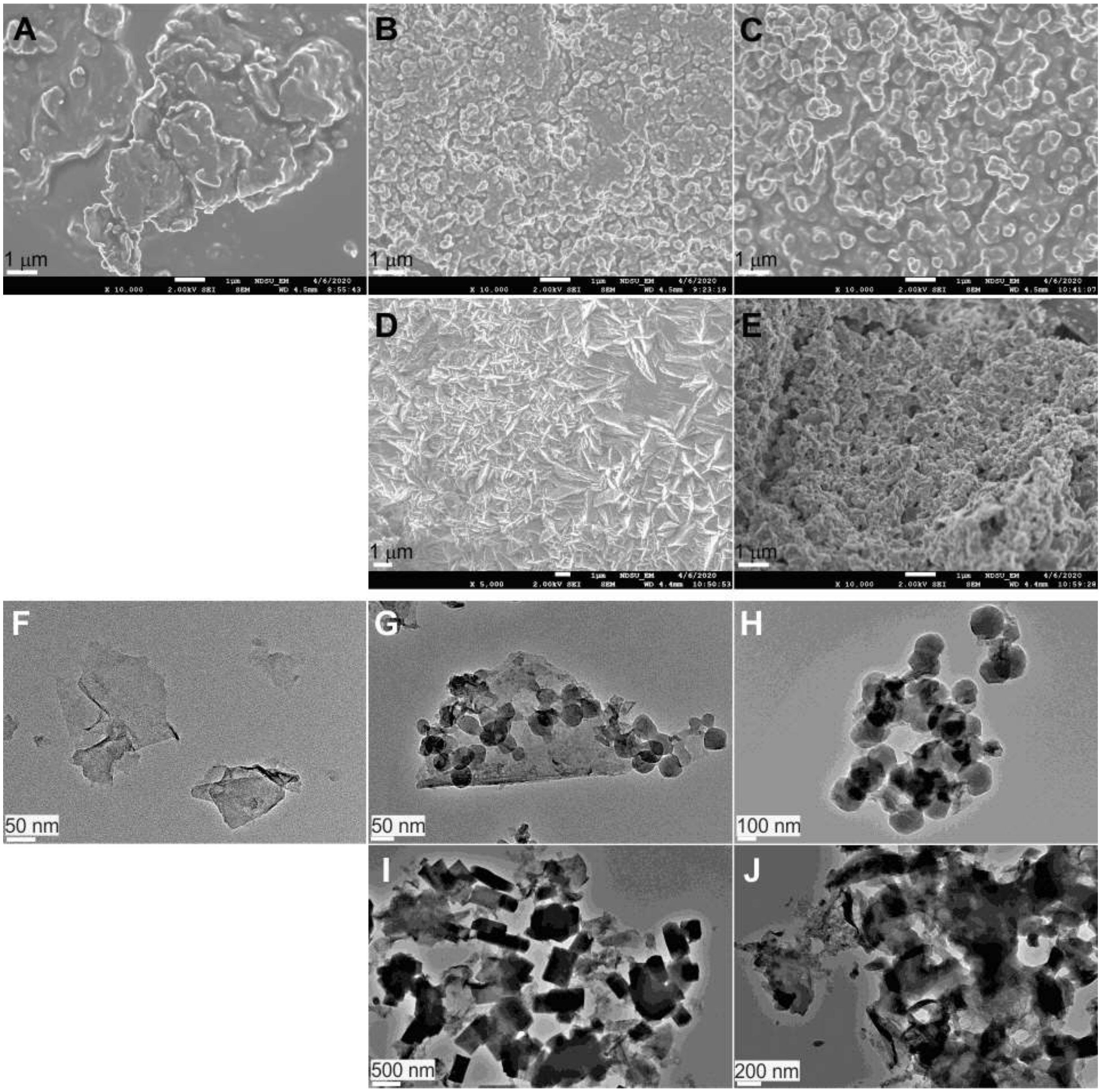

Figure 3.2. SEM images of GO (A), GO/ZIF (B), lys@GO/ZIF (C), GO/CaBDC (D), and lys@GO/CaBDC (E) composites. TEM images of GO (F), GO/ZIF (G), lys@GO/ZIF (H), Go/CaBDC (I), and lys@GO/CaBDC (J) composites.

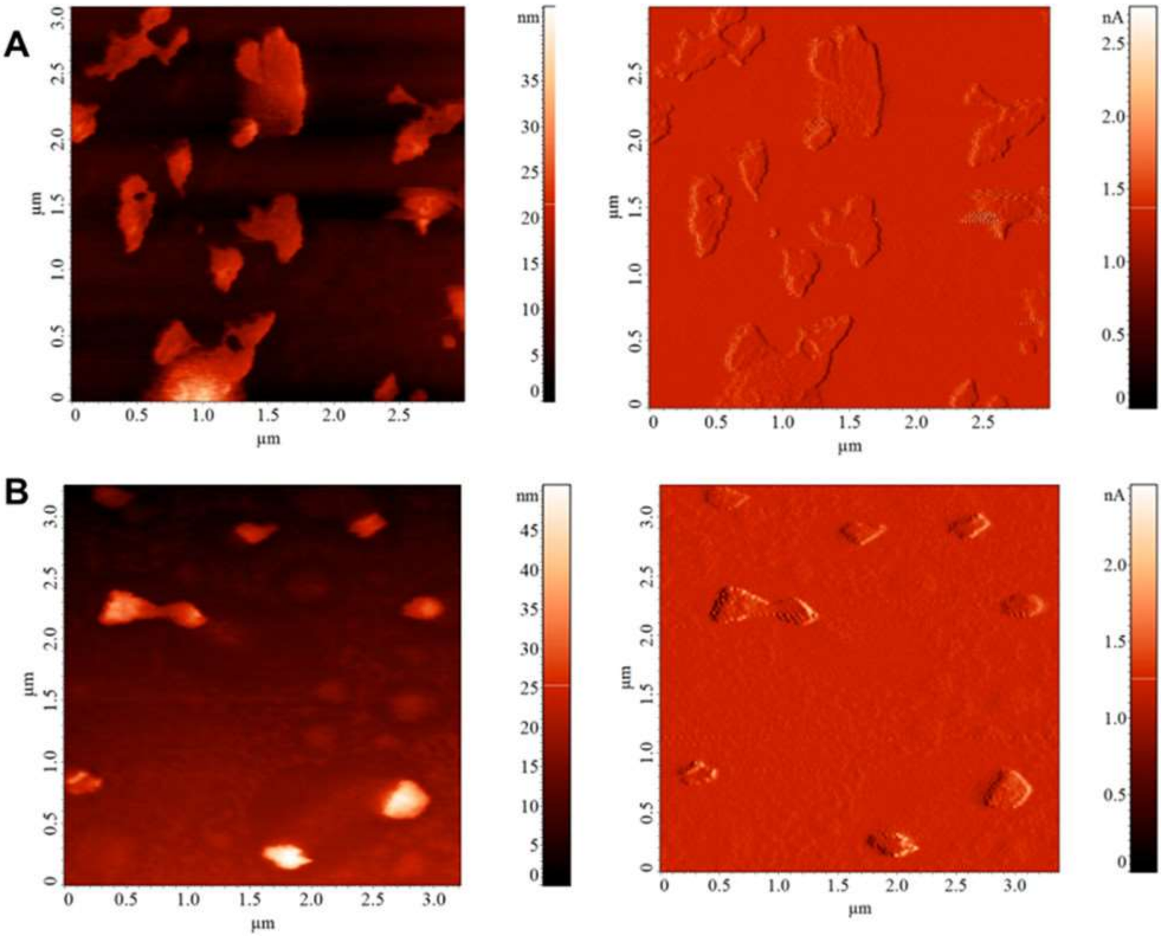

Figure 3.3. AFM images of lys@GO/ZIF (A) and lys@GO/CaBDC (B) composites.

In the presence of BDC (or imidazolate), GO, and possibly broken pieces of CaBDC (or ZIF), it is difficult to use optical methods to determine the enzyme concentrations precisely in the supernatant before and after encapsulation. Gel electrophoresis may encounter relatively high errors as well. Therefore, the loading capacity was estimated based on EPR spin density, which is proportional to the concentration of spin labeled lys[126]. Our results indicated ~225 and 187 mg of lys on 1 mg of GO/ZIF and GO/CaBDC, respectively.

3.4.4. Activity of Formed Composites

To confirm the enzyme is immobilized on the surface of both GO/MOFs, activity was assessed using an established procedure described previously. In brief, the optical density at 450 nm (OD450) is the characteristic absorption of bacterial cells, degradation of which will results in a drop in OD450. For free enzyme in buffer, the slope of the beginning 30−60 s of this drop has been determined to quantify lys activity. However, due to the reduced mobility of the GO/MOF composites (and therefore, reduced substrate contact), the rate of OD450 drop is relatively slower. Therefore, instead of quantitatively measuring OD450 at the beginning 30 s, of the reaction, the reaction was monitored for ∼1 h; the relative catalytic efficiency of the composites is also compared within the same time frame (Figure 3.4). For lys@GO/ZIF, bacterial cell wall breakage was observed at pH 7.4 (in both HEPES and PBS buffers), and no activity at pH 6. The lack of activity at pH 6.2 is likely due to ZIF disassembly which released all encapsulated lys (the composites were washed before the activity test). For lys@ GO/CaBDC, a drop in OD450 was observed at both pH 7.4 (HEPES buffer) and 6.2 (MES buffer) after the same sample preparation/wash procedures, indicating CaBDC stabilized lys on GO. However, PBS buffer in both pHs for CaBDC composites did not result in activity, which is consistent with the fact that phosphate groups destabilize CaBDC (and many other MOFs). Interestingly, the drop in OD450 for lys@GO/ CaBDC at pH 6.2 is more efficient than that at pH 7.4. This is consistent with the optimal pH of free lys in solution (pH dependence of free lys in solution is shown in Figure 3.5). As compared to the nm-size free lys, the reduced lys catalytic efficiency upon immobilization on GO/MOF surface (and partially exposed to the reaction medium) is rationalized to the reduced efficiency of contact with the µm-size bacterial cell walls. A narrow range near lys optimal pH (6.2) was investigated because at higher pHs lys is not as stable (due to the basic isoelectric point of 9.2) and the hydrolysis of bacterial cell walls is not expected to occur under highly basic or acidic conditions which are unrealistic in nature[136,137].

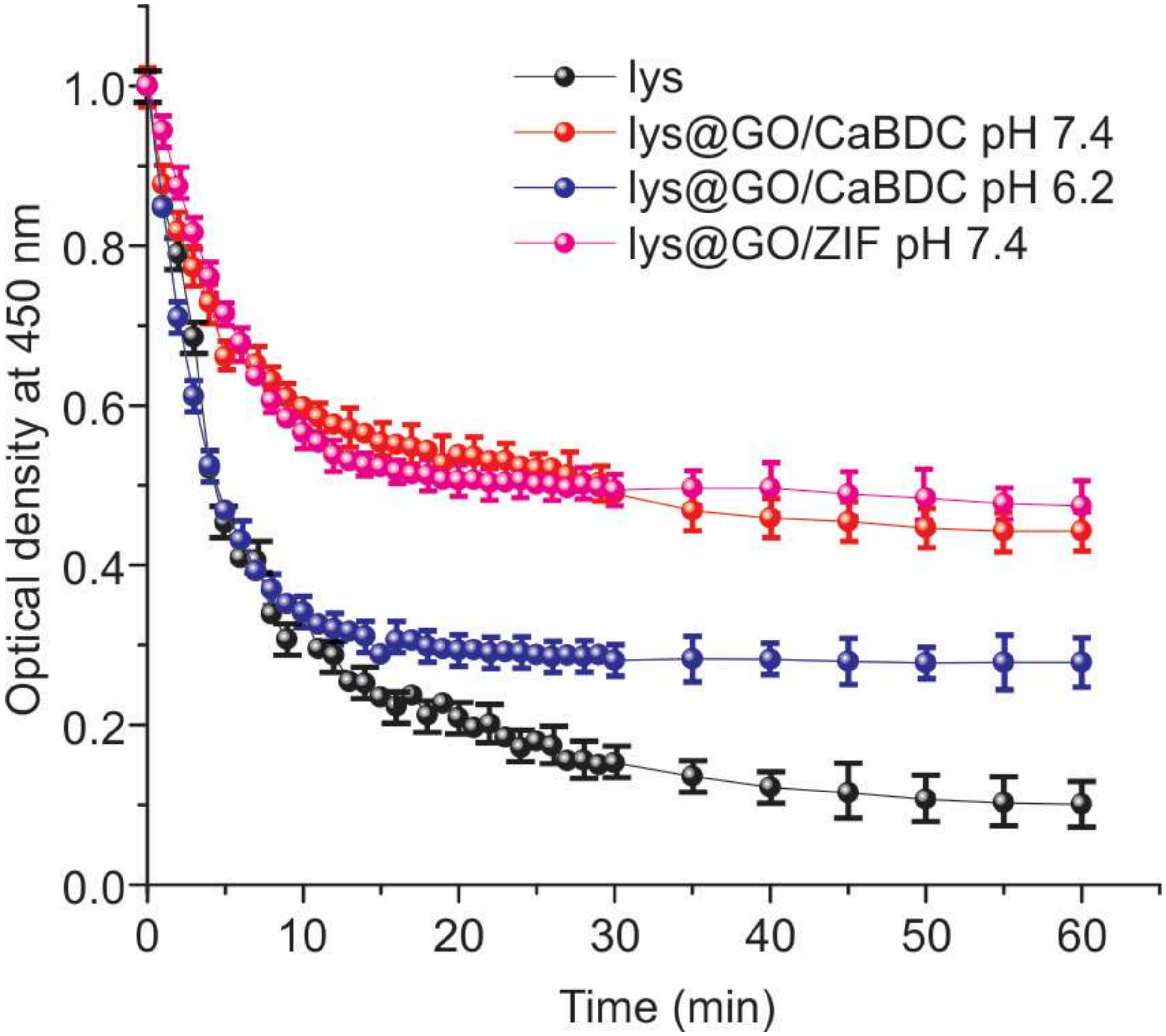

Figure 3.4. Relative catalytic efficiency of lys@GO/ZIF at pH 7.4 (purple), lys@GO/CaBDC at pH 7.0 (red), and lys@GO/CaBDC at pH 6.2 (blue), respectively. The positive control, free lys under pH 6.2, is shown in black. Error bars were obtained by repeating the same measurement three times and acquiring the uncertainty at each time point. Error bars are only shown for alternating time points between 5 and 30 min for clarity of presentation.

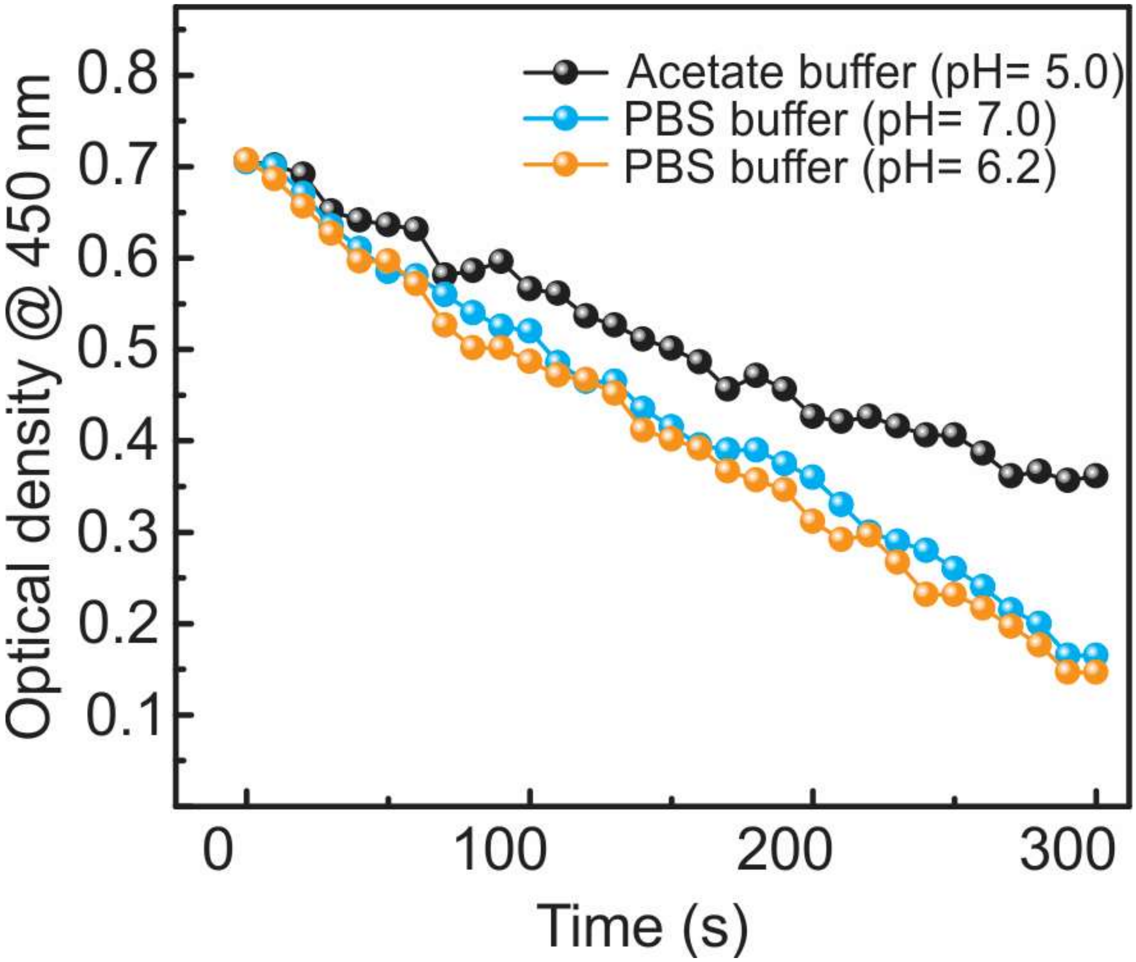

Figure 3.5. The pH dependence of lysozyme determined by the activity assay described above.

3.4.5. Structural Basis of lys Activity on GO/MOF Surfaces.

The activity data clearly indicates that there are lys areas, most likely the active site, exposed on the surface of GO/MOF composites. To understand the extent of active site exposure and determine the enzyme relative orientation on the composite surface, SDSL-EPR studies were carried out using principles introduced in our recent works[24,55]. In brief, surface residues representing the key regions of the model enzyme were spin labeled, followed by spin label dynamics determination using continuous wave (CW) EPR. The CW EPR spectrum of a spin labeled protein depends on three motions, protein rotational tumbling, protein backbone dynamics, and the intrinsic motion of the spin label. The combination of the motions result in two categories of spectral components depending on the location of the spin labeled residue. On an exposed residue, the motion is active and a “mobile” spectral component will be resolved. If the labeled residue is buried under the composite surface, thus restricting motion, an “immobile” component is resolved. If both cases are present, then a linear combination of the two components will be present, which can be decomposed via spectral simulation. Furthermore, certain denaturants can be employed to confirm the surface exposable residues because the encapsulated enzyme is known to be stable under denaturing conditions. Herein, the exposed regions are unfolded by urea, leading to a sharp mobile component due to the enhanced mobility of the local disordering.

Eight surface residues were selected to represent key regions along the protein backbone and each were spin labeled (Figure 3.6A). The CW EPR spectra of all labeled mutants in GO/ZIF and GO/CaBDC composites in the absence and presence of 6 M urea were acquired and presented in Figure 3.6. Overall, both mobile and immobile components (see shades of Figure 3.6) are observed in all sites and urea treatment induces a sharp mobile component in most sites, indicating most sites can be exposed. This is consistent with the fact that lys on both composites have activity. Note that the EPR signal and activity detected in the presented work are originated from immobilized proteins instead of physically adsorbed ones. This finding is based on a negative control where GO/ZIF or GO/CaBDC was mixed with lys physically, followed by a 2 h incubation and wash via sonication and centrifugation. There was neither detectable EPR signal nor activity of lys detected, confirming that the physically adsorbed lys, if any, was removed.

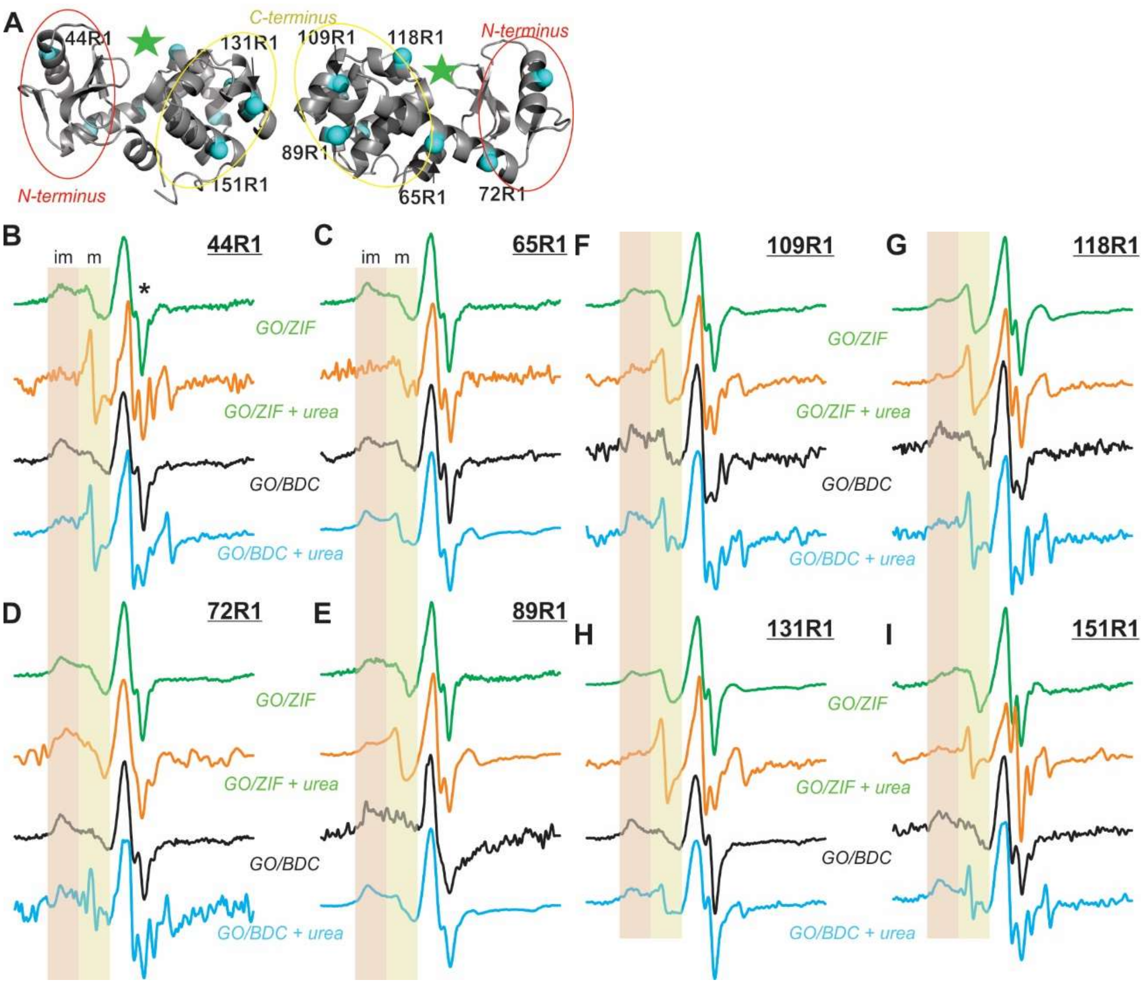

Figure 3.6. (A) Schematic illustration of SDSL. (B)-(I) CW EPR spectra of eight spin labeled mutants upon encapsulation into GO/ ZIF (green) and GO/CaBDC (black) and the corresponding spectra upon treatment with urea. The x-axis is 3300−3400 G. Shades indicate the immobilized and mobile spectral components. The peak indicated by the * is originated from the GO. The pdb file of lys was 3lzm. Green star = active site.

A more detailed look at the data allows one to depict the relative orientation of lys on each composite. In particular, on GO/ZIF, by comparing all green spectra with all orange spectra, it is seen that the N-terminus (represented by 44R1) and the C-terminus (represented by 131R1 and 151R1) of lys are clearly unfolded upon urea treatment, indicating these residues are more likely exposed to the surface of GO/ZIF composite. The long helix of lys (represented by 72R1), on the other hand, is less affected by urea, indicating a higher chance for the long helix to be buried under the surface. Based on this speculation, a favorable enzyme orientation on GO/ZIF surface in proposed in Figure 3.7A. On GO/CaBDC, however almost all studied sites from N- to C-terminus showed the strong tendency to be unfolded by urea, indicating all regions can be exposed, or, a random orientation. It is likely that the orientations shown in Figure 3.7A are also possible and likely of GO/BDC composites, but Figure 3.7B shows additional possible orientations of lys on GO/BDC.

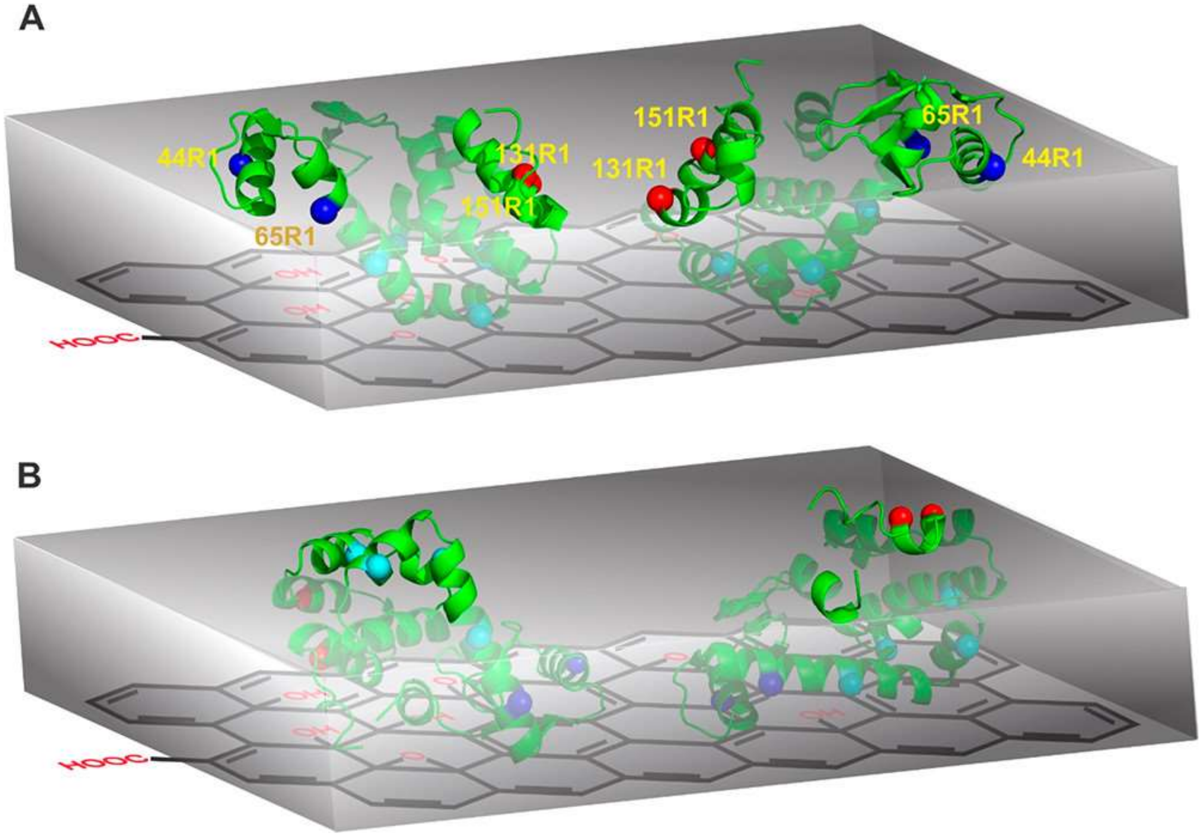

Figure 3.7. Schematic illustration of the possible enzyme orientation on the surface of GO/ZIF (A) and GO/CaBDC (B) composites.

3.4.6. Stability of the Formed Composites

To test the pH stability in acidic solution over time, a representative mutant of lys on each composite, 65R1@GO/MOFs, was selected for EPR study. The principle is that a destabilized composite or MOF will release the encapsulated protein and result in EPR spectra of free enzyme in solution (or, disappearance of the immobile component). Upon preparation, the composites were washed three times with water and then resuspended in pH 4.5 acetate buffer or pH 5.7 MES buffer. Spectra were collected for each of these solutions at various time points from 0.5 to 48 h. Representative EPR spectra at different time points are shown in Figure 3.8.

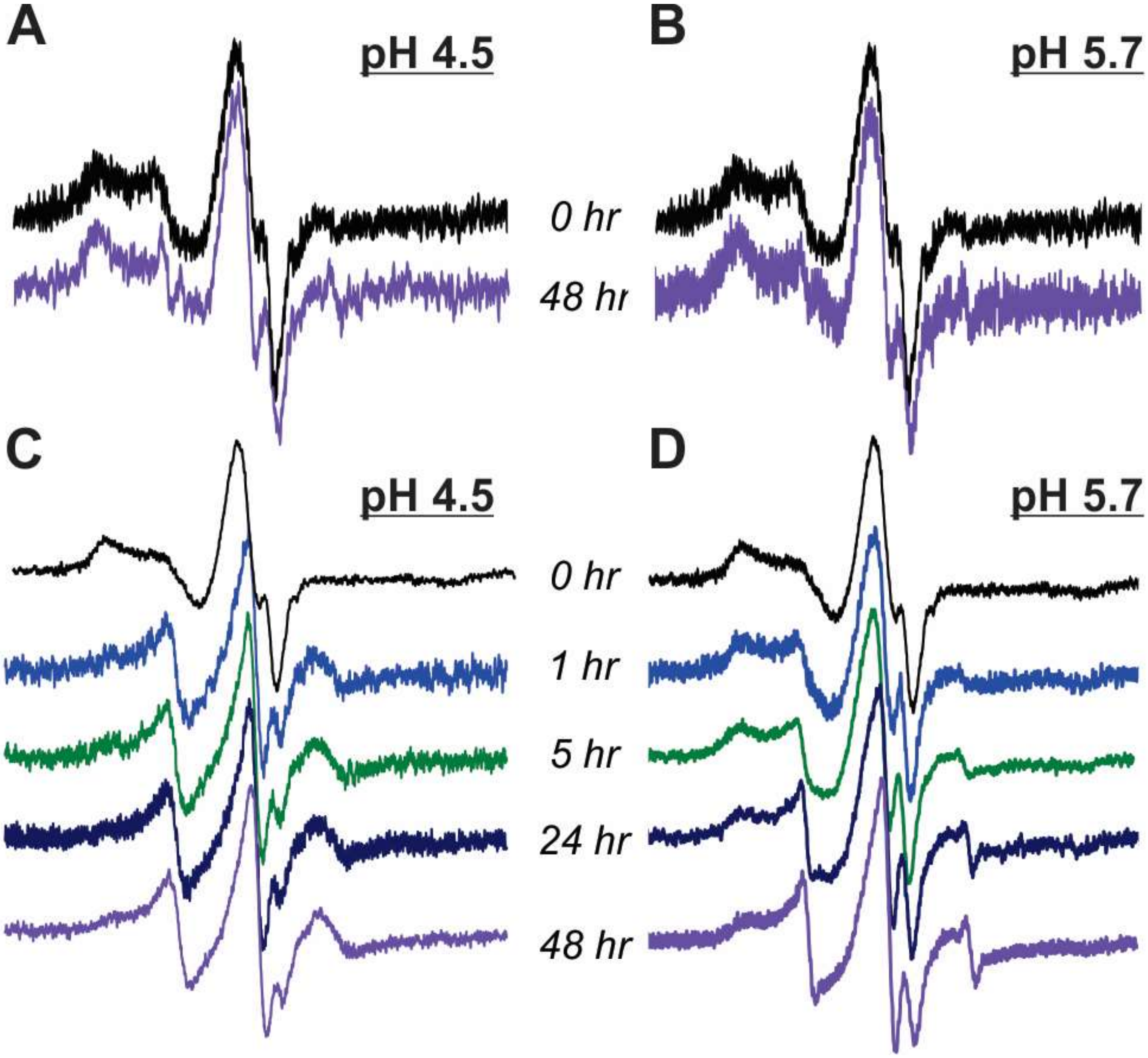

Figure 3.8. CW EPR spectra of the 65R1@GO/CaBDC under pH 4.5 (A) and pH 5.7 (B) at 0 and 48 h; no major change under both pHs was observed over time indicating the acidic stability of GO/CaBDC. Time-resolved CW EPR spectra in GO/ZIF are shown under the same two pHs, (C) and 5.7 (D); a lower pH results in a faster release of enzyme, indicating more rapid disassembly of ZIF. The x-axis is 3300−3400 G.

A notable finding is that the EPR spectrum of 65R1@GO/ CaBDC does not display change over a duration of 48 h in both acidic conditions (Figure 3.8 A,B), confirming that CaBDC is stable in acidic pHs. On the other hand, the EPR spectrum of 65R1@GO/ZIF is influenced by acidic conditions so that the lower the pH, the more rapid the release of free protein (see the gradual increase in the mobile component of spectra shown in Figure 3.8 C,D). This is consistent with the disassembly of ZIF in acidic pHs. Note that GO has increased the acid stability of ZIF because pure ZIF is disassembled much more rapidly under pH 7 (data similar to Figure 3.8 C and not shown). Buffer stability test showed similar findings. In PBS buffer, 65R1@GO/ZIF did not show a spectral change over time while 65R1@GO/CaBDC showed free 65R1 spectrum almost immediately upon buffer exchange[24].

3.5. Conclusions

The feasibility of co-precipitating enzymes, metals, and ligands on the surface of GO is demonstrated in this work. Here, two MOFs, the popular ZIF and an acid-stable MOF, namely CaBDC, were shown to both assist the immobilization of enzyme on GO surface. While using ZIF and/or GO to immobilize enzymes has been done before, this enzyme@GO/ ZIF work shows the hydrolysis of a large-size biological substrate, bacterial cell walls by encapsulating a typical model large-substrate enzyme, lysozyme. Furthermore, the structural basis of such large-substrate catalytic activity was revealed using SDSL-EPR, which depicted that the N- and C-terminal domains of the enzyme are exposed, while the long helix connecting the two domains are preferred to be buried. Although the antimicrobial activity of the lys@GO/ZIF is acceptable, the trapped enzyme is released under acidic pHs. In this context, the second composite, lys@GO/BDC, overcomes this barrier because GO/CaBDC is stable under acidic pHs. Catalytic activity for GO/BDC was observed against the same large substrate under acidic pHs and the orientation of lys on GO/BDC surface revealed to be random. Lastly, the pH stability was monitored over time using EPR spectra which is a convenient way to sense the release of enzyme due to MOF disassembly. This is the first report using acid-stable MOF to encapsulate enzyme on GO surfaces. The enzymes are demonstrated to be immobilized on GO/MOF surfaces and capable of catalyzing large substrate reactions. The structural basis of the activity, namely, enzyme exposable regions on GO/ MOF surfaces, was revealed at the molecular level, which is also the first time in the literature. The platforms reported here can be generalized to other large-substrate enzymes for improving biocatalysis. The structural basis can be used to guide future design of complex enzyme immobilization platforms.

4. BIGGER MAY BE BETTER: ACTIVITY ALTERATIONS OF SITE-SPECIFICALLY PEGYLATED T4 LYSOZYME

4.1. Abstract

Protein-polymer conjugates are exciting prospects for a variety of applications in drug delivery, diagnostics, biocatalysis, and biomaterials. Polyethylene glycol is an attractive and popular polymer for protein-polymer conjugation (PEGylation) because it is FDA approved for use in pharmaceuticals. Although PEGylation can increase the stability of the protein, it often reduces the activity. To maximize stability and enzyme activity, the effects of polymer size and conjugation site on conjugate properties must be investigated. The effect of polymer length and location on the activity of T4 Lysozyme conjugated site-specifically using a maleimide-thiol click reaction at 6 different locations and PEGs with different molecular weights (1.9K and 5K) is studied herein. The conjugates had appreciably different alteration in surface charge, as evidenced the ion exchange chromatography utilized for purification, and in activity. This data showed site-specific alterations which could not be explained by surface charge alteration or steric hinderance alone. These results can guide the rational design of polymer-protein conjugates for applications in many different fields.

4.2. Introduction

Polymer-protein hybrids are attractive because they can fuse the desirable attributes of both polymers and proteins to give a material that is enzymatically active with enhanced stability features[138–140]. Notably, the protein-polymer hybrids can retain enzymatic activity in harsh conditions where the native protein cannot function[14–17]. The polymer's ability to adopt different conformations in various environments plays a central role in enhancing protein stability and in tuning selectivity and/or efficiency of proteins[149,150]. However, this enhanced stability and/or tunability often comes with the cost of reduced enzyme activity which limits the applications of the hybrids[151,152]. Therefore, great efforts have been focused on understanding the impact of polymer properties (size, rigidity, hydrophobicity, thermos-stability, etc) and conjugation site(s) on the functionality of the resultant conjugates in order to engineer them for a wide variety of applications[143,147,151,153,154].

Polymers can be synthesized with many different properties such as size, hydrophobicity, temperature stability, branching degree, ect, to fit different needs and/or to respond to changes in their environment[87]. The combination of “smart” polymers that are designed to respond to changes in the environment with proteins has opened a whole new avenue for tunable hybrids[87,88,155–158]. Among the large spectrum of available polymers, polyethylene glycol (PEG) is an ideal counterpart for protein-polymer conjugates because of its low immunogenicity, toxicity, and cost[33,34,36,37,39,90,159,160]. PEGylation (conjugation of PEG to a drug or protein) has been shown to increase the circulation time and stability of drugs and has been approved by the FDA for use in pharmaceuticals[34,161,162]. The first PEGylated drug on the market, Adagen, was approved in 1990 to treat severe combined immunodeficiency disease[34,36,37]. Since the release of Adagen, many other PEGylated pharmaceuticals have been approved for market use[34].

There are many different ways to combine polymers with proteins[90,163]. Non-specific conjugation has the advantage of simple operation, but suffers from limited control and unpredictability in functionality of the resultant product[142–144,147,164–166]. Site-specific conjugation is an effective alternative and offers not only better control of conjugation site/conjugate structure but also activity[144,145,153,165–167]. Still, the influence of PEGylation on protein activity is a concern. While PEGylation increases the stability and circulation time of the attached protein or molecule, it typically decreases the activity of an attached enzyme[42]. This activity alteration could be a result of multiple factors including steric hinderance of substrate access due to polymer shielding, alterations in protein surface charge, and disruptions in structure/dynamics critical for activity[151,153,157]. To continue development of PEGylated enzymes, the underlying cause of activity loss must be investigated but it is challenging to elucidate these structural details[40,168,169].

Predicting the properties of a conjugate solely based on PEG size and conjugation site(s) is often incorrect because polymer-protein interactions can influence protein structure, dynamics, and function in unexpected ways[88,143]. Additionally, the large size and heterogeneity of the conjugates and the complexities caused by the polymer-protein interactions pose challenges to investigating structural information using most experimental approaches[154]. By combining multiple approaches to create a better understanding of the conjugates, protein-polymer hybrids can be rationally designed to maximize stability while still entirely retaining or enhancing enzyme activity[170]. Accurate property prediction will allow creation of hybrids to fit criteria needed for applications as drugs as well as in other areas such as biomaterials or biocatalysis.

Herein, the synthesis, purification, and activity of 12 hybrids formed from 6 mutants of an antibacterial protein, T4 lysozyme (T4L), and 2 PEGs of molecular weights 1.9K and 5K attached site-specifically is presented. T4L, which degrades bacterial cell walls by cleaving the 1,4-glycosidic bond in bacterial cells, is not only a good model protein due to the widely investigated structure-function relationship, but is also an antibacterial protein, which makes it a desirable protein for the development of antibacterial materials[170,171]; naturally antibiotic products are greatly needed given the increased prevalence of antibiotic resistant bacteria and are a current topic of research[16,18,124,172–175].The hybrids were conjugated via grafting-to using a site-specific reaction between T4L mutants with a cysteine mutation and PEG with a maleimide end group. The conjugates were then separated from unreacted protein and polymer using an ion-exchange column which allowed for separation based on the alteration in surface charge. Each of the 12 hybrids displayed different degrees of surface charge alteration which was dependent not only on polymer size, but on location as well. This process could be adapted for large scale commercial production of a pure conjugate as well as allowing for recapture and use of the unreacted polymer and protein. The activity of the hybrids was assessed using standard procedures and it was found that the alterations in activity were dependent on polymer size as well as the location.

4.3. Materials

Maleic anhydride (≥ 99.5%) was purchased from Chem-Impex. The β-alanine (99%) and poly(ethylene glycol) methyl ether (mPEG-OH, Mn = 5000) was purchased from Sigma-Aldrich. The mPEG-OH (Mn = 1900) were purchased from Alfa Aesar. Other reagents such as dimethylformamide (DMF), ethyl ether, tetrahydrofuran (THF), and dichloromethane were purchased from Fisher Scientific and purified if necessary. The commercial PEGs were modified to include a maleimide group for reaction with protein cysteines (see methods).

4.4. Methods

4.4.1. Project Design

4.4.1.1. Protein Mutations

The T4L mutants used in this study had native cysteine residues 54 and 97 mutated to threonine and alanine, respectively, so that there would only be 1 cysteine residue open for conjugation in each mutant. This ensures that conjugation is done site-specifically at the added cysteine locations only. Polymer conjugation sites where selected as representative sites along the protein backbone (K65C, D72C, D89C) and in proximity to the active site (S44C, V131C, T151C). These sites are also solvent accessible and have been shown in previous papers to have no changes the protein structure or activity due to the mutagenesis alone[40,77,83].

4.4.1.2. Polymer

PEG was chosen for this study because of its wide use in industry, biocompatibility and low cost[36,39,90,159]. Additionally, it can be easily modified to contain a maleimide end group and is soluble in aqueous conditions. To separate the polymer size effects of the resultant conjugates from the site-specific alterations, two molecular weights of PEG were necessary. PEGs of 2K and 5K have been shown in literature to not cause large disruptions in lysozyme structure and have possibilities for activity enhancement[42,142,152,176]. Therefore, 1.9K and 5K PEG chains were chosen to test the system herein. The polymer was obtained from Sigma-Aldrich and modified to have a maleimide end group (Scheme 1).

4.4.1.3. Polymer Attachment

The "grafting-to" conjugation approach based on the thiol-maleimide Michael addition (between a protein cysteine and maleimide-PEG) was selected in this study[144,177,178]. The maleimide-cysteine reaction was chosen for its specificity, efficiency, and ability to be carried out in mild reaction conditions[179,180]. The reaction is popular in biochemistry applications and many antibody-drug conjugates that are clinically approved contain a maleimide linkage[34]. The chosen maleimide-thiol linkage in a grafting-to conjugation approach results in synthesizing the desired conjugate with very little heterogeneity or undesirable side reactions.

4.4.1.4. Purification

To separate the conjugates from unreacted/dimerized protein and polymer, a cation exchange column was chosen. A cation exchange column retains molecules based on the strength of their interactions with the negatively charged resin, and therefore, separates molecules based on charge. Negatively charged and neutral compounds will elute from the column prior to the application of a gradient because they will not adsorb to the resin. It was expected that the conjugates would elute prior to the wildtype because PEG is neutral and known to exhibit a shielding effect on molecules it is attached to[39,42,181]. This shielding effect can, and has, been used to make molecules soluble in solutions they would otherwise be insoluble in[42]. Furthermore, ion-exchange chromatography has also been utilized to separate conjugates of different sizes based on the number of attached PEG chains[42]. Therefore, it was reasonable to hypothesize that the PEG conjugates made herein would elute prior to the wildtype protein from an ion exchange column.

4.4.2. Polymer Modification

4.4.2.1. Synthesis of 2-(2,5-dioxo-2,5-dihydro-1H-pyrrol-1-yl) propionic acid (Maleimide acid)

Maleimide acid was synthesized as reported previously[182,183]. Typically, maleic anhydride (9.8 g, 0.1 mol) and β-alanine (8.9 g, 0.1 mol) were dissolved in acetic acid (200 mL) under constant stirring in a nitrogen atmosphere for 16 hr. The mixture was refluxed for 8 hr, followed by removing the acetic acid under vacuum. The crude product was further purified using the flash column (CH2Cl2 as the eluent): (4.25 g, 25.1 mM yield 25.1%), 1H NMR (400 MHz, Chloroform-d) δ 6.74 (s, 2H), 3.86 (t, 2H), 2.73 (t, J = 7.2 Hz, 1H).

4.4.2.2. Methoxypolyethylene glycol maleimide (mPEG-Maleimide)

mPEG-OH (5K or 1.9K m.w.; 0.6 mmol), maleimide acid (0.54 g, 3 mmol), and 4-dimethylamino-pyridine (0.1 g, 0.6 mmol) were dissolved in 100 mL anhydrous DCM at 0 ºC. DCC (0.74g, 3.6 mmol) was then added into the mixture under nitrogen atmosphere for 2 hr at 0 ºC. The reaction was kept at room temperature for another 46 hr and the cured product filtered to remove the formed precipitate, dicyclohexylurea (DCU). The filtrate was concentrated to ~ 30 mL and further precipitated in 300 mL cold ether twice to remove unreacted chemicals. The purified products were dried under vacuum for 24 hr. For mPEG5k-maleimide, the yield is 90%, 1H NMR (400 MHz, Chloroform-d) δ 6.73 (s, 2H), 3.72 (t, 2H), 3.67 (s, 457H), 2.62 (s, 2H). For mPEG1.9k-maleimide, the yield is 76%, 1H NMR 1H NMR (400 MHz, Chloroform-d) δ 6.73 (s, 2H), 3.72 (t, 2H), 3.67 (s, 167H), 2.62 (s, 2H).

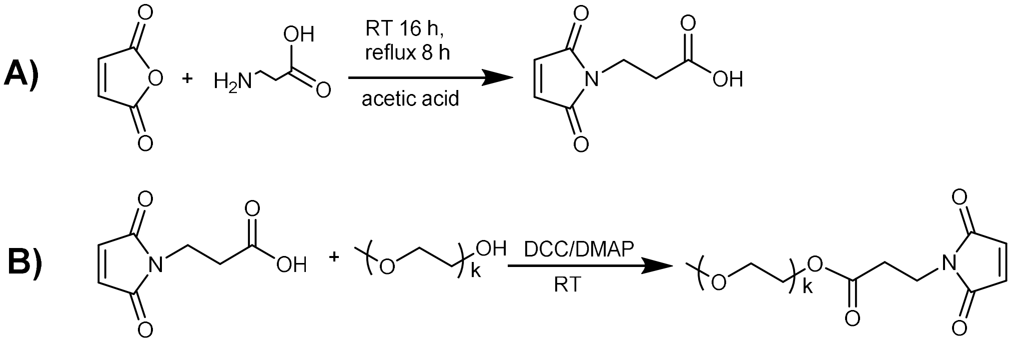

Scheme 4.1. Synthesis of maleimide acid (A) and mPEG-maleimide (B)

4.4.3. T4L Expression and Purification

T4-lysozyme mutants of 44C, 65C, 72C, 89C, 131C, and 151C were prepared as described before[40,77,82,83]. Briefly, vectors of these mutants were generated by QuikChange site-directed mutagenesis of the pET11a-T4L construct containing the pseudo-wild-type mutations C54T and C97A, followed with verification of each mutation by DNA sequencing. These mutants were expressed, purified using an ion-exchange column, and stored at 4C until being desalted for conjugation. The secondary structure and catalytic function of the resultant mutants are shown to be indistinguishable from the wildtype protein in Appendix Figures A1 and A2.

4.4.4. Preparation of PEGylated lysozyme

The T4L samples collected from the ion-exchange purification contained DTT to prevent the formation of disulfide bonds between the proteins. The complete removal of the DTT and immediate addition of polymer is essential to ensure successful conjugation. The T4L samples were applied to a HiPrep 26/10 desalting column to ensure complete removal of DTT using buffer containing 50 mM MOPs, 25 mM NaCl, pH 6.8. Each polymer was immediately added to each of the 6 the desalted protein samples, one at a time, in a 100:1 polymer: protein ratio. The solution was allowed to nutate at room temperature overnight.

4.4.5. Separation

Separation was completed by applying the protein-polymer overnight solution to a HiTrap SPHP 5ml cation exchange column using two buffers as described in the literature[40,82,83,93]. In brief, the percent of low salt and high salt buffers, Buffer A (25 mM Tris-Base, 25 mM MOPS, and 0.1 mM EDTA at pH 7.6) and Buffer B(25 mM Tris-Base, 25 mM MOPS, 1M NaCl, and 0.1 mM EDTA at pH 7.6), respectively, was adjusted to induce elution. The overnight protein-polymer solution was applied to the column with a flow rate of 5 ml/min. The buffer was held 0% B until the first peak had completely eluted and the baseline stabilized. Once the baseline had stabilized, the proteins and conjugates were eluted with a gradient of 0-30% B over 15 min. Each peak was collected, and the identity verified using gel-electrophoresis. It was found that the polymer eluted at 0% B and the conjugates eluted from the column at a lower salt concentration than the wildtype, which typically eluted between 18 % and 25 %.

4.4.6. Sodium Dodecyl Sulfate Polyacrylamide Gel Electrophoresis (SDS-PAGE)

SDS-PAGE was used to determine the purity of the conjugates. Generally, 10 μL of purified conjugate and 2.5 μL Loading Buffer were mixed in a 1.5 mL Eppendorf tube. The mixture was boiled at 95C for five min, loaded into Bio-Rad Mini ROTEAN TGX 4−20% gradient gels, and run at 120 V for ~70 min. Gels were stained with the GelCode Blue protein stain for 2 hr and de-stained using overnight using buffer of 10 %glacial acetic acid, 70% deionized-distilled (DD) water, and 20 % methanol.

4.4.7. Activity of Conjugates

The activity of T4L and T4L-PEG conjugates was measured using a commercial lysozyme activity kit (Micrococcus lysodeikticus, ATCC No. 4698, Sigma-Aldrich). The Micrococcus lysodeikticus cell walls absorb at 450 nm and the decrease in optical density at 450 nm (OD450) is directly related to the amount of cell wall degradation by lysozyme. The OD450 after the addition of 10 µL of a 1.24 mg/ml solution to Micrococcus lysodeikticus cells suspended in pH 6.8 phosphate buffer was measured and recorded at 0, 5, and 10 seconds, then every 10 seconds for 5 min. The data were plotted and the linear range in the first 30 seconds was used to calculate the activity.

4.4.8. UV Spectra

UV spectra were obtained with the NanoDrop UV-vis spectrophotometer (Thermo Scientific ND-2000 C) at the Core Biology Facility of Department of Chemistry and Biochemistry,North Dakota State University (NDSU).

4.4.9. Circular Dichroism (CD)

CD data were obtained with Jasco J- 815 spectropolarimeter at the core facility of Department of Pharmaceutical Sciences, NDSU. The wavelength range used was 260 to 200 nm. Typical sample volume and concentration were 300 µL and 10 µM, respectively. The baseline of each sample was corrected using DD water and the data normalized. The differences in helical content between hybrids and the wild type protein as estimated based on the mean residue ellipticity at 208 and 222 nm are on the order of ~6 % (or ~1-2 helical turn).

4.5. Results and Discussion

4.5.1. Conjugate Preparation and Purification

To separate the conjugates from unreacted/dimerized protein and polymer, the overnight solution was applied to a cation exchange column, each elution peak collected, and the identity verified using gel electrophoresis (details in method section). A representative purification profile is shown in Figure 4.1A, where a conjugate of PEG 1.9K attached at the 65C position (designated as 65P1.9K; other PEGylated mutants are named similarly throughout the remainder of this text) is separated from the unwanted species. Figure 4.1B shows the SDS-PAGE results confirming the identity of the peaks.

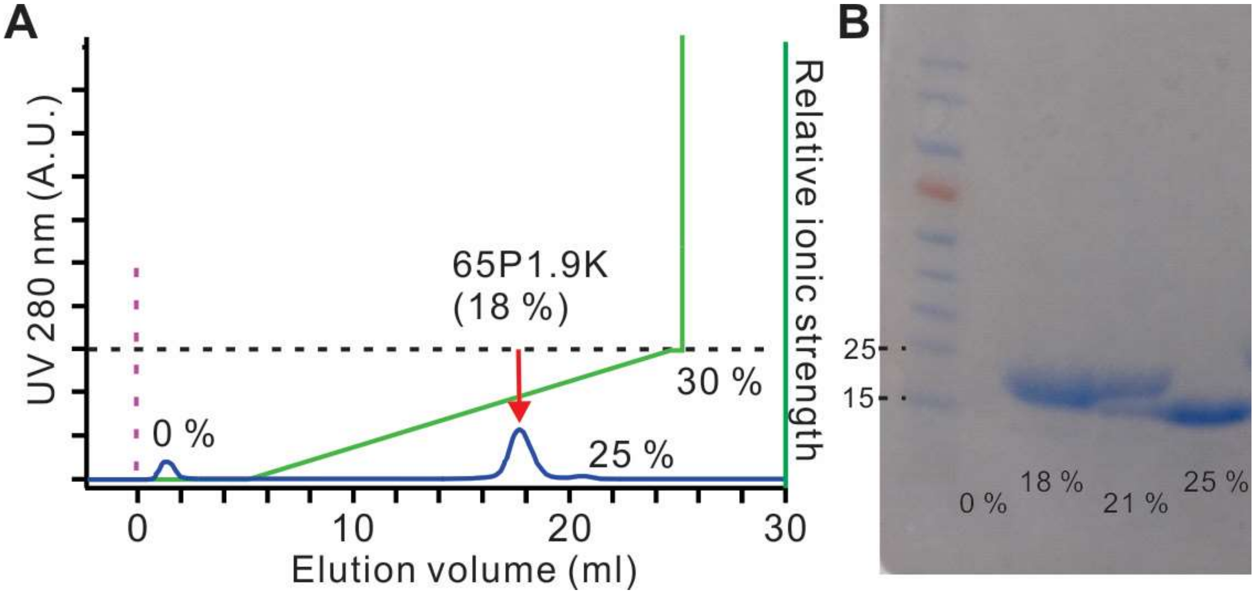

Figure 4.1. (A) The separation of different species after the conjugation of 65C and PEG 1.9K via ion-exchange chromatography. PEG elutes at 0 % while the unconjugated lysozyme elutes at ~ 25 %. The 18 % portion as indicated by the arrow is assigned to the 65P1.9K conjugate elute as confirmed by gel electrophoresis. (B) Gel electrophoresis indicates the successful separation of different components via ion-exchange column.

It was found that the polymer eluted with an average retention time of ~1 min and the conjugates eluted from the column at a lower salt concentration than the unconjugated lysozyme mutant (i.e., ~18 % ionic strength, or, 180 mM NaCl was able to elute 65P1.9K; see Figure 4.1A red arrow); typical ionic strength to elute the unconjugated lysozyme is ~20 – 25 % (200 mM – 250 mM NaCl; Figure 4.1A). Other PEGylated mutants show slightly different profiles (Appendix Figures A3, A4, and A5), but the general trend is similar. Table 4.1 summarizes the elution profiles of the conjugates. It is quantified here that the neutral PEG does indeed reduce the overall charge of the conjugate which leads to a reduced salt concentration necessary for elution.

Table 4.1. Elution percentage of each conjugate formed in this study. On the same conjugation site, the PEG (either 1.9K or 5K molecular weight) that results in a higher charge is bolded.

	44C	65C	72C	89C	131C	151C
PEG1.9K	**10%**	**18%**	**20%**	**10%**	6%	10%
PEG5K	6%	17%	12%	6%	**19%**	**18%**

It was expected was that the 5K polymer would have a greater shielding effect, and thus, all 5K conjugates would require a lower salt concentration to elute as compared to the 1.9K conjugates. As shown in Table 4.1, this hypothesis was incorrect. Most interestingly, the ionic strength needed to elute 131P5K and 151P5K, which are both near the active site, was not lower than their respective 1.9K conjugates. Importantly, the displayed charge differences have potential to effect activity because bacterial cell walls, the substrates of lysozyme, are negatively charged. Alterations in surface charge, especially near the active site, may interfere or repel the negatively charged substrate to result in a lesser activity. Therefore, the conjugates that exhibited greater alterations in surface charge were expected to have correspondingly altered activities. Following the same rationale, it was expected that the conjugates of 44C, 131C, and 151C would exhibit the lowest activities due to the polymer attachment site proximity to the active site and the possibility of the polymer sterically blocking the active site.

The purification method discussed here has potential for applications in commercial hybrid purification due to the versatility of an ion-exchange column which can be manufactured for large-scale production processes. The percent conversion can be calculated using the elution profile which allows for simultaneously purifying the conjugate and monitoring the reaction conditions. Furthermore, the unreacted polymers can be recaptured and reused which can increases the cost efficiency. The recapture of polymer would be significant when working with difficult to manufacture and expensive polymers and proteins.

While it would be ideal to have a conjugation reaction that results in a 100% yield, this is not possible, thus, an efficient purification process is important to the future development of protein-polymer hybrids. The reaction efficiency of the maleimide-thiol reaction can be increased using an anerobic conditions, however, this is difficult to obtain when working with proteins which prefer and aqueous environment and is furthermore unfavorable for commercial production. Another strategy to improve the yield is to carry out the reaction in the presence of TCEP because it does not readily reduce the maleimide-thiol linkage and does not compete with maleimide for interaction with the thiol group. Therefore, TCEP could be left in solution to keep the proteins from dimerizing while still allowing for conjugation. In this study, no consistent statistically significant increase in efficiency was observed with the addition of TCEP, an increase of polymer to protein ratio above 100:1, or an anerobic environment (data not shown).

4.5.2. Conjugate Activity

It was predicted that the activities of all the conjugates would be less than the wildtype due to the polymer sterically hindering substrate access, and correspondingly, the 5K conjugates displaying the least activity due to greater steric hinderance. Additionally, it was hypothesized that conjugates attached nearest the active site (44C,131C, and 151C) would have greater degrees of steric hinderance, and therefore, the least activity. The unanticipated trends discovered during the ion-exchange purification process foreshadowed similarly unpredictable activity results. Surprisingly, the activity prediction that conjugates exhibiting the greatest surface charge reduction (lowest elution %s) would have correspondingly altered activity would prove similarly incorrect.

The activity of the purified conjugates (conjugation sites see Figure 4.2A) was assessed using established procedures (See Methods Section). The activity data collected from each conjugate as well as the wildtype protein is shown in Figure 2B and 2C (for 1.9K and 5K conjugates, respectively). The activity in U/ml of each conjugate was defined as the slope of the linear range of the curves (0 to 30 s) and is presented in Table 4.2. On the same site (but different PEG size), the conjugate of higher activity is bolded in the table for clarity.

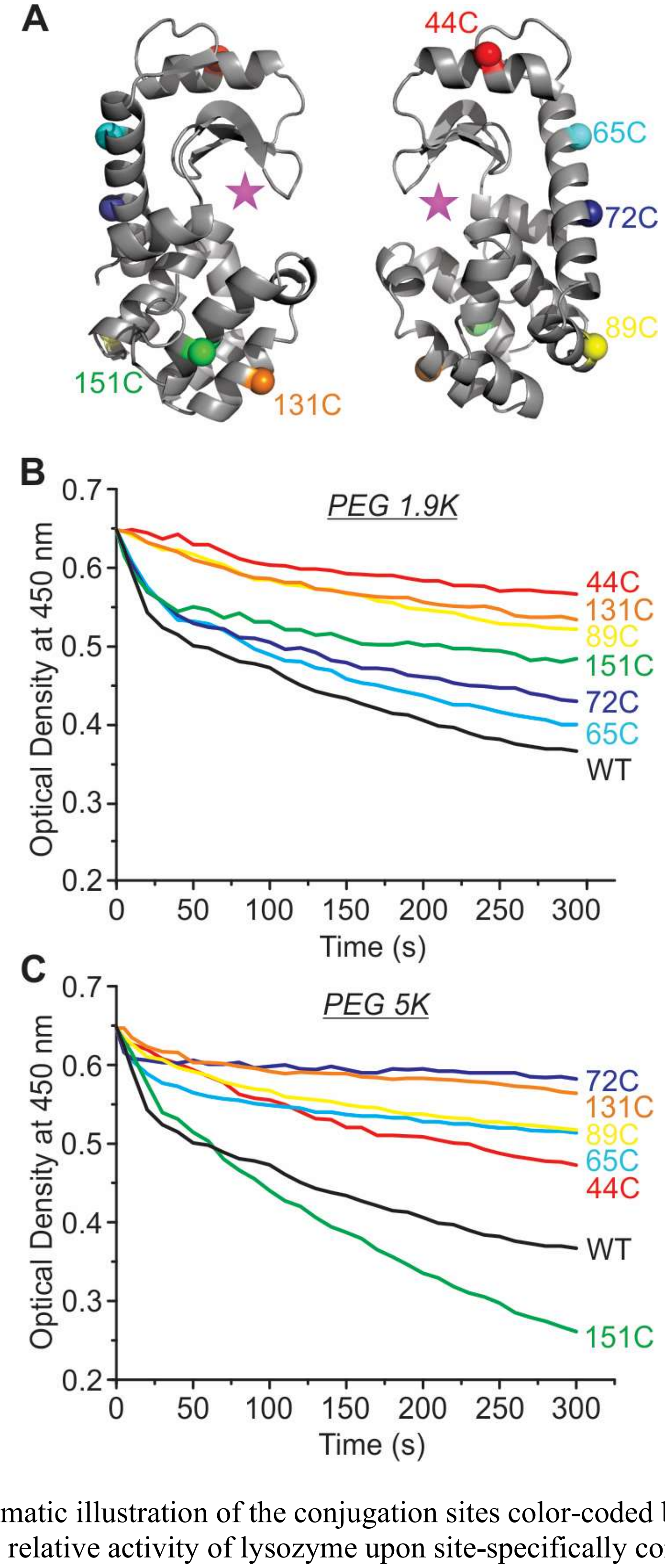

Figure 4.2. (A) Schematic illustration of the conjugation sites color-coded by spheres and the active site (star). The relative activity of lysozyme upon site-specifically conjugated by PEG with 1.9K (B) and 5K (C) molecular weight. The activity of the wildtype enzyme without PEGylation is shown in black (and labeled as WT).

Table 4.2. Quantification of the relative activity of all PEGylated lysozyme mutants. On the same conjugation site, the PEG (either 1.9K or 5K molecular weight) that results in a higher relative activity is bolded. U/ml±0.05.

WT: 4.30	44C	65C	72C	89C	131C	151C
PEG1.9K	0.35	**3.11**	**3.00**	0.86	0.78	2.86
PEG5K	**1.15**	2.17	1.16	**1.37**	**1.11**	**3.62**

Although the factors of steric hindrance and overall surface charge alterations are reasonable basis for predicting relative activity, data in Table 4.2 cannot be explained solely based these factors. For example, the smaller 1.9K PEG should create less hindrance and therefore, yield higher activities as compared to the 5K PEG. However, four out of the six studied sites show the opposite trend. This was especially surprising because there was no correlation between relative catalytic efficiency and the overall charge alteration of the conjugates (see Table 4.1).

Additionally, PEG conjugates of 44C, 131C, and 151C, which are closer to the active site of the protein, should lead to a lower activity as compared to the other sites (Figure 4.2A). However, this trend was not observed either. Furthermore, the 151P5K conjugate had the highest overall activity of the conjugates, being 3.62U/ml, which is comparable to the wildtype activity of 4.30U/ml. Notably, while the 151P5K conjugate had activity lower than the wildtype in the first 30 seconds, at 1 minute the conjugate began to show enhanced activity than that of the wildtype. This finding demonstrates that carefully designed site-specific conjugation can be used to enhance protein activity.

4.5.3. Conjugate Secondary Structure

The surprising activity alterations indicate that there are factors other than steric hindrance and charge alteration affecting conjugate activity. Due to the close structure-function relationship of T4L, the protein secondary structure was probed to seek answers for the activity variation using circular dichroism (CD) spectroscopy. The CD spectra presented in Figure 4.3 shows small deviations in helical content between the conjugates and the wildtype proteins (< 6 %), which is consistent with a small pull of 1-2 turns on an alpha helix. However, the changes in secondary structure are more or less the same for all conjugates and therefore, do not explain the activity trends. This is not surprising because literature shows that PEGylation typically has no large effect on the secondary structure of the attached protein[42,142,152,176].

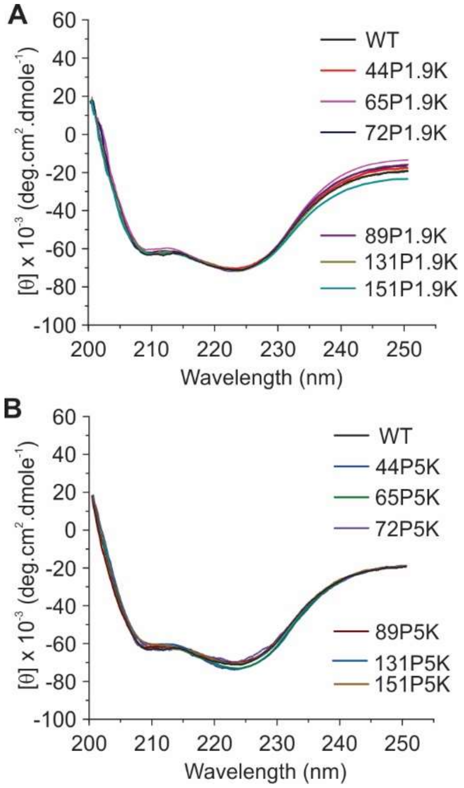

Figure 4.3. The CD spectra of lysozyme upon site-specifically conjugated by PEG with 1.9K (A) and 5K (B) molecular weight. The CD data of the wildtype enzyme without PEGylation is shown in black (and labeled as WT).

4.6. Conclusions

Herein, the synthesis, purification, and activity of 12 hybrids formed from 6 mutants of an antibacterial protein, T4 lysozyme (T4L), and 2 PEGs of molecular weights 1.9K and 5K attached site-specifically was presented. For commercial and biomedical use, purity is of utmost importance. Previously, purification based on the surface charge difference via the ion-exchange column was employed to separate conjugates of different sizes based on the number of attached PEG chains[147,181]. Shown here, a simple conjugate purification methodology is introduced for the effective separation of site-specifically conjugated proteins from unreacted polymers and proteins as well as the recapture and reuse of the latter two. This method is preferential when compared to other common techniques including salting-precipitation and filtration via dialysis or ultracentrifugation. In particular, polymer conjugates commonly salt out at or near where the wildtype does, which makes it hard to separate the conjugate from unreacted protein as well as any contaminants that may be trapped in the precipitation process. Furthermore, the salted-out protein must then be reconstituted, and excess salt removed from solution which adds extra steps to the purification process. Filtration based on size can be a good tool for purification of conjugates, however, for this study, the size difference of 1.9K and 5K was not sufficient to separate the conjugate from wildtype protein.

The site-specific activity alterations of the conjugates displayed no clear trend that followed predictions based only on steric hinderance and charge effects. Yet, the CD data asserted that the activity alteration was not due to large-scale changes in protein structure. This indicates that there are other factors, likely changes in protein dynamics (such as the hinge-motion of T4L) that are providing large contributions to the activity alterations observed herein. This supposition is aided by the purification process used which provided specific numbers for the surface charge alterations. Additionally, 151P5K was able to increase the activity of the protein which is a promising result for the future development of enzymatically-active materials with enhanced catalytic features.

The rationale underlying the surprising results found herein should be further investigated for improved rational design of future protein-polymer hybrid materials. One tool that can shed light on the molecular-level interactions between the polymer and protein surface as well as protein dynamics is molecular modeling. A collaboration with a computational biophysics and soft materials group that studies PEG has been established to further probe the hybrids discussed herein. In brief, the preliminary simulations show enhanced conformational dynamics for 151P5K which accounts for the activity enhancement[2]. The full details of these findings will be released in a published paper. Another future direction of this project is to utilize EPR spectroscopy to study the changes in protein dynamics upon site-specific conjugation.

---

[2] Data obtained from the group of Dr. Coray Colina from the University of Florida and her student Dr. Aravinda Munasinghe.

5. SHORT AND SWEET: A SYSTEMATIC APPROACH TO SIMPLIFIED SOD1 PRODUCTION SUITABLE FOR RESEARCH AND TEACHING

5.1. Abstract

Superoxide Dismutase (SOD) is an antioxidant enzyme important for maintaining safe levels of reactive oxygen species (ROS). Harnessing the natural antioxidant power of SOD is desirable for the prevention and treatment of diseases that cause, or are caused by, oxidative stress[184]. The Cu/Zn containing human Superoxide Dismutase 1 (SOD1) produced in this chapter is also important for research into treatments of amyotrophic lateral sclerosis (ALS), which is a disease characterized by degeneration of motor neurons and subsequent death. 10% of ALS cases are familial and result from deposits of mutated aggregation-prone SOD1. The production of SOD1 mutants (particularly ALS mutants) is difficult due to the increased aggregation propensity. In this chapter, an expression and purification protocol for soluble SOD1 is developed that has minimal steps and can be done at low-cost, making it accessible for both research and teaching laboratories. The systematic approach taken to create the procedure can be followed to tailor production of other proteins and mutants that may be even more prone to aggregation.

5.2. Introduction

Oxidative stress is involved in many disease states, including cancer, diabetes, and neurodegenerative conditions[26,27,29,31]. Oxidative stress occurs when more reactive oxygen species (ROS) are generated than antioxidant defenses can handle. While ROS can come from outside sources, they are also generated during normal metabolic processes such as the mitochondrial energy production pathway[29]. Antioxidant enzymes are an integral part of preventing the ROS from oxidizing essential macromolecules like DNA, protein, and lipids[26].

Superoxide dismutase (SOD) is a powerful antioxidant enzyme responsible for the dismutation of two superoxide anions to less hazardous hydrogen peroxide and molecular oxygen. It is an especially important enzyme because dismutation is the first step in the detoxification process of superoxide anions in cells[26,185]. As a metalloenzyme, it requires a metal cofactor to catalyze the reaction. Various isoforms of SOD exist in both prokaryotes and eukaryotes with different metal cofactors. The typical cofactors are iron(Fe), zinc(Zn), copper(Cu), and manganese(Mn). Cu/Zn-SODs are predominant in eukaryotes and can be found in almost all human tissues[26,28,184].

The widespread distribution of the SOD enzymes and the importance of keeping ROS at optimal levels underpin why a lack of SOD is observed in many pathologies (in both humans and animals)[29,30,186]. In addition, natural levels of SOD decreases and free radical formation increases with age, thus contributing to the natural aging process[27,29]. SOD has also been shown to exhibit protective effects against irradiation, carcinogenesis, and apoptosis[27,29,31]. Therefore, a large body of research dating back to the 80's focuses on administering SOD as a supportive therapy, precautionary measure, or anti-aging supplement[27]. However, this research was greatly slowed in 1991 when bovine SOD was removed from the market[27]. Due to advances in recombinant protein production technologies, recombinant SOD can now be expressed and purified from bacterial cells.

Human Cu/Zn SOD1 is a homodimer localized mainly to the intracellular cytoplasmic spaces which has been linked to Familial Amyotrophic Lateral Sclerosis (FALS)[32,187,188]. ALS is a disease caused by progressive motor neuron degeneration that is characterized by stiff muscles, weakness, twitching, and eventual death. FALS cases are caused by different point mutations in the SOD1 gene which produces especially aggregation-prone SOD proteins[32,186,189,190]. Studies have shown that the progression of ALS is not due to a loss of SOD action, but a gain of toxic function[184,191]. Therefore, any strides made in delivering SOD enzymes is not beneficial for treatment of FALS. Instead, understanding the underlying aggregation mechanisms of the mutant SODs is vital for developing therapeutics to prevent or treat this devastating disease. However, the production of the familial ALS mutants is complicated by their aggregation-prone nature.

Using advances in protein production strategies, a simple, easy to follow protocol for producing the SOD mutant: C6A/C111S/V94C, is described herein. The simple and low-cost procedure focuses on maximizing the stability of the protein so it can be purified from the soluble fraction instead of inclusion bodies. The developed protocol is comprised of 4 main steps: 1. Expression in E. Coli, 2. Protein extraction from cells, 3. Separation from lysate using a nickel affinity column, and 4. Cleavage of the His-tag. These steps are followed by the literature technique of adjusting metal stoichiometry, wherein the metals are removed from the protein and then selectively added back in[192,193]. The metal adjustment steps would be unnecessary for proteins without metal centers or for teaching purposes. The systematic approach to developing the protocol can also serve as a guide to produce other SOD mutants (which each have a differing aggregation propensities), intrinsically disordered proteins, or other aggregation prone proteins.

5.3. Materials

5.3.1. Reagents, Chemicals, and Biologicals

The human SOD1 DNA in the pET28b expression vector was provided by Greg Merz at Cornell University. LB media was purchase from MP biomedical supplies. Kanamycin, Novex Tris-Glycine 15% gels, 10x Tris-Glycine buffer, Coomassie blue, and SOD activity kit were purchased from thermofisher. Dialysis tubing with MWCO 6-8kDa purchased from VWR International.

5.3.2. Instrumentation

An ÄKTA fast protein liquid chromatography instrument was used for protein purification. The HisTrap HP 5ml column and Superdex 75 Column were purchased from GE. The Thrombin CleanCleave Kit was purchased from Sigma-Aldrich. UV spectra were obtained with the NanoDrop UV-vis spectrophotometer (Thermo Scientific ND-2000 C) at the Core Biology Facility of Department of Chemistry and Biochemistry, North Dakota State University (NDSU). CD data were obtained with Jasco J- 815 spectropolarimeter at the core facility of Department of Pharmaceutical Sciences, NDSU.

5.3.3. Buffers

Buffers used were as follows: Lysis Buffer (25mM HEPES, 150mM NaCl, 5mM Imidazole, pH 8), Binding Buffer A (25mM HEPES, 150mM NaCl, 20mM Imidazole, pH 8), Elution Buffer B (25mM HEPES, 150mM NaCl, 200mM Imidazole, pH 8), Superdex Buffer (50mM HEPES, 150mM NaCl, pH 8), Thrombin Buffer (50mM Tris-Base, 10mM $CaCl_2$, pH 8), Cell Shock Solution 1 (20% sucrose, 30mM Tris-HCl, 1mM EDTA, pH to 8), Cell Shock Solution 2 (5mM $MgSO_4$), Dialysis Buffer 1 (50mM Acetate, 10mM EDTA, pH 3.8), Dialysis Buffer 2 (50mM Acetate, 100mM NaCl, pH 3.8), Dialysis Buffer 3 (100mM Acetate, pH 3.8), Dialysis Buffer 4 (100mM Acetate, pH 5.5), Dialysis Buffer 5 (50mM HEPES, 20mM NaCl, pH 7.5), 10X Cleavage Buffer (500mM Tris-HCl, 100mM $CaCl_2$, pH 8), Destaining Buffer(10%glacial acetic acid, 70%DDH_2O, 20%methanol).

5.4. Methods

5.4.1. Transformation

The human SOD1 DNA in the pET28b expression vector was provided by the Merz lab at Cornell University. The vector contained Kanamycin resistance, a lac operon for IPTG induction, and a polyhistidine tag with a thrombin cleavage site. The mutant expressed herein contains the following amino acid substitutions: C6A/C111S/V94C. The vector was transformed into Escherichia coli BL21-DE3 cells for expression.

5.4.2. Expression Tests

Expression conditions were designed by varying commonly used literature values for concentrations of IPTG, copper sulfate, and zinc heptahydrate, as well as growth time and temperature. An expression test was conducted by first expressing the protein using the designed conditions and then evaluating expression levels via gel electrophoresis. All conditions were started by using an overnight culture in LB media supplemented with Kanamycin which was added to 50mL of Kanamycin supplemented LB media the next morning. Each condition was then supplemented with copper and zinc as per the condition number and allowed to grow for 2 hours. Copper was added in the form of copper sulfate anhydrous and zinc was added in the form of zinc sulfate heptahydrate. IPTG was then added in the concentration dictated by the condition number and allowed to grow at 25̊C overnight. The optical density of the sample was recorded to evaluate cell growth levels. To evaluate pre- and post-expression contents of cells from each condition, 1ml samples were collected of each sample condition before and after expression and evaluated via gel electrophoresis. The samples were prepared for electrophoresis by centrifugation for 10min at 1500 rcf, resuspension in 500 µL of 1XSDS-PAGE buffer, heating at

95℃ for 5 minutes, and centrifugation for 5 minutes at 1500rcf. The samples were allowed to come to room temperature and then 10µL of each were loaded into the gel.

5.4.3. Expression Solubility Test

To evaluate the ratio of protein in the soluble and insoluble fractions, 2 ml samples were taken after the designated expression time. These samples were spun at 1500rcf for 10 minutes and the supernatant discarded. The pellet was then resuspended with 50 µL of soluble solution (2mM Tris-Base, 2% Triton-X, 0.002% Lysozyme, and 0.05M EDTA) and incubated for 10 min at room temperature. The samples were then spun down at 1500rcf for 10 min and the supernatant moved to a new tube and labeled soluble fraction. 50 µL of 2x SDS-Page buffer was added to the soluble fraction and 100 µL of 1x SDS-Page buffer was added to the pellet, which was then labeled insoluble fraction. The samples were mixed thoroughly by pipetting up and down then heated at 95℃ for 10 minutes. After the heating period, the samples were allowed to come to room temperature before a final centrifugation at 1500 rcf for 10min. 15 µL of each sample was analyzed using gel electrophoresis.

5.4.4. Expression Conditions

A 25mL starter culture was grown in LB media supplemented with Kanamycin at 37℃ overnight. The starter culture was added to 1L LB media supplemented with Kanamycin and 0.25mM $CuSO_4$ and allowed to grow until OD~0.8 (about 2 hours). Expression was then induced by adding 0.3mM IPTG and allowed to go overnight at 25℃. Cell pellets were harvested by centrifugation at 5,000rcf for 30 minutes.

5.4.5. Sonication

The cell pellets were resuspended using lysis buffer, then sonicated at 50% duty cycle on ice for 5 minutes on, 5 off, and 5 on again. The sonicated samples were then spun at 20,000rcf for 1 hour and the supernatant collected. The supernatants were passed through a 0.22 µm filter before application to the nickel column.

5.4.6. Cell Shock

The harvested cell pellet was suspended in Cell Shock Buffer 1 and incubated at room temperature for 10 minutes. The solution was then centrifuged, and the supernatant saved. The pellet was then resuspended in ice-cold Cell Shock Solution 2 and stirred on ice for 10 minutes. The sample was then centrifuged, and the supernatant collected. The two supernatants were then dialyzed into binding buffer for 4 hours at 4°C. The samples were passed through a 0.22µm filter before application to the nickel column.

5.4.7. Nickel Affinity Column Test

The column was first equilibrated by running 50mL of 20% Ethanol solution, 50mL DDH_2O, 50ml Elution Buffer B, and 50mL of Binding Buffer A, in that order, through with a flow rate of 5ml/min. The flow rate was then dropped to 2ml/min and the cell lysate from 4 1L growths injected onto the column. Once the UV 280 returned to baseline, the flow rate was increased to 5ml/min for at least 15ml or until the UV returned to baseline if a UV increase was observed. The protein was then eluted from the column using a 3-step elution from 0%B to 40%B, 40%-60%B, and 60-100%B. Each step was maintained for 15-20 minutes or until the baseline had stabilized after the peak had been collected. The column was then washed in the same way it was equilibrated, but in reverse order, and stored in 20% ethanol. All collected peaks were evaluated for the presence and purity of SOD1 using gel electrophoresis. It was determined that using this elution technique SOD is present along with contamination in all gradient steps. The peaks were then combined together and run through the nickel column for a second time using the same protocol except that the elution was done via one step from 0%B to

100% B. The 100%B elution peak was collected and determined to be of acceptable purity via gel electrophoresis. The sample was then dialyzed into thrombin cleavage buffer overnight.

5.4.8. Nickel Affinity Column protocol

The column was first equilibrated by running 50mL of 20% Ethanol solution, 50mL DDH_2O, 50ml Elution Buffer B, and 50mL of Binding Buffer A, in that order, through with a flow rate of 5ml/min. The flow rate was then dropped to 2ml/min and the cell lysate from 4 1L growths injected onto the column. Once the UV 280 returned to baseline, the flow rate was increased to 5ml/min for at least 15ml or until the UV returned to baseline if a UV increase was observed. The protein was then eluted from the column using a one-step elution from 0%B to 100%B. The peak was collected and applied to the column with the same settings for a second run the same day. The column was then washed in the same way it was equilibrated, but in reverse order, and stored in 20% ethanol.

5.4.9. Thrombin Bead Cleavage

Commercial thrombin beads were chosen and purchased due to their efficiency and ease of use. The concentration of the samples after dialysis into thrombin buffer was determined using UV 280. The procedure supplied with the commercial beads was followed for the cleavage reaction. In brief, 200 μL of a 50% thrombin bead resin suspension was added for every 1mg of protein. This solution was then diluted as needed to obtain a final solution volume of 1mg of protein per mL and allowed to react for 24 hours at room temperature. The thrombin bead cleavage conditions were evaluated by spinning the sample down at 0, 1, 2, 3, 4, 5, 6, and 24 hours and collecting a 20μL sample. These samples were then evaluated using gel electrophoresis. Cleavage for 4 hours at room temperature was determined to be sufficient for most purposes. After cleavage, the thrombin bead resin is collected via centrifugation, washed, and then stored as a 50% suspension as outlined in the established protocol.

5.4.10. Dialysis

The SOD reconstitution protocol used for this study is as follows. The samples were dialyzed against 1L of dialysis buffers 1-4 sequentially for at least 4 hours each at 4℃. Concentration was calculated using UV 280 and 40-fold molar excess of $ZnSO_4$ added to the beaker then left overnight at 4℃. The next day, 40-fold molar excess of $CuSO_4$ was added for 4 hours at 4℃. The protein was then dialyzed against 1L of dialysis buffer 5 for 4 hours at 4℃ prior to collection.

5.4.11. Characterization

Presence and purity of SOD was evaluated using sodium dodecyl sulfate polyacrylamide gel electrophoresis (SDS-PAGE). Typically, 10 µL sample and 3 µL LDS Sample Buffer were mixed in a 1.5 mL Eppendorf tube. The mixture was heated at 95℃ for five minutes to denature the proteins, then loaded into the Novex Tris-Glycine 15% gels and run at 120 V for ~60-120 mins. Gels were stained with Coomassie blue stain for 2 hours then de-stained using the de-staining buffer overnight. Protein concentration was calculated using A280 and extinction coefficient of 10,800. CD wavelength range used was 260 to 200 nm. Typical sample volume and concentration were 300 µL and 10 µM, respectively. The baseline of each sample was corrected using DD water. Activity was assessed using an SOD activity kit. In brief, xanthine oxidase, WST-1 solution, and SOD 1 were added together and the absorbance at 450nm monitored. Xanthine oxidase produces superoxide anions that interact with WST-1 to produce formazan dye, which absorbs at 450nm. The activity of SOD is measured by the percent inhibition of the formazan dye formation. The greater the activity of SOD, the smaller the absorbance at 450nm will be. The activity units are calculated by finding the percent inhibition as compared to the uninhibited standard.

5.5. Results and Discussion

Despite large advances in protein production strategies, many aggregation-prone proteins remain challenging to produce[30,194,195]. For recombinant production, the process can be carefully designed and adjusted as needed[7,195,196]. Aggregation-prone proteins are typically more sensitive to changes in solution and require more specific conditions to maximize stability[196]. Many factors such as design of expression vectors, bacterial host strains, expression conditions, and purification system greatly affect the degree of protein aggregation[196]. By screening conditions systematically at each step, a procedure can be developed that minimizes aggregation to produce larger amounts of soluble protein. Herein, each step is systematically adjusted for an aggregation-prone metal-containing protein, namely, human Cu/Zn SOD1.

5.5.1. Expression System Design

The BL21 DE3 cells were chosen because they have been shown to be good for SOD expression[197], but other cell lines may be better for other types of proteins. E. Coli is generally a good expression system because it grows easily in culture, is non-toxic, and is cheap, which makes it suitable for use with undergraduate students. For some proteins, the vector may need to be adjusted to include chaperones and/or fusion partners, or even change codons[195]. However, vector design was not carried out here because the vector was obtained from the Merz group[192,193].

5.5.2. Expression Conditions

Expression is a key step in the recombinant protein production pipeline that is especially troubling for aggregation-prone proteins which are commonly sequestered into inclusion bodies[196]. The process of aggregation is a complex interplay between many factors, some of which are intrinsic to the protein, such as self-association/nucleation, which can occur from native or non-native conformations[196]. However, aggregation can be minimized at the expression step by adjusting conditions such as inducer concentration, temperature, time, and media composition. While aggregated proteins can be purified out of inclusion bodies, soluble protein expression is preferential in most cases because it provides a simpler purification scheme.

The general rule for preventing aggregation is to lower the concentration of the protein in solution and prevent any localized areas of higher concentration. The addition of an inducer to the cell culture initiates protein production. The quicker protein production is, or the longer it goes, the opportunities for aggregation increase. Inducer concentration effects mRNA production; the local concentration of the mRNA influences the local concentration of elongating peptides, and consequently, localized protein concentrations[196]. Slowing down elongation rate by reducing temperature and using a lower inducer concentration allows time for diffusion which can prevent localized areas of high concentrations, as well as allow time for proper folding and chaperone interactions.

However, there is a fine line between appropriately low concentration and temperature and too low. While too much inducer can cause aggregation, too little inducer will cause insufficient protein production. Similarly, too low of a temperature will negatively affect cell growth and reduce protein yield. Therefore, temperature must be high enough for the cells to continue producing, but low enough to prevent or minimize aggregation. To compensate for the lower induction rate and temperature, induction time can be elongated, but should not be so long that protein concentration reaches aggregation levels. Consequently, optimizing protein production rate by adjusting inducer concentration, time, and temperature can have a large effect on the net yield of soluble protein. Generally, for aggregation-prone proteins, lower temperatures and inducer concentration combined with a longer induction time yields less aggregation[196].

Another factor to consider is media composition because it provides nutrients for the cells to grow and the materials for producing proteins. Generally, commercially bought media is more than sufficient for producing recombinant proteins, but for a metallated protein such as SOD, the media might need to be supplemented. Luria Broth contains some metals including copper and zinc, but it may not be a high enough concentration when it is being incorporated into the recombinant protein. However, high levels of metals can inhibit bacterial growth, and therefore, negatively impact expression[196]. If the concentration of the metal isn't high enough to fill the proteins as they are produced, they are more likely to misfold and nucleate aggregation. For these reasons, it is vital to ensure there is enough metal to make a stable protein, but not so much that it inhibits bacterial cell growth.

To identify the expression conditions that result in an optimal amount of soluble protein for this construct and mutant, an expression test was run. Expression conditions from published papers on superoxide dismutase were compared, with special emphasis on human SOD and on E-Coli systems, and commonly used values selected for this study[188,192,193,197–199]. Special emphasis was placed on varying metal concentrations, which is unnecessary for non-metalated proteins. The 6 conditions that were tested are shown in Table 5.1.

Table 5.1. Expression conditions.

Condition Number	IPTG Concentration	Cu Concentration	Zn Concentration	Optical Density at 600 nm
1	0.3mM	0.25mM	0	1.09
2	0.3mM	0.25mM	0.05mM	0.947
3	0.3mM	1mM	0	0.344
4	0.3mM	1mM	0.05mM	0.423
5	0.5mM	0.25mM	0	0.404
6	0.5mM	1mM	0.1mM	0.341

All conditions were expressed as per the protocol in the methods section using the values listed here. In brief, an overnight culture was added to LB media supplemented with Kanamycin and the metals. After 2 hours of growth at 37̊C, a sample of each was saved, and the IPTG added. The cells were left overnight at 25̊C, optical density (OD) at 600nm recorded, and a sample saved. The before and after induction samples were run on a gel to compare the relative expression levels for the conditions. This gel is shown in Figure 1.

By comparing OD600 values, some conclusions about overall cell growth can be made because optical density at 600nm is dependent on cell concentration. As seen in Table 5.1, the cell concentration generally decreases as the metal concentration is increased, indicating that cell growth was inhibited as expected. It is also observed that a higher level of IPTG also decreased cell growth. This observation can be attributed to the fact that induction reallocates cell machinery from growth to production. To assess overall protein production, samples of pre- and post-induction for each condition were run on a gel which is shown in Figure 5.1.

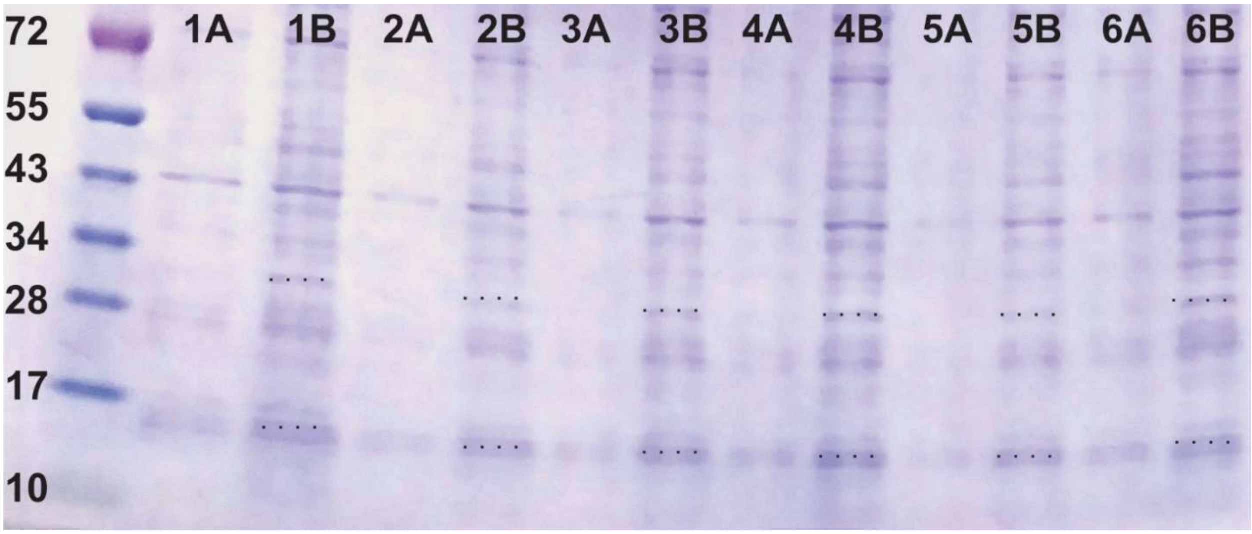

Figure 5.1. Gel of pre- and post-induction. Lanes are labeled by condition number, with pre-induction labeled as A and post-induction labeled as B. Conditions are as follows: 1- 0.3mM IPTG, 0.25mM Cu,2- 0.3mM IPTG, 0.25mMCu, 0.05mM Zn, 3- 0.3mM IPTG, 1mM Cu, 4- 0.3mM IPTG, 1mM Cu, 0.05mM Zn, 5- 0.5mM IPTG, 0.25mM Cu, 0.1mM Zn, and 6- 0.5mM IPTG, 1mM Cu, 0.1mM Zn. Relevant bands of ~32kDa representing SOD dimers and ~16kDa representing monomers are marked with dots. Here we see that conditions 1, 4, and 6 have the highest concentration of SOD.

The human Cu/Zn mutant in this paper is a homodimer of 16kDa monomers. Generally, in an SDS-PAGE gel it is expected that any dimers would be broken into monomers, and thus, it is expected that the 16kDa band is the SOD. However, we also see a band around 32kDa that is not present in the pre-induction cells, indicating that there might be some dimers that were not fully reduced. It was hypothesized that the band at 32kDa may represent unreducible insoluble dimers from aggregates or inclusion bodies. This gel shows a small band in the 16kDa region prior to expression, which could be from a native protein or from leaky expression. It was expected that the SOD bands would be light because, according to literature, it is typical for recombinant SOD to account for around 10% of the total expressed protein[188,199–201].

Comparing the expression conditions from Figure 5.1, it is observed that conditions 1, 4, and 6 had the darkest bands, indicating those conditions were the best for expression. Interestingly, the relative darkness of the bands did not follow the trend of OD numbers which asserts that the optical density cannot be used to make conclusions about protein expression levels. However, a better expression does not necessarily mean more soluble protein, especially in the case of aggregation-prone proteins. To probe which conditions resulted in the highest amount of soluble protein, the post-induction samples were processed to separate the soluble and insoluble fractions as described in the methods section and evaluated using gel electrophoresis (shown in Figure 5.2).

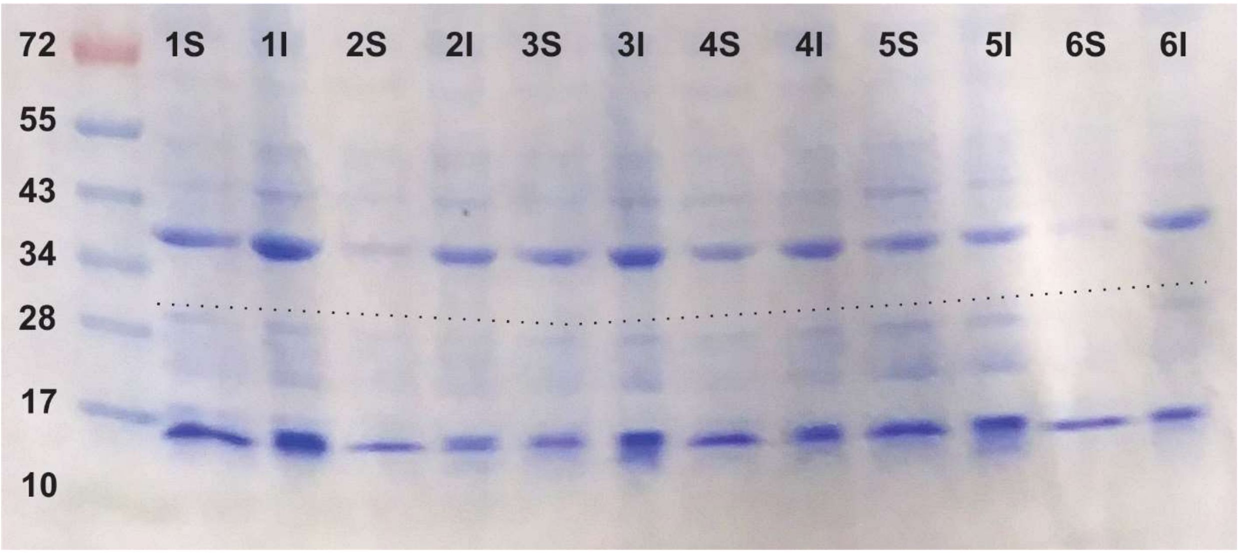

Figure 5.2. Soluble Vs. insoluble gel test. Lanes are labeled by condition number with S for soluble or I for insoluble. Conditions are as follows: 1- 0.3mM IPTG, 0.25mM Cu,2- 0.3mM IPTG, 0.25mMCu, 0.05mM Zn, 3- 0.3mM IPTG, 1mM Cu, 4- 0.3mM IPTG, 1mM Cu, 0.05mM Zn, 5- 0.5mM IPTG, 0.25mM Cu, 0.1mM Zn, and 6- 0.5mM IPTG, 1mM Cu, 0.1mM Zn. Notable 16kDa bands are clearly observed and the ~32kDa line where the dimer would sit has been highlighted with a dotted line across the gel.

As shown in Figure 5.2, the band around 32kDa, which is highlighted using a dotted line, has all but disappeared. This fits with the hypothesis that the thick band at 32kDa from Figure 5.1 was from aggregated dimers which are broken apart during the solubilization steps. Condition 1 clearly had the most soluble protein. Furthermore, condition 1 produced good cell growth as evidenced by the optical density shown in Table 5.1, and therefore, was chosen as optimal for this mutant. From Figure 5.1, conditions 1, 4, and 6 were identified as the conditions with the best overall expression. Figure 5.2 illustrates the point that while expression may appear better for some conditions, the expressed protein may not be soluble. The insoluble proteins will not purify using soluble protein techniques, and thus, the yield will be drastically lower than anticipated.

Herein, expression conditions were screened for soluble recombinant protein levels. However, the same tests could be used to select for conditions that maximize the amount of insoluble proteins which can be purified from inclusion bodies. Inclusion body purification can be challenging because it typically requires the protein to be unfolded entirely or in part during the purification. SOD has been successfully purified in high yield amounts from inclusion bodies[197,202]. If this route is desired, the same expression tests could be run to identify conditions that give the most insoluble proteins with minimal cell death. For proteins where aggregation is not anticipated or suspected, the solubility screening is unnecessary.

5.5.3. Purification Conditions

With aggregation-prone proteins, the challenges do not stop after successfully expressing soluble protein. Aggregation can happen at any point in the purification process. Similar to expression, a lower temperature and concentration of the protein can mitigate the aggregation process. However, unlike expression, a longer time allows more opportunity for the nucleation process, so purification should be carried out as quickly as possible.

In addition, the choice of buffers used during purification is vital to maintain solubility. Changes in pH and salt concentration can be used to precipitate proteins out of solution, but these conditions should be avoided when maintaining soluble proteins is the goal. Another factor that may nucleate aggregation is stresses to the system such as changes in pH, temperature, agitation, and contact with different surfaces. To prevent aggregation, system stresses and changes should be minimized. Therefore, focus is placed on a quick and efficient means of purification herein.

5.5.4. Extraction

Cell lysis can have some impact on the net yield of proteins, but is generally a standard step that does not require fine-tuned optimization[196]. A common method of extraction is cell lysis using sonication to procure a cell lysate that contains the contents of the cells. However, for SOD1, the protein is often localized primarily in the periplasm of the E. Coli cells, and thus can be extracted using a cell shock method[188,200]. Sonication can cause denature proteins and lead to protein misfolding, which gives further opportunity for aggregation which is not present in the cell shock method. The denaturing effect of sonication is often utilized to break apart inclusion bodies so that the protein may be solubilized and purified[202,203].

Extraction by cell shock is advantageous because it extracts the proteins in the periplasm without releasing the entire contents of the cell. It also keeps the membranes largely intact, and therefore, the extraction contains less cellular debris and contaminant proteins, such as proteases that can degrade the protein, which minimizes interactions within the solution that may nucleate aggregation and/or degrade the protein. To evaluate the merits of the extraction methods for the purification of this SOD mutant, both were carried out as described in the methods section then run through the nickel affinity column. The samples were evaluated using gel electrophoresis which will be discussed later and are shown in Figure 5.3.

5.5.5. Nickel Column Purification

Affinity chromatography allows for an efficient one-step isolation of a tagged molecule from a solution[203]. In the case of proteins, purification using a poly-histidine tag and an immobilized metal affinity column is commonly employed. This approach is advantageous because the small histidine tag typically does not greatly alter the expression or structure of the protein, but allows for specific binding to the column resin[100,204]. Although many proteins have histidine residues, none naturally have 6 in a row, which allows for selection of recombinant proteins from solution. Samples do not need to be concentrated before application to the column and the selective nature of the interaction eliminates the need for further separation steps like ammonium sulfate precipitation or additional columns. Ammonium salt precipitation is another common choice for separation. However, in the case of aggregation prone proteins, the precipitation may nucleate aggregates that may not go back into solution and thus, lower the yield[196].

While immobilized metal affinity columns have advantages, they have drawbacks as well. The metal affixed to the resin leaches off in harsh conditions as well as over time. Extra metal in solution is particularly troublesome when working with a metallated protein, such as SOD 1, because the metal can compete for binding in the active site. When using mild buffer solutions, the metal leached off is negligible, but still a consideration. In the case of recombinant human Cu/Zn SOD 1, a standard metal removal and then reconstitution is used regardless of purification technique. Because the all metals will be removed and the protein reconstituted, the possibility of metal kicking out or replacing the copper and zinc ions is not a concern.

A common concern with an immobilized metal affinity column is the accessibility of the poly-histidine tag. Sometimes the folding of the protein or interface between dimers can prevent the tag from binding to the column[203]. In this case, unfolding or partially unfolding the protein will expose the tag to the solution where it can bind to the column. Unfolding proteins is not an ideal situation because the re-folding process can be troublesome and result in yield reduction, especially with aggregation prone proteins[196]. However, SOD 1 has been purified from inclusion bodies by unfolding prior to a nickel column[203]. Because unfolding is necessary to remove proteins from an inclusion body, an immobilized metal affinity column is a wise choice for inclusion body purifications. Including a histidine tag on the protein allows for flexibility if the soluble purification proves too difficult and purification from inclusion bodies is necessary.

Immobilized metal affinity columns come in many varieties, and nickel is a common metal choice due to its tight binding to the histidine-tag. Nickel columns have been used for the purification of recombinant SOD1[192,193,203] and the plasmid used here contains a his-tag, so a nickel column was an obvious choice for this study. An automated fast protein liquid chromatography instrument was chosen due to the ability to tightly control flow rate and gradient which allows for more reproducible results. Automated systems also allow for real-time monitoring via UV280 to make informed decisions on what changes can be made to improve the elution. However, a non-automated column could be used as well. A non-automated nickel column would be ideal for a teaching lab due to its low cost and ease of use.

When using a column on an automated system, many different factors can be adjusted, including buffer composition, flow rate, and elution gradient. Incomplete binding to the column results in proteins being eluted in the flow through. The flow rate for loading was set at 2ml/min to give the tag time to bind tightly to the column. The flow rate was increased to 5ml/min prior to elution to dislodge any un-tagged proteins that were stuck in the column through non-specific interactions. First a gradient of 0-100%B was tried over 100 minutes. However, the peaks were shallow and difficult to discern through the baseline shift (data not shown). Several other slow gradients were tried with similar results. Therefore, a step wise gradient of 0-40%B, 40-60%B, and 60-100%B was employed as illustrated in Figure 5.3.

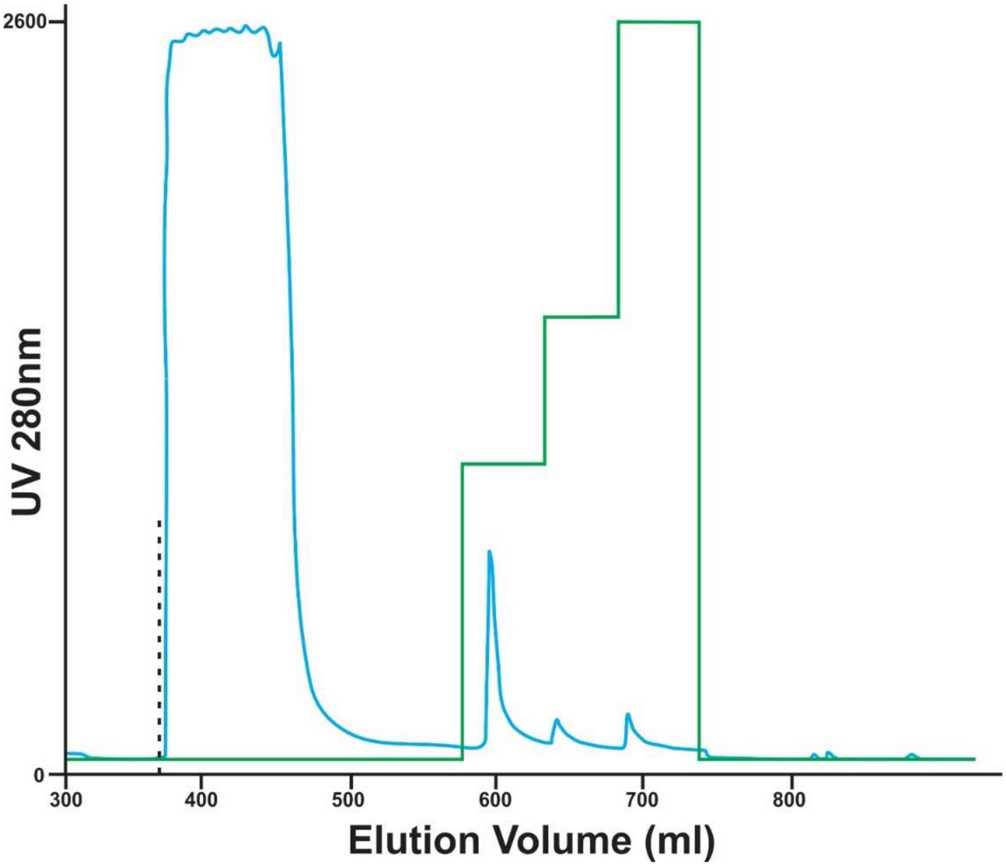

Figure 5.3. FPLC elution graph of sonicated samples. The ultraviolet absorbance at 280nm is plotted using a blue line and represents the concentration of proteins being eluted. The dotted line marks where the sample was injected into the system. The green line traces the percentage of buffer B and the 3 steps represent 40%B, 60%B and 100% B respectively. The buffer compositions are as follows: Binding Buffer A 25mM HEPES, 150mM NaCl, 20mM Imidazole, pH 8) and Elution Buffer B, 25mM HEPES, 150mM NaCl, 200mM Imidazole. The 3 elution peaks are clearly visible in this elution scheme. The peaks were collected and run on a gel which is shown in Figure 5.4.

For the samples extracted using cell shock methods, there was a peak observed only at 100%B, but for the samples extracted using sonication, 3 well-defined peaks were observed as shown in Figure 5.3. Samples of before and after the column and the flow through for each of the extraction methods as well as each peak collected were run on a gel shown in Figure 5.4. For the cell lysis method, the 3 peaks were added together and run back through the column using the same procedure and only a peak at 100% was observed and collected. Samples of the pre-column, flowthrough, and 100% elution of the second run sample were collected and also run on the gel shown in Figure 5.4.

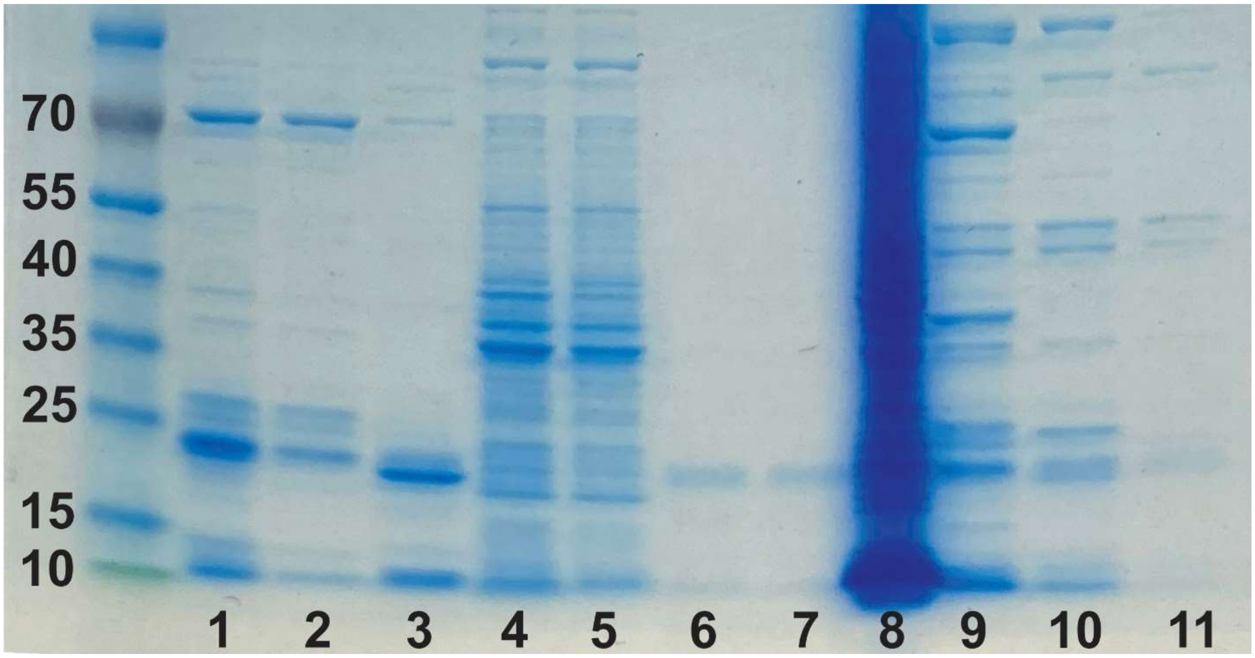

Figure 5.4. Gel electrophoresis of samples evaluating extraction method and nickel column elution purity. The lanes are as follows: 1-second run pre-column, 2- second run flowthrough, 3- second run 100%B, 4- cell shock solution 1 pre-column, 5- cell shock solution 2 pre-column, 6- cell shock buffer 1 100% elution, 7-cell shock buffer 2 100% elution, 8- sonication pre-column, 9- sonication 40%B, 10- sonication 60%B, 11-sonication 100%B. Buffers are as follows: Binding Buffer A 25mM HEPES, 150mM NaCl, 20mM Imidazole, pH 8) and Elution Buffer B, 25mM HEPES, 150mM NaCl, 200mM Imidazole. Samples collected using Cell Shock Solution 1 (20% sucrose, 30mM Tris-HCl, 1mM EDTA, pH to 8) and Cell Shock Solution 2 (5mM $MgSO4$), were both dialyzed into buffer A prior to application to the column. The ladder kDa values are labeled on the left side of the gel. The SOD protein band should appear around 16kDa.

Using the gel results to compare the pre-column content of the extractions procured from cell shock solutions 1(lane 4) and 2 (lane 5) as well as sonication (lane 8), we see that, as expected, the cell shock extractions had a much lower concentration of overall protein. We also see that the 100% B peak for the cell shock methods (lanes 6 and 7) were very pure, but the yield was low. This is expected because there is likely protein inside the organelles which would be extracted using sonication but not cell shock. Additionally, the cell shock method also requires dialysis prior to application to the nickel column which takes at least 4 hours, whereas the sonication method is ready to be applied to the column within an hour. The longer dialysis time allows opportunity for the SOD to aggregate out of solution and interact with any proteases in solution which can lower the yield. The cell shock method also puts the sample through more stresses and steps (changes in buffer, agitation, and contact with more surfaces), which could nucleate aggregation.

As shown from lanes 9, 10, and 11, we see that the sonication elution peaks all contained some SOD and contaminant proteins. The samples from lanes 9, 10, and 11 were combined together and left overnight in the fridge. They were concentrated and washed with binding buffer using a 10,000kDa centrifugal concentrator before re-application to the nickel column. We see in lane 1 that the sample left overnight lost some of the bands that were present in the individual elution lanes 9, 10, and 11. This could be due to proteases in the solution cleaving some of the proteins into smaller segments. Segments smaller than 10,000kDa would have been removed during the centrifugal concentration step. We see that the flowthrough in lane 2 contains some of the SOD protein band, but also many contaminant proteins. Figure 4 lane 3 shows the 100%B elution for the second run samples which has a dark SOD band and a band near 10,000kDa. The dark band around 10,000kDa could be chunks of SOD protein that were partially cleaved by the proteases but still contained the poly-histidine tag which allowed it to stick to the column.

Given the results of the gel, it was determined that the sonication method gave acceptably pure samples when run through the nickel column twice. Therefore, it was determined that the column should be run by employing one step from 0%to 100%B with the entire peak collected and run through the column a second time on the same day to minimize any protease degradation. Since the cell shock method did not provide any enhancements in yield or purity, even when the two solutions were added together, and required more stresses to the system, sonication was chosen as the extraction method for the remainder of the study.

5.5.6. His-Tag Removal

For many applications, the his-tag may be left on the protein. However, in the case of SOD1, the poly-histidine tag must be removed prior to reconstitution because it will capture the metals that are meant for the protein. To remove a tag, a cleavage site can be included in the sequence which will allow for site specific cleavage by proteases. The plasmid was constructed with a thrombin cleavage site, so thrombin was chosen as the protease for cleavage. After the tag has been cleaved, the thrombin and cleaved tag must be removed from solution. A common choice in literature is a Superdex 75 column after thrombin cleavage[192,193]. However, Superdex 75 is an expensive and sensitive column which is not suitable for use with undergraduates or in teaching labs. Therefore, an alternative route was desired.

Some other alternatives to the Superdex column are benzamide or heparin columns which can be used to remove serine-like proteases from solution. Another option is biotynilated thrombin which can be removed from solution with an affinity column that has a streptavin resin. However, commercially available thrombin attached to sepharose beads can be easily removed from solution via centrifugation and reused. The commercial thrombin beads provide simplicity and efficiency that are suitable for research and teaching purposes.

Thrombin beads were chosen because they are easily operable, reusable, and cheap which makes them perfect for use with undergraduate students. After elution from the nickel column, the protein was dialyzed into the thrombin buffer suggested by the handbook (50mM Tris-Base, 10mM $CaCl_2$, pH 8), and the procedure in the methods section followed. The reaction was then allowed to go for 48 hours and samples taken at every hour for 6 hours and then after 24 hours.

Shown in Figure 5.5 is the gel electrophoresis comparison of the timepoints taken during the thrombin bead test. As observed in Figure 5, there was no thrombin contamination in the samples and cleavage was complete in 4 hours. It can also be observed that even after 24 hours there is no great amount of protein cleaved in non-specific locations, which allows for some flexibility with timing.

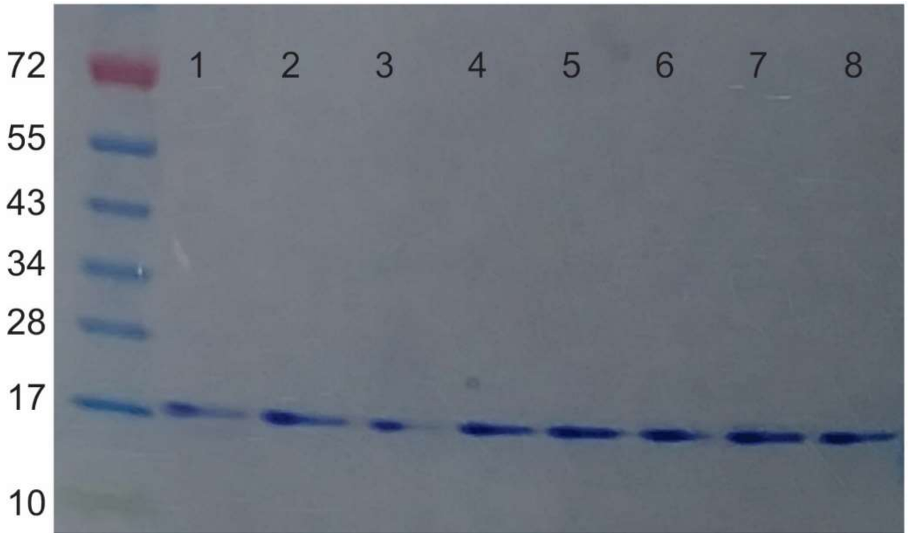

Figure 5.5. Thrombin test. The procedure supplied with the commercial beads was followed for the cleavage reaction. In brief, 200 µL of a 50% thrombin bead resin suspension was added for every 1mg of protein and diluted to obtain a final solution volume of 1mg protein per mL. The reaction left for 24 hours at room temperature. Timepoints were collected by spinning the sample down at 0, 1, 2, 3, 4, 5, 6, and 24 hours and collecting a 20µL sample. These samples were loaded as lanes 1-0hrs, 2-1hr, 3-2hrs, 4-3hrs, 5-4hrs, 6-5hrs, 7-6hrs, and 8-24hrs. Cleavage for 4 hours at room temperature was determined to be sufficient for most purposes.

5.5.7. Dialysis for Protein Reconstitution

The dialysis reconstitution method used for SOD 1 is an important step because it helps adjust the metal stoichiometry to a 1:1 ratio. Zinc must be added first and allowed ample binding time because zinc is more preferential to its own site[193,199]. At pH 5.5, the copper can kick out any zinc that might be occupying its site and binds more quickly. By removing all metals in solution and then adding one molar equivalent of zinc, then an excess of copper we can obtain a sample that is by and large the correct stoichiometry. This method is commonly used with very little alteration, so no attempt was made to optimize the protocol. For other proteins, this step can obviously be skipped, which would further simplify purification.

5.5.8. Characterization

Pure recombinant SOD1 with the histidine tag removed was successfully produced as shown in Figure 5.5. The typical yield using the protocol herein was 1.06±.02 mg of protein was produced for each 1L culture (data not shown). The CD spectra and activity data for the final SOD1 protein were obtained and are shown in panels A and B, respectively, of Figure 5.6. As shown in Figure 5.6 panel A, the CD of the recombinant protein resembles the wildtype[205]. To further investigate the protein produced, the activity was measured using a standard procedure as outlined in the methods section. The activity results are shown in panel B of Figure 5.6. The activity was found to be 79.65±4.57% inhibition of dye formation, which was calculated to equal 272U/mg activity total.

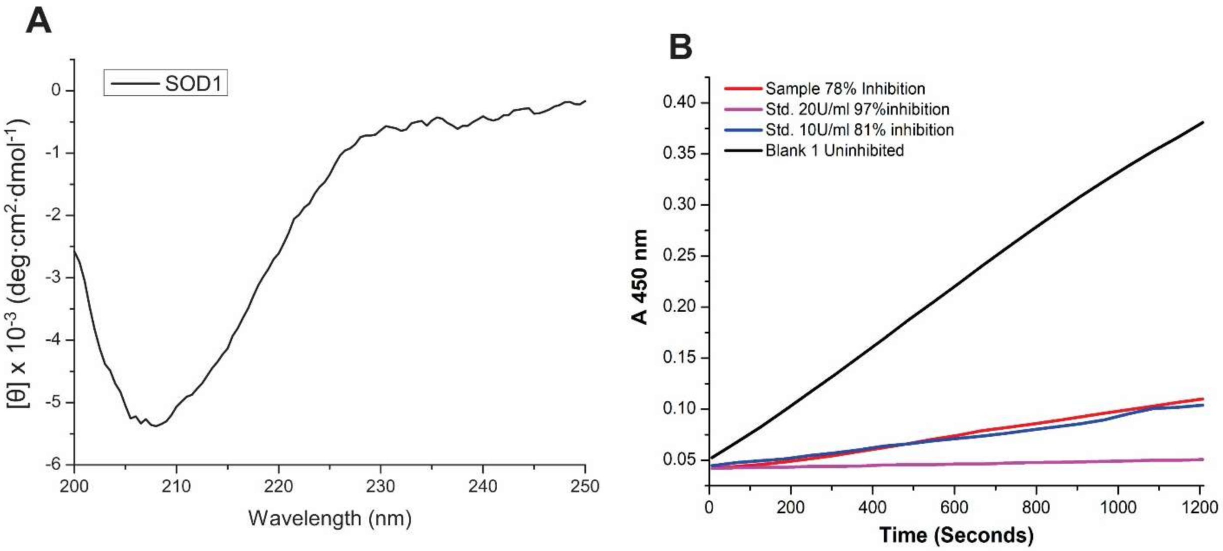

Figure 5.6. SOD1 characterization. CD spectra of the recombinant SOD1 protein shown in panel A. Activity graph obtained from utilizing the commercial activity kit. Activity is monitored via the absorbance of light at 450nm. The oxidation of the dye complex in solution causes absorbance at 450nm. Active SOD inhibits the formation of the dye and therefore, the absorbance at 450nm. The sample, 10U/mg standard, 20 U/mg standard, and Blank 1 are plotted as red, blue, pink, and black lines, respectively.

5.6. Conclusion

Superoxide dismutase is an important protein to study for the prevention and treatment of many diverse diseases. However, the production of recombinant SOD1 is complicated by its aggregation-prone nature. There are many approaches to producing recombinant proteins and herein an approach focusing on keeping the protein soluble throughout the process is presented. The systematic approach to developing the protocol can be generalized and applied to other proteins as well as used in teaching labs. The procedure produces a protein that is pure enough for research purposes while being simple enough to be operated by undergraduate students. The yield of 1.06±.02mg per liter is sufficient for both research and teaching. However, the protocol is not suited for large-scale commercial production. Each FALS mutant displays different aggregation tendencies and the systematic approach can be repeated as needed for each mutant to troubleshoot when a decrease in yield is observed. The approach may also be utilized to screen and select conditions for inclusion body purifications. Future directions of this project include studying the underlying forces relating to the stability of the SOD-1 protein as well as the mechanisms of the aggregation process.

6. CONCLUSION

The work described herein expands the current knowledge of enzymatically-active materials by examining the behavior of an antibacterial enzyme, T4 lysozyme, in two different material systems, specifically, GO/MOF (ZIF and CaBDC) and protein-polymer hybrids (PEG of 1.9K and 5K m.w.). Additionally, a simple 4-step protocol for production of human superoxide dismutase, which is an important antioxidant protein attractive for development of antioxidant materials and therapeutics, is presented. Electron Paramagnetic Resonance spectroscopy is a technique that is especially well suited for studying enzymatically active materials and is utilized in Chapter 3. The fundamental principles behind this structure probing approach are explored in Chapter 2. An understanding of this experimental tool aids in future enzyme structure studies with or without materials.

First, the orientation of T4L within two different GO/MOF composites, one made with GO and ZIF, and the other constructed from GO and CaBDC, was probed using Electron Paramagnetic Resonance spectroscopy. It was found that the orientation of the lysozyme was preferential within the GO/ZIF composite but not within the GO/CaBDC composite. This finding demonstrates that protein orientation, and thus function, could be tuned by varying MOF composition. Furthermore, the composites retained activity against a large substrate and had enhanced acid stability which provides evidence that material properties can be improved using layering techniques.

Next, the site-specific properties of 12 PEGylated T4L hybrids were investigated. PEGs of 1.9K and 5K molecular weights were attached to 6 different locations, one at a time, along the T4L backbone to give 12 total hybrids. The conjugation was achieved by using site-directed mutagenesis to create T4L mutants with 1 solvent-accessible cysteine residue that the PEG was conjugated to using a thiol-maleimide reaction. It was discovered that alterations in surface charge, as evidenced by the ion-exchange purification profile, depended not only on the size of the polymer, but the location as well. The relative charge differences followed no clear trend. Similarly, the respective activities of the hybrids did not align with the charge differences or any other expected trend. The secondary structure of the protein was largely unaltered as evidenced by CD spectra which indicates that the changes in protein dynamics should be investigated to more accurately predict resultant conjugate properties. We, therefore, established a collaboration with a simulation group and found a possible explanation of the high activity of one of the conjugates.

Finally, the systematic approach used to optimize a simplified protocol to produce recombinant human superoxide dismutase 1 (SOD1) is presented. Superoxide dismutase is an antioxidant protein that could be utilized for therapeutics, cosmetics, food preservation, and many other applications. Unfortunately, SOD1 is an aggregation-prone enzyme which complicates the expression and purification process. Additionally, mutations along the superoxide dismutase backbone that induce aggregation are implicated in familial amyotrophic lateral sclerosis, which is a neurodegenerative disease. For future studies, it is desirable to produce the mutated SOD1 proteins to study the aggregation process behind neurodegenerative disorders, as well as for incorporation into materials. The simplified production method of human superoxide dismutase 1 opens the door to future studies of this important antioxidant protein and can be generalized to aid in the design and troubleshooting of other protein productions as well.

The knowledge encompassed herein is one brick to add in process of paving the road to successful development of enzymatically-active materials for a wide variety of applications in drug delivery, biocatalysis, materials science, and protein engineering. The future of these projects has far-reaching consequences across many fields including, but not limited to, the development of multi-enzyme MOF complexes, stimuli-responsive polymer-protein hybrids, and treatments of oxidative stress. There are still many questions to be answered and much work to be done in these areas. Especially valuable results may be extracted by collaborations across all STEM disciplines, including structural biologists, biochemists, material science researchers, physical chemistry experts, and molecular dynamics specialists, to deepen the overall understanding necessary for improvement in these areas and harness the wide-sweeping potentials in this intersection of fields.

REFERENCES

1. Neelam Gurung, Sumanda Ray, Sutapa Bose, and V. R. A Broader View: Microbial Enzymes and Their Relevance in Industries, Medicine, and Beyond. *Biomed Res. Int.* **2013**, 18 (2013).

2. Ellis, G. A. *et al.* Artificial Multienzyme Scaffolds: Pursuing in Vitro Substrate Channeling with an Overview of Current Progress. *ACS Catal.* **9**, 10812–10869 (2019).

3. Bommarius, A. S. & Paye, M. F. Stabilizing biocatalysts. *Chem. Soc. Rev.* **42**, 6534–6565 (2013).

4. Wong, L. S., Khan, F. & Micklefield, J. Selective covalent protein immobilization: Strategies and applications. *Chem. Rev.* **109**, 4025–4053 (2009).

5. Sheldon, R. A. & van Pelt, S. Enzyme immobilisation in biocatalysis: Why, what and how. *Chem. Soc. Rev.* **42**, 6223–6235 (2013).

6. Cao, L. Immobilised enzymes: Science or art? *Curr. Opin. Chem. Biol.* **9**, 217–226 (2005).

7. Muhammad Nazif, A. Maximizing Stability in Industrial Enzymes: Rational Design Approach – A Review. *Am. J. Chem. Eng.* **5**, 135 (2017).

8. Di Cosimo, R., Mc Auliffe, J., Poulose, A. J. & Bohlmann, G. Industrial use of immobilized enzymes. *Chem. Soc. Rev.* **42**, 6437–6474 (2013).

9. Rodrigues, R. C., Ortiz, C., Berenguer-Murcia, Á., Torres, R. & Fernández-Lafuente, R. Modifying enzyme activity and selectivity by immobilization. *Chem. Soc. Rev.* **42**, 6290–6307 (2013).

10. Hermanová, S., Zarevúcká, M., Bouša, D., Pumera, M. & Sofer, Z. Graphene oxide immobilized enzymes show high thermal and solvent stability. *Nanoscale* **7**, 5852–5858 (2015).

11. Vellard, M. The enzyme as drug: Application of enzymes as pharmaceuticals. *Curr. Opin. Biotechnol.* **14**, 444–450 (2003).

12. Hanefeld, U., Gardossi, L. & Magner, E. Understanding enzyme immobilisation. *Chem. Soc. Rev.* **38**, 453–468 (2009).

13. Zhang, Y., Ge, J. & Liu, Z. Enhanced Activity of Immobilized or Chemically Modified Enzymes. *ACS Catal.* **5**, 4503–4513 (2015).

14. Mehta, J., Bhardwaj, N., Bhardwaj, S. K., Kim, K. H. & Deep, A. Recent advances in enzyme immobilization techniques: Metal-organic frameworks as novel substrates. *Coord. Chem. Rev.* **322**, 30–40 (2016).

15. Lysozyme and Its Function. in *Advances in Protein Chemistry* 176 (Academic Press, 1991).

16. Ragland, S. A. & Criss, A. K. From bacterial killing to immune modulation: Recent insights into the functions of lysozyme. *PLoS Pathog.* **13**, 1–22 (2017).

17. Ercan, D. & Demirci, A. Recent advances for the production and recovery methods of lysozyme. *Crit. Rev. Biotechnol.* **36**, 1078–1088 (2016).

18. Hughey, V. L. & Johnson, E. A. Antimicrobial activity of lysozyme against bacteria involved in food spoilage and food-borne disease. *Appl. Environ. Microbiol.* **53**, 2165–2170 (1987).

19. Canfield, R. E. The Amino Acid Sequence of Egg White Lysozyme. *J. Biol. Chem.* **238**, 2698–2707 (1963).

20. Vocadlo, D. J. *et al.* Catalysis by hen egg-white lysozyme proceeds via a covalent intermediate. *Nature* **412**, 835–838 (2001).

21. Phillips, D. C. The hen egg white lysozyme molecule. *Proc. Natl Acad. Sci.* 484–495 (1967).

22. Sarkar, S., Gulati, K., Mishra, A. & Poluri, K. M. Protein nanocomposites: Special inferences to lysozyme based nanomaterials. *Int. J. Biol. Macromol.* **151**, 467–482 (2020).

23. Baase, W. A., Liu, L., Tronrud, D. E. & Matthews, B. W. Lessons from the lysozyme of phage T4. *Protein Sci.* **19**, 631–641 (2010).

24. Poteete, A. R. & Hardy, L. W. Genetic analysis of bacteriophage T4 lysozyme structure and function. *J. Bacteriol.* **176**, 6783–6788 (1994).

25. Matthews, B. W., Remington, S. J., Grütter, M. G. & Anderson, W. F. Relation between hen egg white lysozyme and bacteriophage T4 lysozyme: Evolutionary implications. *J. Mol. Biol.* **147**, 545–558 (1981).

26. Ighodaro, O. M. & Akinloye, O. A. First line defence antioxidants-superoxide dismutase (SOD), catalase (CAT) and glutathione peroxidase (GPX): Their fundamental role in the entire antioxidant defence grid. *Alexandria J. Med.* **54**, 287–293 (2018).

27. Bafana, A., Dutt, S., Kumar, S. & Ahuja, P. S. Superoxide dismutase: An industrial perspective. *Crit. Rev. Biotechnol.* **31**, 65–76 (2011).

28. Mondola, P., Damiano, S., Sasso, A. & Santillo, M. The Cu, Zn superoxide dismutase: Not only a dismutase enzyme. *Front. Physiol.* **7**, 1–8 (2016).

29. Carillon, J., Rouanet, J. M., Cristol, J. P. & Brion, R. Superoxide dismutase administration, a potential therapy against oxidative stress related diseases: Several routes

of supplementation and proposal of an original mechanism of action. *Pharm. Res.* **30**, 2718–2728 (2013).

30. Kim, S. *et al.* Enhancement of potency and stability of human extracellular superoxide dismutase. *BMB Rep.* **48**, 91–96 (2015).

31. Yen, C. C. *et al.* Aerosolized human extracellular superoxide dismutase prevents hyperoxia-induced lung injury. *PLoS One* **6**, 1–9 (2011).

32. DiDonato, M. *et al.* ALS mutants of human superoxide dismutase form fibrous aggregates via framework destabilization. *J. Mol. Biol.* **332**, 601–615 (2003).

33. R, D. & Duncan, R. Polymer therapeutics as nanomedicines: new perspectives. *Curr. Opin. Biotechnol.* **22**, 492–501 (2011).

34. Alconcel, S. N. S., Baas, A. S. & Maynard, H. D. FDA-approved poly(ethylene glycol)-protein conjugate drugs. *Polym. Chem.* **2**, 1442–1448 (2011).

35. Davis, F. F. The origin of pegnology. *Adv. Drug Deliv. Rev.* **54**, 457–458 (2002).

36. Turecek, P. L., Bossard, M. J., Schoetens, F. & Ivens, I. A. PEGylation of Biopharmaceuticals: A Review of Chemistry and Nonclinical Safety Information of Approved Drugs. *J. Pharm. Sci.* **105**, 460–475 (2016).

37. MJ, D. R. & V., Duncan, R. & Vicent, M. J. Polymer Therapeutics-Prospects for 21st Century: The End of the Beginning. *Adv. Drug Deliv. Rev.* **65**, 60–70 (2013).

38. Fordtran, J. S. & Hofmann, A. F. Seventy Years of Polyethylene Glycols in Gastroenterology: The Journey of PEG 4000 and 3350 From Nonabsorbable Marker to Colonoscopy Preparation to Osmotic Laxative. *Gastroenterology* **152**, 675–680 (2017).

39. Caliceti, P. & Veronese, F. M. Pharmacokinetic and biodistribution properties of poly(ethylene glycol)-protein conjugates. *Adv. Drug Deliv. Rev.* **55**, 1261–1277 (2003).

40. Pan, Y. *et al.* Insights on the Structure, Molecular Weight and Activity of an Antibacterial Protein–Polymer Hybrid. *ChemPhysChem* **19**, 651–658 (2018).

41. Top, A. & Kiick, K. L. Multivalent protein polymers with controlled chemical and physical properties. *Adv. Drug Deliv. Rev.* **62**, 1530–1540 (2010).

42. Morgenstern, J., Baumann, P., Brunner, C. & Hubbuch, J. Effect of PEG molecular weight and PEGylation degree on the physical stability of PEGylated lysozyme. *Int. J. Pharm.* **519**, 408–417 (2017).

43. Jia, F., Narasimhan, B. & Mallapragada, S. Materials-based strategies for multi-enzyme immobilization and co-localization: A review. *Biotechnol. Bioeng.* **111**, 209–222 (2014).

44. Bornscheuer, U. T. Immobilizing enzymes: How to create more suitable biocatalysts. *Angew. Chemie - Int. Ed.* **42**, 3336–3337 (2003).

45. Jesionowski, T., Zdarta, J. & Krajewska, B. Enzyme immobilization by adsorption: A review. *Adsorption* **20**, 801–821 (2014).

46. Laurent, N., Haddoub, R. & Flitsch, S. L. Enzyme catalysis on solid surfaces. *Trends Biotechnol.* **26**, 328–337 (2008).

47. Krishnan, S. K., Singh, E., Singh, P., Meyyappan, M. & Nalwa, H. S. A review on graphene-based nanocomposites for electrochemical and fluorescent biosensors. *RSC Adv.* **9**, 8778–8781 (2019).

48. Kuila, T. *et al.* Recent advances in graphene-based biosensors. *Biosens. Bioelectron.* **26**, 4637–4648 (2011).

49. Secundo, F. Conformational changes of enzymes upon immobilisation. *Chem. Soc. Rev.* **42**, 6250–6261 (2013).

50. Zhang, Y. *et al.* Assembly of graphene oxide-enzyme conjugates through hydrophobic interaction. *Small* **8**, 154–159 (2012).

51. Liu, Y. & Yu, J. Oriented immobilization of proteins on solid supports for use in biosensors and biochips: a review. *Microchim. Acta* **183**, 1–19 (2016).

52. Cipolatti, E. P. *et al.* Nanomaterials for biocatalyst immobilization-state of the art and future trends. *RSC Adv.* **6**, 104675–104692 (2016).

53. Yang, Q. *et al.* Three dimensional reduced graphene oxide/ZIF-67 aerogel: Effective removal cationic and anionic dyes from water. *Chem. Eng. J.* **348**, 202–211 (2018).

54. Jahan, M., Bao, Q., Yang, J. X. & Loh, K. P. Structure-directing role of graphene in the synthesis of metal-organic framework nanowire. *J. Am. Chem. Soc.* **132**, 14487–14495 (2010).

55. Yu, G., Xia, J., Zhang, F. & Wang, Z. Hierarchical and hybrid RGO/ZIF-8 nanocomposite as electrochemical sensor for ultrasensitive determination of dopamine. *J. Electroanal. Chem.* **801**, 496–502 (2017).

56. Pinto, A. M., Gonçalves, I. C. & Magalhães, F. D. Graphene-based materials biocompatibility: A review. *Colloids Surfaces B Biointerfaces* **111**, 188–202 (2013).

57. Hu, Y. *et al.* Zeolitic imidazolate framework/graphene oxide hybrid nanosheets as seeds for the growth of ultrathin molecular sieving membranes. *Angew. Chemie - Int. Ed.* **55**, 2048–2052 (2016).

58. Liu, J., Cui, L. & Losic, D. Graphene and graphene oxide as new nanocarriers for drug delivery applications. *Acta Biomater.* **9**, 9243–9257 (2013).

59. Zhu, Z. *et al.* A critical review of Glucose biosensors based on Carbon nanomaterials: Carbon nanotubes and graphene. *Sensors (Switzerland)* **12**, 5996–6022 (2012).

60. Kumar, P., Huo, P., Zhang, R. & Liu, B. Antibacterial properties of graphene-based nanomaterials. *Nanomaterials* **9**, 1–32 (2019).

61. Bai, Y. *et al.* Influence of graphene oxide and reduced graphene oxide on the activity and conformation of lysozyme. *Colloids Surfaces B Biointerfaces* **154**, 96–103 (2017).

62. Smith, S. C., Ahmed, F., Gutierrez, K. M. & Frigi Rodrigues, D. A comparative study of lysozyme adsorption with graphene, graphene oxide, and single-walled carbon nanotubes: Potential environmental applications. *Chem. Eng. J.* **240**, 147–154 (2014).

63. Neupane, S. *et al.* Enhancing Enzyme Immobilization on Carbon Nanotubes via Metal-Organic Frameworks for Large-Substrate Biocatalysis. *ACS Appl. Mater. Interfaces* **11**, 12133–12141 (2019).

64. Fan, Z. *et al.* Metal-organic frameworks/graphene oxide composite: A New enzymatic immobilization carrier for hydrogen peroxide biosensors. *J. Electrochem. Soc.* **163**, B32–B37 (2016).

65. Zhu, Q. *et al.* Nano-Biocatalysts of Cyt c@ZIF-8/GO Composites with High Recyclability via a de Novo Approach. *ACS Appl. Mater. Interfaces* **10**, 16066–16076 (2018).

66. Lian, X. *et al.* Enzyme-MOF (metal-organic framework) composites. *Chem. Soc. Rev.* **46**, 3386–3401 (2017).

67. Gkaniatsou, E. *et al.* Metal-organic frameworks: A novel host platform for enzymatic catalysis and detection. *Mater. Horizons* **4**, 55–63 (2017).

68. Srimuk, P., Luanwuthi, S., Krittayavathananon, A. & Sawangphruk, M. Solid-type supercapacitor of reduced graphene oxide-metal organic framework composite coated on carbon fiber paper. *Electrochim. Acta* **157**, 69–77 (2015).

69. Drout, R. J., Robison, L. & Farha, O. K. Catalytic applications of enzymes encapsulated in metal–organic frameworks. *Coord. Chem. Rev.* **381**, 151–160 (2019).

70. Liao, F. S. *et al.* Shielding against Unfolding by Embedding Enzymes in Metal-Organic Frameworks via a de Novo Approach. *J. Am. Chem. Soc.* **139**, 6530–6533 (2017).

71. Hou, C. *et al.* Facile synthesis of enzyme-embedded magnetic metal-organic frameworks as a reusable mimic multi-enzyme system: Mimetic peroxidase properties and colorimetric sensor. *Nanoscale* **7**, 18770–18779 (2015).

72. Nadar, S. S. & Rathod, V. K. Magnetic-metal organic framework (magnetic-MOF): A novel platform for enzyme immobilization and nanozyme applications. *Int. J. Biol. Macromol.* **120**, 2293–2302 (2018).

73. George, P., Das, R. K. & Chowdhury, P. Facile microwave synthesis of Ca-BDC metal organic framework for adsorption and controlled release of Curcumin. *Microporous Mesoporous Mater.* **281**, 161–171 (2019).

74. Lyu, F., Zhang, Y., Zare, R. N., Ge, J. & Liu, Z. One-pot synthesis of protein-embedded metal-organic frameworks with enhanced biological activities. *Nano Lett.* **14**, 5761–5765 (2014).

75. Chen, S., Lucier, B. E. G., Chen, M., Terskikh, V. V. & Huang, Y. Probing Calcium-Based Metal-Organic Frameworks via Natural Abundance 43Ca Solid-State NMR Spectroscopy. *Chem. - A Eur. J.* **24**, 8732–8736 (2018).

76. We, B. *et al.* Mof Materials From Design To Applications : Case Studies of Calcium- and Magnesium-Based. *Science (80-.).* **500**, 408–418 (2016).

77. Wayne Hubbel, Carlos Lopez, Christian Altenbach, and Z. Y., Hubbell, W. L., López, C. J., Altenbach, C. & Yang, Z. Technological advances in site-directed spin labeling of proteins. *Curr. Opin. Biol.* **23**, 725–733 (2013).

78. Liang, Z., Lou, Y., Freed, J. H., Columbus, L. & Hubbell, W. L. A multifrequency electron spin resonance study of T4 lysozyme dynamics using the slowly relaxing local Structure model. *J. Phys. Chem. B* **108**, 17649–17659 (2004).

79. Mchaourab, H. S., Oh, K. J., Fang, C. J. & Hubbell, W. L. Conformation of T4 lysozyme in solution. Hinge-bending motion and the substrate-induced conformational transition studied by site-directed spin labeling. *Biochemistry* **36**, 307–316 (1997).

80. Langen, R., Oh, K. J., Cascio, D. & Hubbell, W. L. Crystal structures of spin labeled T4 lysozyme mutants: Implications for the interpretation of EPR spectra in terms of structure. *Biochemistry* **39**, 8396–8405 (2000).

81. Fleissner, M. R. X-ray Structures of Nitroxide Side Chains in Proteins: A Basis for Interpreting Distance Measurements and Dynamic Studies by Electron Paramagnetic Resonance. (2007).

82. Pan, Y. *et al.* How Do Enzymes Orient When Trapped on Metal-Organic Framework (MOF) Surfaces? *J. Am. Chem. Soc.* **140**, 16032–16036 (2018).

83. Farmakes, J. *et al.* Enzyme Immobilization on Graphite Oxide (GO) Surface via One-Pot Synthesis of GO/Metal − Organic Framework Composites for Large- Substrate Biocatalysis. (2020). doi:10.1021/acsami.0c04101

84. Hubbell, W. L., Cafiso, D. S. & Altenbach, C. Identifying conformational changes with site-directed spin labeling. *Nat. Struct. Biol.* **7**, 735–739 (2000).

85. Ding, S., Cargill, A. A., Medintz, I. L. & Claussen, J. C. Increasing the activity of immobilized enzymes with nanoparticle conjugation. *Curr. Opin. Biotechnol.* **34**, 242–250 (2015).

86. Matsumura, M., Wozniak, J. A., Dao-Pin, S. & Matthews, B. W. Structural studies of mutants of T4 lysozyme that alter hydrophobic stabilization. *J. Biol. Chem.* **264**, 16059–16066 (1989).

87. Hoffman, A. S. Bioconjugates of intelligent polymers and recognition proteins for use in diagnostics and affinity separations. *Clin. Chem.* **46**, 1478–1486 (2000).

88. Cummings, C., Murata, H., Koepsel, R. & Russell, A. J. Tailoring enzyme activity and stability using polymer-based protein engineering. *Biomaterials* **34**, 7437–7443 (2013).

89. Harada, A. & Kataoka, K. Novel polyion complex micelles entrapping enzyme molecules in the core: Preparation of narrowly-distributed micelles from lysozyme and poly(ethylene glycol)-poly(aspartic acid) block copolymer in aqueous medium. *Macromolecules* **31**, 288–294 (1998).

90. Veronese, F. M. Peptide and protein PEGylation: A review of problems and solutions. *Biomaterials* **22**, 405–417 (2001).

91. Lopez, C. Mapping molecular flexibility of spin labeled proteins on the nanosecond and longer time scales via CW lineshape analysis and osmolyte-perturbation EPR (2012).

92. Mchaourab, H. S., Lietzow, M. A., Hideg, K. & Hubbell, W. L. Motion of spin-labeled side chains in T4 lysozyme. Correlation with protein structure and dynamics. *Biochemistry* **35**, 7692–7704 (1996).

93. Neupane, S. *et al.* Probing the Aggregation Mechanism of Gold Nanoparticles Triggered by a Globular Protein. *J. Phys. Chem. C* **121**, 1377–1386 (2017).

94. Chen, W.-H.; Vazquez-Gonza´ lez, M.; Zoabi, A.; Abu-Reziq, R.;´ Willner, I. Biocatalytic Cascades Driven by Enzyme Encapsulated in Metal-Organic Framework Nanoparticles. *Nat. Catal.* **1**, 689–695 (2018).

95. Zakharchenko, A.; Guz, N.; Laradji, A. M.; Katz, E.; Minko, S. Magnetic Field Remotely Controlled Selective Biocatalysis. *Nat. Catal.* **1**, 73–81 (2018).

96. Wang, M.; Mohanty, S. K.; Mahendra, S. Nanomaterial Supported Enzymes for Water Purification and Monitoring in Point-of-Use Water Supply Systems. *Acc. Chem. Res.* **52**, 876–885 (2019).

97. MH, C. R. & S. All Wrapped up: Stabilization of Enzymes within Single Enzyme Nanoparticles. *ournal Am. Chem. Soc.* **141**, 2754–2769 (2019).

98. Li, H.; Pan, Y.; Farmakes, J.; Xiao, F.; Hu, J.; Chen, B.; Rao, J.; Yang, Z. A Sulfonated Mesoporous Silica Nanoparticle for Enzyme Protection against Denaturants and Controlled Release under Reducing Conditions. *J. Colloid Interface Sci.* **556**, 292–300 (2019).

99. Hudson, S.; Cooney, J.; Magner, E. Proteins in Mesoporous Silicates. *Angew. Chem., Int. Ed.* **47**, 8582–8594 (2008).

100. Chen, Y. P. *et al.* A new strategy for intracellular delivery of enzyme using mesoporous silica nanoparticles: Superoxide dismutase. *J. Am. Chem. Soc.* **135**, 1516–1523 (2013).

101. Lu, G.; Li, S.; Guo, Z.; Farha, O. K.; Hauser, B. G.; Qi, X.; Wang, Y.; Wang, X.; Han, S.; Liu, X.; DuChene, J. S.; Zhang, H.; Zhang, Q.; Chen, X.; Ma, J.; Loo, S. C. J.; Wei, W. D.; Yang, Y.; Hupp, J. T.; Huo, F. Imparting Functionality to a Metal-Organic Framework Material by Controlled Nanoparticle Encapsulation. *Nat. Chem* **4**, 310–316 (2012).

102. Ulbrich, K.; HolÃ, K.; Š ubr, V.; Bakandritsos, A.; TuŠ ek, J.; Zboril, R. Targeted Drug Delivery with Polymers and Magnetic ˇNanoparticles: Covalent and Noncovalent Approaches, Release Control, and Clinical Studies. *Chem. Rev.* **116**, 5338–5431 (2016).

103. Kudina, O.; Zakharchenko, A.; Trotsenko, O.; Tokarev, A.; Ionov, L.; Stoychev, G.; Puretskiy, N.; Pryor, S. W.; Voronov, A.; Minko, S. Highly Efficient Phase Boundary Biocatalysis with Enzymogel Nanoparticles. *Angew. Chem., Int. Ed.* **53**, 483–487 (2014).

104. Lee, Y.; Ishii, T.; Cabral, H.; Kim, H. J.; Seo, J.-H.; Nishiyama, N.; Oshima, H.; Osada, K.; Kataoka, K. Charge-Conversional Polyionic Complex Micelles-Efficient Nanocarriers for Protein Delivery into Cytoplasm. *Angew. Chem., Int. Ed.* **48**, 5309–5312 (2009).

105. Pan, Y.; Zholobko, O.; Li, H.; Jin, J.; Hu, J.; Chen, B.; Voronov, A.; Yang, Z. Spatial Distribution and Solvent Polarity-Triggered Release of a Polypeptide Incorporated into Invertible Micellar Assemblies. *ACS Appl. Mater. Interfaces* **12**, 12075–12082 (2020).

106. Zhang, Y.; Ge, J.; Liu, Z. Enhanced Activity of Immobilized or Chemically Modified Enzymes. *ACS Catal.* **5**, 4503–4513 (2015).

107. Lee, M.-H.; Thomas, J. L.; Chen, Y.-C.; Wang, H.-Y.; Lin, H.-Y. Hydrolysis of Magnetic Amylase-Imprinted Poly(ethylene-co-vinyl alcohol) Composite Nanoparticles. *ACS Appl. Mater. Interfaces* **4**, 916–921 (2012).

108. Debacq-Chainiaux, F.; Erusalimsky, J. D.; Campisi, J.; Toussaint, O. Protocols to Detect Senescence-Associated BetaGalactosidase (SA-Bgal) Activity, a Biomarker of Senescent Cells in Culture and In Vivo. *Nat. Protoc.* **4**, 1798–1806 (2009).

109. Karadzic, I.; Masui, A.; Zivkovic, L. I.; Fujiwara, N. 22. Karadzic, I.; Masui, A.; Zivkovic, L. I.; Fujiwara, N. Purification and Characterization of an Alkaline Lipase from Pseudomonas Aeruginosa Isolated from Putrid Mineral Cutting Oil as Component of Metalworking Fluid. *J. Biosci. Bioeng.* **102**, 82–89 (2006).

110. Salgaonkar, M.; Nadar, S. S.; Rathod, V. K. Combi-Metal Organic Framework (Combi-MOF) of α-Amylase and Glucoamylase for One Pot Starch Hydrolysis. *Int. J. Biol. Macromol.* **113**, 464–475 (2018).

111. Howarth, A. J.; Liu, Y.; Li, P.; Li, Z.; Wang, T. C.; Hupp, J. T.; Farha, O. K. Chemical, Thermal and Mechanical Stabilities of Metal Organic Frameworks. *Nat. Rev. Mater.* **1**, 15018 (2016).

112. Gao, S.; Hou, J.; Deng, Z.; Wang, T.; Beyer, S.; Buzanich, A. G.; Richardson, J. J.; Rawal, A.; Seidel, R.; Zulkifli, M. Y.; Li, W.; Bennett, T. D.; Cheetham, A. K.; Liang, K.; Chen, V. Improving the Acidic Stability of Zeolitic Imidazolate Frameworks by Biofunctional Molecules. *Mol. Chem.* **5**, 1597–1608 (2019).

113. Wei, T.-H.; Wu, S.-H.; Huang, Y.-D.; Lo, W.-S.; Williams, B. P.; Chen, S.-Y.; Yang, H.-C.; Hsu, Y.-S.; Lin, Z.-Y.; Chen, X.-H.; Kuo, P.- E.; Chou, L.-Y.; Tsung, C.-K.; Shieh, F.-K. Rapid Mechanochemical Encapsulation of Biocatalysts into Robust Metal-Organic Frameworks. *Nat. Commun.* **10**, 5002 (2019).

114. Wang, Y., Li, Z., Wang, J., Li, J. & Lin, Y. Graphene and graphene oxide: Biofunctionalization and applications in biotechnology. *Trends Biotechnol.* **29**, 205–212 (2011).

115. Liang, K.; Ricco, R.; Doherty, C. M.; Styles, M. J.; Bell, S.; Kirby, N.; Mudie, S.; Haylock, D.; Hill, A. J.; Doonan, C. J.; Falcaro, P. Biomimetic Mineralization of Metal-Organic Frameworks as Protective Coatings for Biomacromolecule. *Nat. Commun.* **6**, 7240 (2015).

116. Schwizer, F.; Okamoto, Y.; Heinisch, T.; Gu, Y.; Pellizzoni, M. M.; Lebrun, V.; Reuter, R.; Köhler, V.; Lewis, J. C.; Ward, T. R. Artificial Metalloenzymes: Reaction Scope and Optimization Strategies. *Chem. Rev.* **118**, 142–231 (2018).

117. Li, S.; Liu, X.; Chai, H.; Huang, Y. Recent Advances in the Construction and Analytical Applications of Metal-Organic Frameworks-based Nanozymes. *TrAC, Trends Anal. Chem.* **105**, 391–403 (2018).

118. Liang, M.; Yan, X. Nanozymes: From New Concepts, Mechanisms, and Standards to Applications. *Acc. Chem. Res.* **52**, 2190–2200 (2019).

119. Huang, Y.; Ren, J.; Qu, X. Nanozymes: Classification, Catalytic Mechanisms, Activity Regulation, and Applications. *Chem. Rev.* **119**, 4357–4412 (2019).

120. Fleissner, M. R.; Bridges, M. D.; Brooks, E. K.; Cascio, D.; Kalai, T.; Hideg, K.; Hubbell, W. L. Structure and Dynamics of A´ Conformationally Constrained Nitroxide Side Chain and Applications in EPR Spectroscopy. *Proc. Natl. Acad. Sci.* **108**, 16241–16246 (2011).

121. Lopez, C. J.; Fleissner, M. R.; Guo, Z.; Kusnetzow, A. K.;´ Hubbell, W. L. Osmolyte Perturbation Reveals Conformational Equilibria in Spin-Labeled Proteins. *Protein Sci.* **18**, 1637–1652 (2009).

122. Bower, C. K.; Sananikone, S.; Bothwell, M. K.; McGuire, J. Activity Losses Among T4 Lysozyme Charge Variants after Adsorption to Colloidal Silica. *Biotechnol. Bioeng.* **64**, 373–376 (1999).

123. Qu, K.; Vaughn, J. L.; Sienkiewicz, A.; Scholes, C. P.; Fetrow, J. S. Kinetics and Motional Dynamics of Spin-Labeled Yeast Iso-1- cytochrome c: 1. Stopped-Flow Electron Paramagnetic Resonance as a Probe for Protein Folding/Unfolding of the C-Terminal Helix Spin Labeled at Cysteine 102. *Biochemistry* **36**, 2884–2897 (1997).

124. Abouhmad, A., Dishisha, T., Amin, M. A. & Hatti-Kaul, R. Immobilization to Positively Charged Cellulose Nanocrystals Enhances the Antibacterial Activity and Stability of Hen Egg White and T4 Lysozyme. *Biomacromolecules* **18**, 1600–1608 (2017).

125. Kiristi, M.; Singh, V. V.; Esteban-Fernandez de A´´ vila, B.; Uygun, M.; Soto, F.; Aktaş Uygun, D.; Wang, J. Lysozyme-Based Antibacterial Nanomotors. *ACS Nano* **9**, 9252–9259 (2015).

126. Pan, Y. *et al.* Insights on the Structure, Molecular Weight and Activity of an Antibacterial Protein-Polymer Hybrid. *ChemPhysChem* (2018). doi:10.1002/cphc.201701097

127. Compton, O. C. & Nguyen, S. T. Graphene oxide, highly reduced graphene oxide, and graphene: Versatile building blocks for carbon-based materials. *Small* **6**, 711–723 (2010).

128. Lam, E.; Luong, J. H. T. Carbon Materials as Catalyst Supports and Catalysts in the Transformation of Biomass to Fuels and Chemicals. *ACS Catal.* **4**, 3393–3410 (2014).

129. Tiwari, J. N.; Vij, V.; Kemp, K. C.; Kim, K. S. Engineered Carbon-Nanomaterial-Based Electrochemical Sensors for Biomolecules. *ACS Nano* **10**, 46–80 (2016).

130. Huo, D.; Liu, G.; Li, Y.; Wang, Y.; Guan, G.; Yang, M.; Wei, K.; Yang, J.; Zeng, L.; Li, G.; Zeng, W.; Zhu, C. Construction of Antithrombotic Tissue-Engineered Blood Vessel via Reduced Graphene Oxide Based Dual-Enzyme Biomimetic Cascade. *ACS Nano* **11**, 10964–10973 (2017).

131. Xu, W.; Fu, Z.; Chen, G.; Wang, Z.; Jian, Y.; Zhang, Y.; Jiang, G.; Lu, D.; Wu, J.; Liu, Z. Graphene Oxide Enabled Long-Term Enzymatic Transesterification in an Anhydrous Gas Flux. *Nat. Commun.* **10**, 2684 (2019).

132. Jin, L.; Yang, K.; Yao, K.; Zhang, S.; Tao, H.; Lee, S.-T.; Liu, Z.; Peng, R. Functionalized Graphene Oxide in Enzyme Engineering: A Selective Modulator for Enzyme Activity and Thermostability. *ACS Nano* **6**, 4864–4875 (2012).

133. Novak, M. J.; Pattammattel, A.; Koshmerl, B.; Puglia, M.; Williams, C.; Kumar, C. V. ″Stable-on-the-Table″ Enzymes: Engineering the Enzyme-Graphene Oxide Interface for Unprecedented Kinetic Stability of the Biocatalyst. *ACS Catal.* **6**, 339–347 (2016).

134. Hummers, W. S.; Offeman, R. E. Preparation of Graphitic Oxide. *J. Am. Chem. Soc.* **80**, 1339–1339 (1958).

135. Supporting Information Enhancing Enzyme Immobilization on Carbon Nanotubes (CNTs) via Metal-Organic Frameworks (MOFs) for Large Substrate Biocatalysis. 1–24

136. Davies, R. C.; Neuberger, A.; Wilson, B. M. The Dependence of Lysozyme Activity on pH and Ionic Strength. *Biochim. Biophys. Acta − Enzym.* **28**, 116–122 (1972).

137. Jensen, H. B.; Kleppe, K. Effect of Ionic Strength, pH, Amines and Divalent Cations on the Lytic Activity of T4 Lysozyme. *Eur. J. Biochem.* **28**, 116–122 (1972).

138. Seidi F, Jenjob R, & C. D. Designing Smart Polymer Conjugates for Controlled Release of Payloads. *Chem. Rev.* **118**, 3965–4036 (2018).

139. Trzebicka B, et al. Thermoresponsive polymer-peptide/protein conjugates. *Prog. Polym. Sci.* **68**, 35–76 (2017).

140. GJL, B. O. & B. Advances in Chemical Protein Modification. *Chem. Rev.* **115**, 2174–2195 (2015).

141. Yu J, Panganiban B, & X. T. Peptide-Polymer Conjugates: From Fundamental Science to Application. *Annu. Rev. Phys. Chem.* **64**, 631–657 (2013).

142. Caro, A. *et al.* Grafting of lysozyme and/or poly(ethylene glycol) to prevent biofilm growth on stainless steel surfaces. *J. Phys. Chem. B* **113**, 2101–2109 (2009).

143. Lucius, M. *et al.* Investigating the Impact of Polymer Functional Groups on the Stability and Activity of Lysozyme-Polymer Conjugates. *Biomacromolecules* **17**, 1123–1134 (2016).

144. Ko, J. H. & Maynard, H. D. A guide to maximizing the therapeutic potential of protein-polymer conjugates by rational design. *Chem. Soc. Rev.* **47**, 8998–9014 (2018).

145. Lu, H. Site-specific protein-polymer conjugate micelles with dramatically enhanced pharmacology. *Sci. China Mater.* **61**, 1627–1628 (2018).

146. Vandermeulen, G. W. M. & Klok, H. A. Peptide/protein hybrid materials: Enhanced control of structure and improved performance through conjugation of biological and synthetic polymers. *Macromol. Biosci.* **4**, 383–398 (2004).

147. Baker, S. L. *et al.* Transforming protein-polymer conjugate purification by tuning protein solubility. *Nat. Commun.* **10**, 1–12 (2019).

148. Yan M, et al. A novel intracellular protein delivery platform based on single-protein nanocapsules. *Nat. Nanotechnol.* **5**, 48–53 (2010).

149. Panganiban B, et al. Random heteropolymers preserve protein function in foreign environments. *Science (80-.).* **359**, 1239 (2018).

150. Nguyen TD, Qiao B, & O. de la C. M. Efficient encapsulation of proteins with random copolymers. *Proc. Natl. Acad. Sci.* **115**, 6578 (2018).

151. Ramberg, K. O., Antonik, P. M., Cheung, D. L. & Crowley, P. B. Measuring the Impact of PEGylation on a Protein-Polysaccharide Interaction. *Bioconjug. Chem.* **30**, 1162–1168 (2019).

152. Zielenkiewicz, W., Swierzewski, R., Attanasio, F. & Rialdi, G. Thermochemical, volumetric and spectroscopic properties of lysozyme-poly(ethylene) glycol system. *J. Therm. Anal. Calorim.* **83**, 587–595 (2006).

153. Miyake, T. *et al.* Regioselective Chemical Modification of Cysteine Residues on Protein Surfaces Focusing on Local Environment around the Conjugation Site. *Bioconjug. Chem.* (2020). doi:10.1021/acs.bioconjchem.9b00869

154. Munasinghe, A., Mathavan, A., Mathavan, A., Lin, P. & Colina, C. M. PEGylation within a confined hydrophobic cavity of a protein. *Phys. Chem. Chem. Phys.* **21**, 25584–25596 (2019).

155. De, P., Li, M., Gondi, S. R. & Sumerlin, B. S. Temperature-regulated activity of responsive polymer-protein conjugates prepared by grafting-from via RAFT polymerization. *J. Am. Chem. Soc.* **130**, 11288–11289 (2008).

156. Baugh L, et al. Probing the Orientation of Surface-Immobilized Protein G B1 Using ToF-SIMS, Sum Frequency Generation, and NEXAFS Spectroscopy. *Langmuir* **26**, 16434–16441 (2010).

157. Zaghmi A, et al. Mechanisms of activity loss for a multi-PEGylated protein by experiment and simulation. *Mater. Today Chem.* **12**, 121–131 (2019).

158. Chiang C-W, et al. Polymerization-Induced Coassembly of Enzyme-Polymer Conjugates into Comicelles with Tunable and Enhanced Cascade Activity. *Nano Lett.* **20**, 1383–1387 (2020).

159. Suk, J. S., Xu, Q., Kim, N., Hanes, J. & Ensign, L. M. PEGylation as a strategy for improving nanoparticle-based drug and gene delivery. *Adv. Drug Deliv. Rev.* **99**, 28–51 (2016).

160. Mishra, P., Nayak, B. & Dey, R. K. PEGylation in anti-cancer therapy: An overview. *Asian J. Pharm. Sci.* **11**, 337–348 (2016).

161. Pelegri-O'Day EM, Lin E-W, & M. H. Therapeutic Protein-Polymer Conjugates: Advancing Beyond PEGylation. *J. Am. Chem. Soc.* **136**, 114323–14332 (2014).

162. Fach M, Radi L, & W. P. Nanoparticle Assembly of Surface-Modified Proteins. *J. Am. Chem. Soc.* **138**, 1543–1559 (2016).

163. IW, H. PEG-Peptide Conjugates. *Biomacromolecules* **15**, 1543–1559 (2014).

164. Daly, S. M., Przybycien, T. M., Tilton, R. D. & Daly SM, Przybycien TM, & T. R. Adsorption of Poly(ethylene glycol)-Modified Lysozyme to Silica. *Langmuir* **21**, 1328–1337 (2005).

165. Roberts, M. J., Bentley, M. D. & Harris, J. M. Chemistry for peptide and protein PEGylation. *Adv. Drug Deliv. Rev.* **64**, 116–127 (2012).

166. Pfister, D. & Morbidelli, M. Process for protein PEGylation. *J. Control. Release* **180**, 134–149 (2014).

167. CPR, N. N. & H. Site-specific PEGylation of Proteins: Recent Developments. *J. Org. Chem.* **79**, 10727–10733 (2014).

168. Lund R, Shu J, & X. T. A Small-Angle X-ray Scattering Study of α-helical Bundle-Forming Peptide-Polymer Conjugates in Solution: Chain Conformations. *Macromolecules* **46**, 1625–1632 (2013).

169. Cattani G, Vogeley L, & C. P. Structure of a PEGylated protein reveals a highly porous double-helical assembly. *Nat. Chem.* **7**, 1007–1011 (2015).

170. Kuroki R, Weaver LH, & M. B. Structure-based design of a lysozyme with altered catalytic activity. *Nat. Struct. Biol.* **2**, 1007–1011 (1995).

171. Bower CK, Xu Q, & M. J. Activity losses among T4 lysozyme variants after adsorption to colloidal silica. *Biotechnol. Bioeng.* **58**, 658–662 (2000).

172. Horn, D. W. *et al.* Dispersion state and fiber toughness: Antibacterial lysozyme-single walled carbon nanotubes. *Adv. Funct. Mater.* **23**, 6082–6090 (2013).

173. Abouhmad, A., Mamo, G., Dishisha, T., Amin, M. A. & Hatti-Kaul, R. T4 lysozyme fused with cellulose-binding module for antimicrobial cellulosic wound dressing materials. *J. Appl. Microbiol.* **121**, 115–125 (2016).

174. Wang, Z. *et al.* Flower-like Surface of Three-Metal-Component Layered Double Hydroxide Composites for Improved Antibacterial Activity of Lysozyme. *Bioconjug. Chem.* **29**, 2090–2099 (2018).

175. Tripathy, N., Ahmad, R., Bang, S. H., Min, J. & Hahn, Y. B. Tailored lysozyme-ZnO nanoparticle conjugates as nanoantibiotics. *Chem. Commun.* **50**, 9298–9301 (2014).

176. Bloustine, J., Virmani, T., Thurston, G. M. & Fraden, S. Light scattering and phase behavior of lysozyme-poly(ethylene glycol) mixtures. *Phys. Rev. Lett.* **96**, 1–4 (2006).

177. Lorenzo MM, Decker CG, Kahveci MU, Paluck SJ, & M. H. Homodimeric Protein-Polymer Conjugates via the Tetrazineâ€“trans-Cyclooctene Ligation. *Macromolecules* **49**, 30–37 (2016).

178. JW, W. C. & B. PEGylation and Dimerization of Expressed Proteins under Near Equimolar Conditions with Potassium 2-Pyridyl Acyltrifluoroborates. *ACS Cent. Sci.* **4**, 197–206 (2018).

179. Bernardim B, et al. Efficient and irreversible antibody-cysteine bioconjugation using carbonylacrylic reagents. *Nat. Protoc.* **14**, 86–99 (2019).

180. Northrop BH, Frayne SH, & C. U. Thiol-maleimide 'click' chemistry: evaluating the influence of solvent, initiator, and thiol on the reaction mechanism, kinetics, and selectivity. *Polym. Chem.* **6**, 3415–3430 (2015).

181. Sookkumnerd, T. & Hsu, J. T. Purification of PEG-protein conjugates by countercurrent distribution in aqueous two-phase systems. *J. Liq. Chromatogr. Relat. Technol.* **23**, 497–503 (2000).

182. Jing Han, Lidan Sun, Yingying Chu, Zheng Li, Dandan Huang, Xiaoyun Zhu, Hai Qian*, and W. H. Design, Synthesis, and Biological Activity of Novel Dicoumarol Glucagon-like Peptide 1 Conjugates. *J. Med. Chem.* **56**, 9955–9968 (2013).

183. Landa Purushottam, a Srinivasa Rao Adusumalli, a M. C. and V. R. O. logo *a. Chemoselective and site-selective peptide and native protein modification enabled by aldehyde auto-oxidation†. *Chem. Commun.* **53**, 959–962 (2017).

184. Perry, J. J. P., Shin, D. S., Getzoff, E. D. & Tainer, J. A. The structural biochemistry of the superoxide dismutases. *Biochim. Biophys. Acta - Proteins Proteomics* **1804**, 245–262 (2010).

185. Rae, T. D., Torres, A. S., Pufahl, R. A. & O'Halloran, T. V. Mechanism of Cu,Zn-Superoxide Dismutase Activation by the Human Metallochaperone hCCS. *J. Biol. Chem.* **276**, 5166–5176 (2001).

186. Carrì, M. T., Battistoni, A., Polizio, F., Desideri, A. & Rotilio, G. Impaired copper binding by the H46R mutant of human Cu,Zn superoxide dismutase, involved in amyotrophic lateral sclerosis. *FEBS Lett.* **356**, 314–316 (1994).

187. Qualls, D. A. *et al.* Features of wild-type human SOD1 limit interactions with misfolded aggregates of mouse G86R Sod1. *Mol. Neurodegener.* **8**, 1–15 (2013).

188. Boissinot, M. *et al.* Function of the Greek key connection analysed using circular permutants of superoxide dismutase. *EMBO J.* **16**, 2171–2178 (1997).

189. Nishida, C. R., Gralla, E. B. & Valentine, J. S. Characterization of three yeast copper-zinc superoxide dismutase mutants analogous to those coded for in familial amyotrophic lateral sclerosis. *Proc. Natl. Acad. Sci. U. S. A.* **91**, 9906–9910 (1994).

190. Tompa, D. R. & Kadhirvel, S. Molecular dynamics of a far positioned SOD1 mutant V14M reveals pathogenic misfolding behavior. *J. Biomol. Struct. Dyn.* **36**, 4085–4098 (2018).

191. Crow, J. P., Sampson, J. B., Zhuang, Y., Thompson, J. A. & Beckman, J. S. Decreased Zinc Affinity of Amyotrophic Lateral Sclerosis-Associated Superoxide Dismutase Mutants Leads to Enhanced Catalysis of Tyrosine Nitration by Peroxynitrite. *J. Neurochem.* **69**, 1936–1944 (2002).

192. Pratt, A. J. *et al.* Aggregation propensities of superoxide dismutase G93 hotspot mutants mirror ALS clinical phenotypes. *Proc. Natl. Acad. Sci. U. S. A.* **111**, E4568–E4576 (2014).

193. Merz, G. E. *et al.* Copper-based pulsed dipolar ESR spectroscopy as a probe of protein conformation linked to disease states. *Biophys. J.* **107**, 1669–1674 (2014).

194. Hallewell, R. A. *et al.* Genetically engineered polymers of human CuZn superoxide dismutase. Biochemistry and serum half-lives. *J. Biol. Chem.* **264**, 5260–5268 (1989).

195. Nallamsetty, S. & Waugh, D. S. A generic protocol for the expression and purification of recombinant proteins in Escherichia coli using a combinatorial His6-maltose binding protein fusion tag. *Nat. Protoc.* **2**, 383–391 (2007).

196. Lebendiker, M. & Danieli, T. Production of prone-to-aggregate proteins. *FEBS Lett.* **588**, 236–246 (2013).

197. Marisch, K., Bayer, K., Cserjan-Puschmann, M., Luchner, M. & Striedner, G. Evaluation of three industrial Escherichia coli strains in fed-batch cultivations during high-level SOD protein production. *Microb. Cell Fact.* **12**, 1–11 (2013).

198. Hartman, J. R. *et al.* High-level expression of enzymatically active human Cu/Zn superoxide dismutase in Escherichia coli. *Proc. Natl. Acad. Sci. U. S. A.* **83**, 7142–7146 (1986).

199. Leinweber, B. *et al.* Aggregation of als mutant superoxide dismutase expressed in Escherichia coli. *Free Radic. Biol. Med.* **36**, 911–918 (2004).

200. Yoo, H. Y., Kim, S. S. & Rho, H. M. Overexpression and simple purification of human superoxide dismutase (SOD1) in yeast and its resistance to oxidative stress. *J. Biotechnol.* **68**, 29–35 (1999).

201. Kim, T. S., Jung, Y., Na, B. K., Kim, K. S. & Chung, P. R. Molecular cloning and expression of Cu/Zn-containing superoxide dismutase from Fasciola hepatica. *Infect. Immun.* **68**, 3941–3948 (2000).

202. Son, Y. J. *et al.* Expression, high cell density culture and purification of recombinant EC-SOD in escherichia coli. *Appl. Biochem. Biotechnol.* **162**, 1585–1598 (2010).

203. Zhu, X. Q., Li, S. X., He, H. J. & Yuan, Q. S. On-column refolding of an insoluble His6-tagged recombinant EC-SOD overexpressed in Escherichia coli. *Acta Biochim. Biophys. Sin. (Shanghai).* **37**, 265–269 (2005).

204. Hou, E. W., Prasad, R., Beard, W. A. & Wilson, S. H. High-level expression and purification of untagged and histidine-tagged HIV-1 reverse transcriptase. *Protein Expr. Purif.* **34**, 75–86 (2004).

205. Banci, L. *et al.* Metal-free superoxide dismutase forms soluble oligomers under physiological conditions: A possible general mechanism for familial ALS. *Proc. Natl. Acad. Sci. U. S. A.* **104**, 11263–11267 (2007).

APPENDIX. CHAPTER FOUR SUPPORTING FIGURES

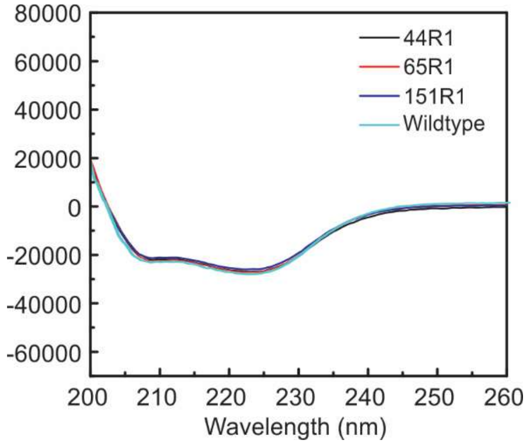

Figure A1. CD spectra of three representation T4L mutants and the wildtype T4L. The mutation clearly does not cause any perturbation to the secondary structure of T4L.

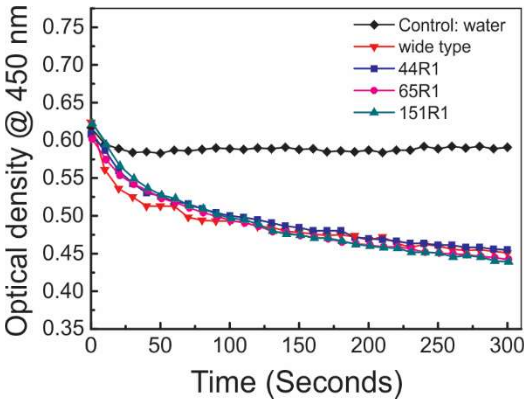

Figure A2. The activity assay of three representative T4L mutants and the wildtype protein. A drop in OD450 was observed for all protein samples. The "control" was acquired by mixing deionized-distill water with the bacterial cell walls.

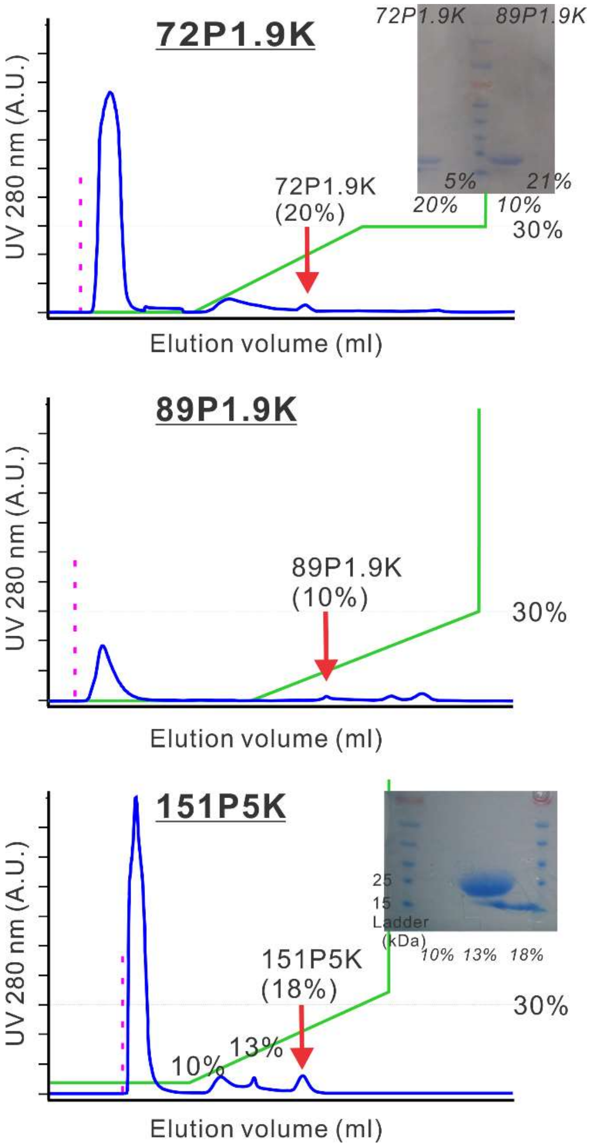

Figure A3. Three representative data on using the ion-exchange chromatography to separate the PEGylated T4L, unreacted mutants, and PEG. Each component resolved and collected from the chromatography is confirmed with gel-electrophoresis.

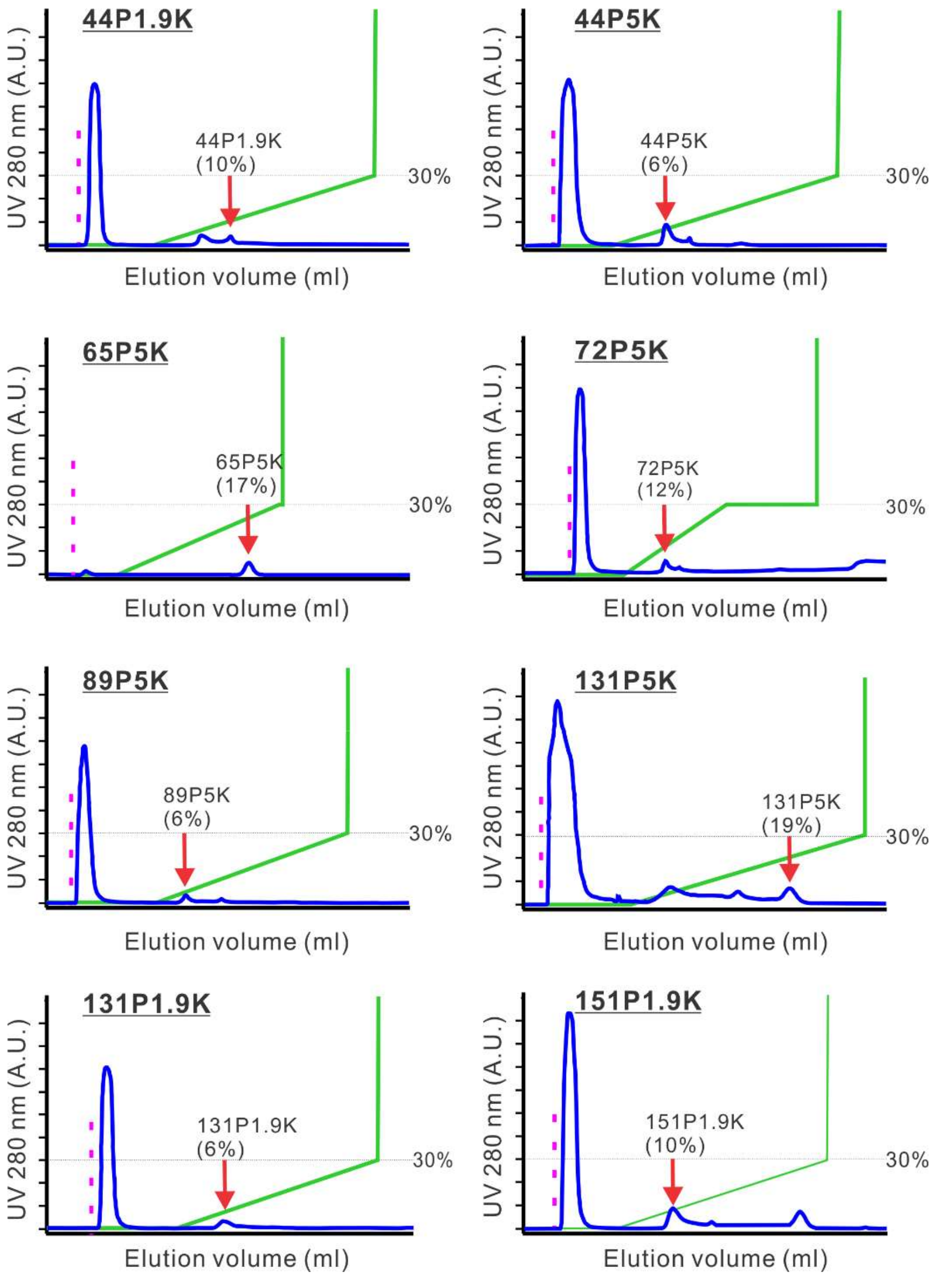

Figure A4. Additional chromatographs indicating the separation of the PEGylated T4L, unreacted mutants, and PEG using the ion-exchange chromatography.

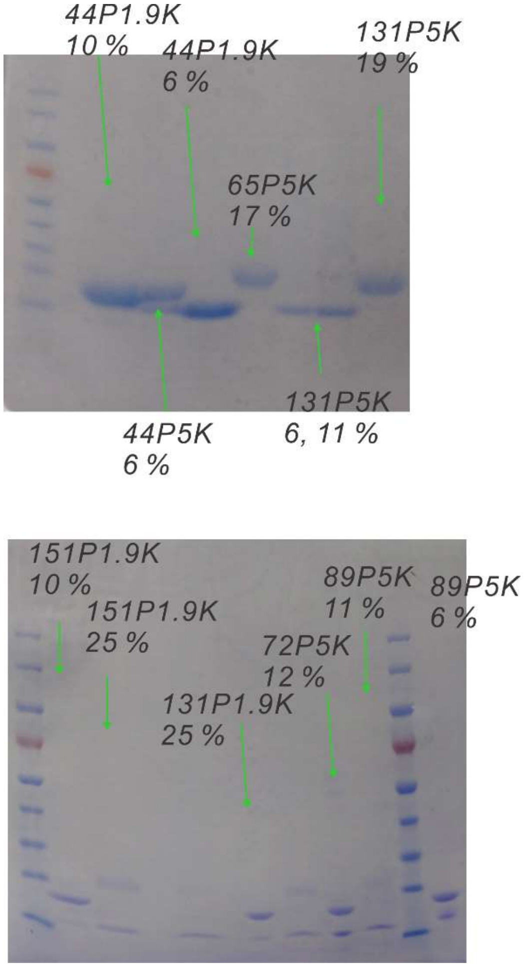

Figure A5. Additional gel-electrophoresis data to confirm the separation of the PEGylated T4L, unreacted mutants, and PEG using the ion-exchange chromatography.